FOTONİK 2026

Ulusal Optik, Elektro-Optik ve Fotonik Çalıştayı

Bilkent Üniversitesi Mithat Çoruh Konferans Salonu

11 Eylül 2026

İÇİNDEKİLER

AMAÇ

Bu toplantı, ulusal boyutta optik, elektro-optik ve fotonik konularına yönelik yıllık tek bilimsel toplantı serisi olan Ulusal Optik, Elektro-Optik ve Fotonik Çalıştaylarının 27.'sini oluşturmaktadır. Optik, elektro-optik ve fotonik alanlarının yüksek teknoloji dahilinde ekonomik katkısı büyük, savunma ve sağlık gibi stratejik sanayilerde uygulamaları geniştir. Bu nedenlerden dolayı, bu konularda ulusal düzeyde gelişmemizle birlikte bulunduğumuz düzeyin bilinmesi ve ilerletilmesi önemlidir.

Bu toplantıda, ülke çapında optik, elektro-optik ve fotonik konularında akademide ve endüstride araştırma ve geliştirme çalışması yapan gruplar (bilim insanları, yöneticiler, mühendisler, lisansüstü öğrencileri vs.) bir araya gelecek ve çalışmalarını birbirlerine sunup, tanışma, görüşme ve tartışma olanağı bulacaklardır. Bu, gruplar arası ortak çalışmaların başlatılmasına, karşılıklı destek ve fikir alışverişinde bulunulmasına ve ortak proje başvuruları (örneğin, Avrupa Birliği Çerçeve Programları) için çalışmalar yapılmasına ön ayak olacaktır.

Bu şekilde, bu toplantının optik, elektro-optik ve fotonik konularında ülkemizin bilim ve teknoloji çalışmalarına yarar ve katkı sağlaması beklenmektedir.

Toplantı Konuları

- Fotoalgılayıcılar
- Elektro-Optik Malzeme ve Cihazlar
- Lazerler
- Doğrusal Olmayan Optik Aygıtlar
- Tümleşik Optik
- Optik Lifler
- Modelleme ve Simulasyon Yöntemleri
- Ölçüm ve Değerlendirme Teknikleri
- Kuantum Optiği
- Nanofotonik Aygıtlar ve Sistemler

ORGANİZASYON

Alpan Bek, ODTÜ
Alper Kiraz, Koç Üniversitesi
Alphan Sennaroğlu, Koç Üniversitesi
Arda Deniz Yalçınkaya, Boğaziçi Üniversitesi
Arif Engin Çetin, İzmir Biyotıp ve Genom Merkezi (İBG)
Bülent Çakmak, Erzurum Teknik Üniversitesi
Bülent Öktem, ROKETSAN
Ekmel Özbay, Bilkent Üniversitesi
Erkan Demirci, TÜBİTAK UEKAE-BİLGEM
Evren Mutlugün, Abdullah Gül Üniversitesi
Gül Yağlıoğlu, Ankara Üniversitesi
İbrahim Özdur, TOBB ETÜ
İsmail Özsaraç, ASELSAN
Kürşat Şendur, Sabancı Üniversitesi
Onur Ferhanoğlu, İstanbul Teknik Üniversitesi
Serkan Ateş, Sabancı Üniversitesi

BİLİMSEL PROGRAM

08:30-09:45	Kayıt İşlemleri
09:45-10:00	Açılış Konuşmaları
10:00-10:45 10:45-11:30	İsmail Özsaraç, ASELSAN MEOS Zübeyde Arslanoğlu, SSB
11:30-12:00	Kahve Arası
12:00-12:30 12:30-13:00	Güven Turgut, Erzurum Teknik Üniversitesi Hümbet Nasibli, TÜBİTAK
13:00-15:00	Yemek Arası ve Poster Sunumları
15:00-15:30 15:30-16:00 16:00-16:30	Muhammed Ali Keçebaş, Gebze Teknik Üniversitesi Onur Külçe, Hacettepe Üniversitesi Ahmet Karatay, Ankara Üniversitesi
16:30-17:00	Poster Ödül Töreni ve Kapanış Konuşmaları

DAVETLİ KONUŞMACI BİLDİRİLERİ LİSTESİ

POSTER BİLDİRİLERİ LİSTESİ

DAVETLİ KONUŞMACI BİLDİRİ ÖZETLERİ

Fotonik Teknolojiler ile Gelen Operasyonel Üstünlük

İsmail Özsaraç
ASELSAN MEOS

Savunma Sanayii Alanında Fotonik ve Kuantum Teknolojileri Alanındaki Gelişmeler

Zübeyde Arslanoğlu
SSB

Optik Biyosensörler İçin İki Boyutlu Malzeme Mühendisliği

Güven Turgut[1]

[1]*Temel Bilimler Bölümü, Fen Fakültesi, Erzurum Teknik Üniversitesi, Yakutiye, Erzurum.*

guven.turgut@erzurum.edu.tr

Canlı sistemler tarafından üretilen belirteç niteliğindeki biyomoleküllerin analitik olarak saptanması, hastalıkların erken tanısı ve prognoz değerlendirmesi açısından büyük önem taşır. Biyomoleküllerin tespitinde optik biyosensörler yüksek hassasiyet, çoklu analit tespiti yapabilme yeteneği ve düşük maliyetli olması nedeni ile kullanım açısından önemli hale gelmiştir. Optik biyosensörler için madde-molekül etkileşiminde etkinliği iyi malzemelere ihtiyaç duyulmaktadır.

İki boyutlu malzemeler, atomik kalınlıkları, olağanüstü optik özellikleri ve ortama karşı güçlü duyarlılıkları nedeniyle optik temelli biyosensörlerde kullanışlı olduğu ortaya çıkmıştır. Malzeme seçiminin ötesinde, kalınlık kontrolü, heteroyapı oluşumu, yüzey fonksiyonelleştirme, gerilim modülasyonu ve kusur kontrolü dahil olmak üzere iki boyutlu malzemelerde yapılabilen malzeme mühendisliği, ışık-madde-biyomolekül etkileşimleri üzerinde benzeri görülmemiş bir kontrol sağlamaktadır.

Malzeme mühendisliği stratejileri ile madde-molekül etkileşimini artırarak malzemenin ve malzeme temelinde üretilecek optik aygıt platformlarının optik sinyal süreçleri kontrol edilebilerek molekül tanılaması yapılabilecektir.

Yüksek Enerjili Lazer ve Uzay Sınıfı Optik Bileşenler için İleri Optik Metroloji: Standardizasyonda İlerlemeler ve Zorluklar

(Advanced Optical Metrology for High-Energy Laser and Space-Grade Optical Components: Progress and Challenges in Standardization)

Hümbet NASİBLİ

TÜBİTAK- UME, Ulusal Metroloji Enstitüsü, PO 54, 41470, Gebze, Kocaeli, Türkiye
(National Metrology Institute, The Scientific and Technological Research Council of Türkiye)
humbet.nasibli@tubitak.gov.tr

Yüksek enerjili lazer sistemleri ve uzay kalifiye optik bileşenler, aşırı yüksek radyasyon, sıcaklık ve vakum ortamlarında çalışmakta olup; optik performans, dayanıklılık ve metrolojik izlenebilirlik açısından son derece katı gereksinimlere ihtiyaç duymaktadır. Başta lazer-uyarılmış hasar eşiği (LIDT), ultra-zayıf optik soğurma ve saçılma olmak üzere temel parametrelerin güvenilir ve karşılaştırılabilir biçimde ölçülmesi, ileri optik metroloji ve fonksiyonel çok katmanlı kaplama teknolojileri için merkezi bir zorluk haline gelmiştir.

Bu konuşmada, ölçüm metodolojilerindeki son gelişmeleri sunmakta olup havacılık/uzay ve yüksek enerjili lazer uygulamalarına yönelik optik karakterizasyon tekniklerinin standardizasyonunda karşılaşılan güncel zorlukları tartışmaktadır. Çevresel kontrolün, hasar başlatma mekanizmaları ve lazer–malzeme etkileşiminin termodinamiği üzerindeki rolü de ele alınmaktadır.

Gelişmiş kaplama tasarımları arayüzeylerdeki elektrik alan dağılımını optimize ederek içsel LIDT değerlerini iyileştirse de, kusur kaynaklı hasar mekanizmaları lazer dayanımını sınırlayan baskın faktör olmaya devam etmektedir. Bu bağlamda, yaygın olarak kullanılan "1-on-1", "S-on-1" ve "Raster Scan" LIDT protokollerinin mevcut durumu, avantajları ve sınırlamaları eleştirel bir bakış açısıyla değerlendirilmektedir. Mevcut yöntemler standart sistemler için iyi yerleşmiş olsa da, kısa dalga boylu ve yüksek güçlü lazerlerin yaygınlaşması yeni test gereksinimleri doğurmuştur. Bu kapsamda; optik bileşenlerin zorlu atmosfer, vakum ve çevre koşulları altındaki LIDT sonuçları değerlendirilmektedir.

Ayrıca, yüksek güçlü sürekli dalga lazer uygulamaları ve termal hasar direncinin değerlendirilmesi açısından kritik öneme sahip olan yüksek saflıkta alttaş camlar ve çok katmanlı dielektrik kaplamalardaki ppm-altı seviyedeki optik soğurma ölçüm teknikleri ele alınmaktadır. Standardize edilmiş lazer kalorimetrisi ile fototermal tabanlı yöntemler arasındaki tutarlılık vurgulanmaktadır.

Gelecek nesil lazer ve uzay optik sistemlerinde güvenilirlik, birlikte çalışabilirlik ve görev başarısının sağlanabilmesi için sağlam, SI izlenebilirliğine sahip ve uluslararası düzeyde, uyumlaştırılmış standartların oluşturulması kritik öneme sahiptir. Sunum, TÜBİTAK UME'nin lazer metrolojisi alanındaki uluslararası iş birlikleri ve yürütülen standardizasyon faaliyetlerine genel bir bakış ile sonlandırılmaktadır.

Türkiye Bilimsel ve Teknolojik Araştırma Kurumu (TÜBİTAK) ARDEB 2568 programına destekleri (Proje No: 224N066) için teşekkür ederim.

High-energy laser systems and space-grade optical components operate under extreme radiative, thermal, and vacuum environments, imposing stringent requirements on optical performance, durability, and metrological traceability. Reliable and comparable measurement of key parameters—most notably laser-induced damage threshold (LIDT), ultra-weak optical absorption, and scatter—has become a central challenge in advanced optical metrology and functional multilayer coating technologies.

This work presents recent progress in measurement methodologies and discusses ongoing challenges in the standardization of optical characterization techniques for high-energy and aerospace applications. Particular emphasis is placed on LIDT testing under both atmospheric and vacuum conditions, as well as on high-quality coatings produced by ion beam sputtering and e-beam deposition technologies. The role of environmental control in damage initiation mechanisms and in the thermodynamics of laser–material interaction is addressed.

Although advanced coating designs reduce electric field intensity and improve intrinsic LIDT, defect-driven damage remains the dominant limitation to laser resistance. In this context the current status, advantages, and limitations of several LIDT protocols—1-on-1, S-on-1, and Raster Scan—are critically examined. While these methods are well established for 1064 nm systems, the rapid expansion of high-power, short-wavelength lasers has shifted attention toward second- and third-harmonic testing. LIDT experimental results are presented for 532 nm and 355 nm polarizers, mirrors and gamma-irradiation exposed windows evaluated under atmospheric and vacuum conditions, including components subjected to combined environmental stresses.

The second part of the talk addresses sub-ppm-level optical absorption in high-purity substrate glasses and multilayer dielectric coatings, which is crucial for high-power continuous-wave applications and thermal failure resistance assessment. The consistency between standardized laser calorimetry and photothermal-based methods is highlighted.

Establishing robust, SI-traceable, and internationally harmonized standards is essential to ensure reliability, interoperability, and mission success in next-generation laser and space optical systems. The presentation concludes with an overview of TÜBİTAK UME's international collaborations and ongoing standardization activities in laser metrology.

Hermityen Olmayan Fotonik Yapılarda Yansıma ve Soğurma Kontrolü

(Non-Hermitian Control of Reflection and Absorption in Photonic Structures)

Ali Keçebaş
Gebze Teknik Üniversitesi, 41400, Gebze, Kocaeli, Türkiye
(*Gebze Technical University, 41400, Gebze, Kocaeli, Türkiye)*
akec ebas@gtu.edu.tr

Işık ve termal radyasyonun dalga boyu altı (subwavelength) yapılarla etkileşiminin kontrolü, elektromanyetiğin bir alt alanı olarak, son birkaç on yılda büyük önem taşımış ve taşımaya devam edecektir. Yıllar içinde araştırmacılar, bu etkileşimleri geniş bir spektrum boyunca ayarlamak amacıyla dalga boyu altı yapılardan oluşan çeşitli kaplama türleri geliştirmiştir. Optik ve termal dalga boylarında ortaya çıkan yüzey plazmonları, epsilon-near-zero (ENZ) tepkileri ve optik boşluklar (kaviteler) gibi zengin fiziksel olgularla birleştirildiğinde, bu etkileşimleri kontrol etme yeteneğimiz giderek artmaktadır. Bu tür olguları etkin şekilde kullanmak ve sonteknoloji fotonik cihazlara entegre etmek için ters tasarım (inverse design) yöntemleri de yaygın olarak kullanılmaktadır. Tasarım probleminin bu ikili doğası nedeniyle, fiziksel içgörü ile ters tasarım arasındaki bağlantı giderek daha önemli hale gelmiştir.

Bu bağlantıyı daha da güçlendirmek amacıyla, son yıllarda önemli ilgi gören bir alt alan olan non-Hermityen fotonikten yararlanılabilir. Kökeni kuantum fiziğine dayanan ve daha sonra klasik fotoniğe uyarlanan non-Hermityen çerçeve, fotonik yapıların yansıma (reflectance) ve soğurma (absorptance) özelliklerini belirleyen temel mekanizmaların analizinde güçlü bir yaklaşım sunar. Özellikle bu çerçeve, istisnai noktalar (exceptional points, EPs) olarak bilinen özgün tekilliklerin incelenmesine olanak tanır. Bu noktalar; tek yönlü yansıma, kayıp kaynaklı saydamlık (loss-induced transparency), koherent mükemmel soğurma (coherent perfect absorption) ve dış bozuculara karşı artmış hassasiyet gibi ilgi çekici olgularla ilişkilidir.

Bu konuşmada, öncelikle non-Hermityen çerçevenin mükemmel soğurma ve artırılmış hassasiyet sağlayan fotonik yapıların tasarımında nasıl kullanılabileceğini ele alacağım. Ardından, farklı fotonik platformlarda istisnai noktaların nasıl gerçekleştirilebileceğini sunacağım. Son olarak, bu kavramların yapı karmaşıklığı arttıkça nasıl genişlediğini tartışarak konuşmayı tamamlayacağım.

Controlling how light and thermal radiation interact with subwavelength features—a subfield of electromagnetics—has been of great importance over the past few decades and will continue to be so. Over the years, researchers have developed various types of coatings composed of subwavelength structures to tailor these interactions across a broad spectrum. When combined with rich physical phenomena present at optical and thermal wavelengths, such as surface plasmons, epsilon-near-zero responses, and optical cavities, our ability to control these interactions continues to improve. To harness these phenomena and incorporate them into state-of-the-art photonic devices, inverse design methods have also been widely employed. Due to this dual nature of the design problem, the connection between physical insight and inverse design has become increasingly important.

To further strengthen this connection between physical understanding and inverse problems, non-Hermitian photonics—a subfield that has attracted significant recent interest—can be utilized. Originating from quantum physics and later extended to classical photonics, the non-Hermitian framework provides a powerful approach for analyzing the underlying mechanisms governing the reflectance and absorptance characteristics of photonic structures. In particular, this framework enables the exploration of unique singularities known as exceptional points (EPs), which are associated with intriguing phenomena such as unidirectional reflectance, loss-induced transparency, coherent perfect absorption, and enhanced sensitivity to external perturbations.

In this talk, I will first discuss how the non-Hermitian framework can be leveraged to design photonic structures for perfect absorption and enhanced sensitivity. I will then present methods for realizing exceptional points in different photonic platforms. Finally, I will conclude by discussing how these concepts extend as the structural complexity increases.

Gelecek Nesil Hesaplama ve Ekranlar için Kırınımsal Optik İşlemciler ve Elektromanyetik Alan Sentezi

Onur Külçe
Elektrik-Elektronik Mühendisliği Bölümü, Mühendislik Fakültesi, Hacettepe Üniversitesi, Ankara
onurkulce@ee.hacettepe.edu.tr

Özet

Klasik optik görüntüleme ve ekran teknolojileri, analiz ve hesaplama kolaylığı sağlaması adına uzun yıllardır büyük ölçüde skaler dalga teorisi ve paraksiyel (yakın eksenli) yaklaşımlar altında modellenmiştir. Ancak günümüzde, geniş görüş açılı (wide-viewing-angle) holografik üç boyutlu televizyonlar (3DTV), artırılmış ve sanal gerçeklik (AR/VR) sistemleri ile head-up display (HUD) gibi yeni nesil ekran teknolojileri, paraksiyel sınırların ötesinde geniş açılı dalga yayımlarını zorunlu kılmaktadır. Benzer şekilde, yapay zekâ ve derin öğrenme modellerinin donanımsal hızlandırma ihtiyaçları, hesaplamayı ışık hızında ve sıfıra yakın enerji tüketimiyle gerçekleştirebilen kırınımsal optik ağlara ve tüm-optik işlemcilere (all-optical processors) olan ilgiyi artırmıştır.

Bu konuşmada, skaler dalga teorisinden elektromanyetik dalga teorisine geçişte paraksiyel olmayan geniş açılı alanlarda karşılaşılan kısıtlamalar ve bu kısıtlamaların sinyaller ve sistemler (signals and systems) çerçevesinde nicel olarak nasıl analiz edilebileceği ele alınacaktır. Klasik eşlemelerde, ihmal edilen boylamsal (longitudinal) elektrik alan bileşeni nedeniyle geniş açılarda ortaya çıkan yüksek frekans gürültüleri ve aşırı güç spektrumu sapmaları, geliştirilen ters filtreleme (inverse filtering) ve güç spektrumu eşitleme yöntemleriyle sistemli bir şekilde giderilmektedir. Geliştirilen "koordinat çerçevesi dönüşümü ve lokal polarizasyon kısıtı" algoritmaları, geniş görüş açılı holografik ekranlarda gözlemcinin farklı açılardan paraksiyel olmayan segmentleri hatasız ve istenen polarizasyon durumunu koruyarak yakalamasını mümkün kılmaktadır.

Konuşmanın ikinci bölümünde ise, uzamsal olarak tasarlanan kırınımsal yüzeylerin (diffractive surfaces) tüm-optik doğrusal dönüşüm (linear transform) işlemcileri olarak kullanımı sunulacaktır. Kırınımsal sinir ağlarının (diffractive neural networks) bilgi işleme kapasitesi doğrusal cebir yaklaşımlarıyla incelenecek; hem veri-bağımsız matris genelleştirilmiş tersi yöntemleri hem de derin öğrenme tabanlı optimizasyon stratejileri karşılaştırmalı olarak tartışılacaktır. Çok katmanlı (derin) kırınımsal mimarilerin, tek katmanlı geniş yapılara kıyasla doğrusal dönüşüm doğruluğu, genelleme yeteneği ve kırınım verimliliği (diffraction efficiency) açısından sunduğu derinlik avantajları (depth advantages) teorik ve nümerik simülasyon sonuçlarıyla ortaya konulacaktır.

Sonuç olarak, elektromanyetik alan sentezi ile derin öğrenme tabanlı kırınımsal işlemci tasarımlarının birleşimi, gelecek nesil hesaplama ve ekran teknolojilerinin optik donanım altyapısını şekillendirmektedir. Gelecek perspektifinde ise bu yaklaşımlar, hesaplamalı optik (computational optics) ve hesaplamalı görüntüleme (computational imaging) prensipleri doğrultusunda yeniden ele alınacaktır. Geliştirilen kırınımsal mimariler, dinamik ışık kontrolü sağlayan uyarlanabilir optik (adaptive optics) sistemleriyle entegre edilerek; faz bozulmalarına karşı dirençli, yüksek verimli ve ölçeklenebilir optik hesaplama (optical computing) platformlarının önünü açacaktır. Bu entegrasyon, fiziksel dünya ile algoritmik hesaplamayı fotonik evrende birleştiren işlemcilerin öncülü olmaya güçlü bir adaydır.

Fotonik Teknolojilerde Doğrusal Olmayan Optik Ve Ultrahızlı Lazer Spektroskopisi

Ahmet Karatay

Optik Malzemeler Araştırma Laboratuvarı, Ankara Üniversitesi Fizik Mühendisliği Bölümü, 06100, Ankara, Türkiye

akaratay@eng.ankara.edu.tr

Ultrahızlı lazer spektroskopisi, malzemelerde gerçekleşen elektronik, titreşimsel ve yapısal dinamiklerin femtosaniye zaman ölçeğinde incelenmesi için güçlü bir araştırma platformu sunmaktadır. Doğrusal olmayan optik tekniklerle birlikte kullanıldığında, yarı iletkenler, nanoyapılar, iki boyutlu malzemeler, moleküler sistemler ve güçlü korelasyonlu katılar gibi çok çeşitli sistemlerde meydana gelen karmaşık ışık–madde etkileşimlerinin ayrıntılı biçimde karakterize edilmesine ve etkin bir şekilde kontrol edilmesine olanak sağlamaktadır.

Yarı iletken kristallerde, katkılama (doping) konsantrasyonuna ve dolayısıyla kusur yoğunluğuna bağlı olarak değişen doğrusal olmayan soğurma mekanizmaları, açık yarık Z-tarama (OA Z-scan) ölçümleri kullanılarak nicel olarak analiz edilebilir. Benzer şekilde, organik moleküllerde yan grupların ve çözücü ortamın etkisiyle şekillenen ultrahızlı süreçleri, pompa–gözlem spektroskopisi aracılığıyla ayrıntılı biçimde ortaya konulabilir. Ayrıca, biyogörüntüleme ve fotodinamik terapi uygulamaları için tasarlanan nanokompozit yapılarda meydana gelen yük transferi dinamikleri ve doğrusal olmayan soğurma davranışları da bu ultrahızlı deneysel teknikler kullanılarak etkin biçimde incelenebilmektedir.

Tüm bu olanaklar, ultrahızlı ve doğrusal olmayan optik yöntemlerin yalnızca maddede gerçekleşen geçici süreçlerin temel düzeyde anlaşılmasına katkı sağlamakla kalmadığını; aynı zamanda ultrahızlı optik anahtarlar, optik sınırlayıcılar ve fotodinamik terapi kaynakları gibi gelişmiş fotonik teknolojilerin geliştirilmesinde de önemli bir rol oynadığını göstermektedir.

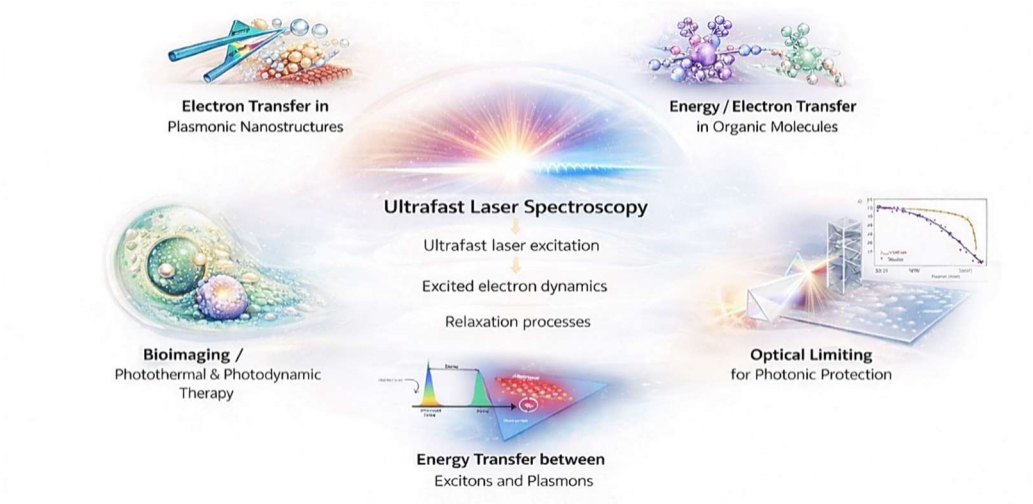

Şekil 1. Doğrusal olmayan optik dinamiklerin ultrahızlı lazer spektroskopisi ile incelenmesi ve fotonik uygulamaları

A.K., TÜBİTAK'ın 124F168 ve 122F211 numaralı projelerinden sağlanan destek için teşekkür etmektedir.

POSTER BİLDİRİ ÖZETLERİ

Lazer Mesafe Ölçer Sistemlerinde Ayarlanabilir Eşik Seviyesi

Hasan Mert KARABACAK
Aviyonik Mühendisliği Tezli Yüksek Lisans, Yıldız Teknik Üniversitesi, ASELSAN, İstanbul-Ankara, Türkiye
mert.karabacak@std.yildiz.edu.tr / hasanmertk@aselsan.com

Özet

Lazer mesafe ölçer (LRF) sistemlerinde ölçüm doğruluğu ve güvenilirliği, özellikle yüksek ortam ışığı bulunan koşullarda, alıcıya ulaşan arka plan gürültüsü nedeniyle önemli ölçüde etkilenebilmektedir. Avalanche fotodiyot (APD) tabanlı alıcıların yüksek hassasiyetleri, düşük ışık seviyelerinde avantaj sağlarken, yoğun ortam ışığı altında gürültü ve yanlış alarm olasılığını artırabilmektedir.

Bu çalışmada, değişken ortam ışığı koşullarında LRF sistemlerinin ölçüm güvenilirliğini artırmak amacıyla gerçek zamanlı çalışan bir adaptif gürültü eşikleme yöntemi önerilmiştir. Önerilen yöntemde, lazer atışı gerçekleştirilmeden önce fotodiyot üzerinden ortam gürültüsü izlenmekte ve ölçülen gürültü seviyesine bağlı olarak algılama eşik gerilimi otomatik olarak ayarlanmaktadır. Eşik gerilimi, dijital potansiyometre ve karşılaştırıcı devresi kullanılarak mikrodenetleyici tarafından iteratif biçimde artırılmakta; ortam gürültüsünün eşik seviyesinin altında kaldığı noktada mevcut eşik değeri belirlenerek lazer atışı gerçekleştirilmektedir. Böylece sabit eşikleme yöntemlerinde ortaya çıkabilen yanlış alarmların ve zayıf geri dönüş sinyallerinin gözden kaçırılması problemlerinin azaltılması hedeflenmiştir.

Önerilen yaklaşımın doğrulanması amacıyla fotodiyot, ayarlanabilir gerilim bölücü, karşılaştırıcı ve mikrodenetleyiciden oluşan bir donanım prototipi geliştirilmiş ve lazer mesafe ölçer alıcı sistemi ile bütünleştirilmiştir. Osiloskop ölçümleri, eşik seviyesinin ortam gürültüsündeki değişimlere bağlı olarak otomatik biçimde güncellendiğini göstermiştir. Elde edilen sonuçlar, önerilen adaptif eşik ayarlama yönteminin değişken ortam ışığı koşullarında arka plan kaynaklı yanlış algılamaların azaltılmasına ve lazer geri dönüş sinyalinin daha güvenilir biçimde algılanmasına katkı sağladığını göstermektedir.

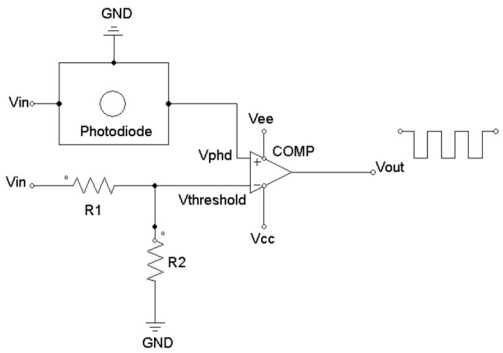

Şekil 1: Almaç devre yapısı

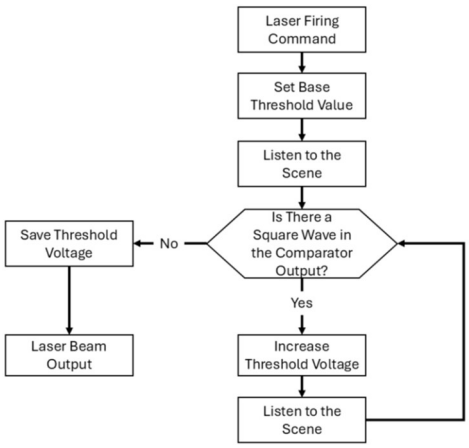

Şekil 2: Algoritma tanımı

Adaptive Spatial-Temporal 2D Non-Local Means Denoising for Raman Distributed Temperature Sensing

Soner Mülayim*[1], Erkan Özkan[2]
[1]SAMM Teknoloji, Türkiye
[2]SAMM Teknoloji, Türkiye

corresponding author, E-mail: soner.mulayim@samm.com

Abstract

Raman distributed temperature sensing (DTS) estimates temperature from the intensity ratio of spontaneous Stokes and Anti-Stokes backscatter. At long sensing distances, measurement precision is increasingly limited by stochastic fluctuations, particularly in the weaker Anti-Stokes channel. This work evaluates a causal spatial-temporal two-dimensional Non-Local Means (2D NLM) denoising approach that exploits redundancy in sequential Raman traces while preserving the distance-dependent physical envelope. The Stokes and Anti-Stokes channels are filtered independently before formation of the temperature-sensitive logarithmic ratio, preventing the nonlinear ratio operation from mixing the noise statistics of the two channels [1-4].

The experimental dataset contains 180 sequential records, each with 9771 Stokes and 9771 Anti-Stokes spatial samples at 0.81 m/sample. A 20-trace time-distance buffer is maintained. For each channel, the NLM bandwidth is adapted using a robust median-absolute-deviation estimate obtained from temporal first differences. The causal search uses the current and previous traces, with a 5-sample spatial patch (±2), an 11-sample spatial search window (±5), and channel-wise weighting. Figure 1(a) summarizes the processing chain. Figure 1(b) shows the last approximately 1 km of the log-ratio, where the raw scatter is strongly reduced after independent channel denoising.

For quantitative evaluation, the final 1235 spatial samples were linearly detrended to avoid counting deterministic attenuation as noise. The standard deviation was reduced by 79.2% for Stokes, 88.4% for Anti-Stokes, and 91.1% for the log-ratio. These values correspond to equivalent noise-suppression gains of 13.63 dB, 18.68 dB, and 21.00 dB, respectively, as shown in Figure 1(c). The results support causal 2D NLM as a practical software-domain method for improving long-range Raman-DTS precision without optical hardware modification. Since the dataset does not include an independent absolute-temperature calibration record, the reported improvement represents signal and log-ratio precision rather than absolute temperature accuracy; transient response and temperature bias should be validated separately for certification-oriented operation.

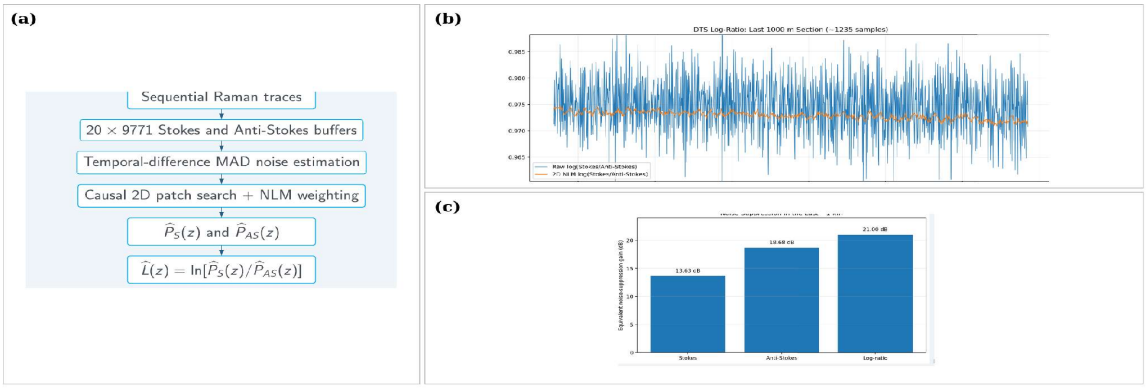

Figure 1: (a) Causal 2D NLM processing pipeline. (b) Raw and denoised log-ratio in the last ~1 km. (c) Equivalent noise-suppression gains for Stokes, Anti-Stokes and log-ratio.

Keywords: Raman distributed temperature sensing, Non-Local Means, spatial-temporal denoising, Stokes, Anti-Stokes, log-ratio

References

[1] M. A. Farahani and T. Gogolla, "Spontaneous Raman scattering in optical fibers with modulated probe light for distributed temperature Raman remote sensing," J. Lightwave Technol., 17(8), 1379-1392, 1999.
[2] A. Buades, B. Coll, and J.-M. Morel, "A review of image denoising algorithms, with a new one," Multiscale Model. Simul., 4(2), 490-530, 2005, doi:10.1137/040616024.
[3] M. A. Soto, J. A. Ramírez, and L. Thévenaz, "Intensifying the response of distributed optical fibre sensors using 2D and 3D image restoration," Nat. Commun., 7, 10870, 2016, doi:10.1038/ncomms10870.
[4] M. A. Soto, J. A. Ramírez, and L. Thévenaz, "Reaching millikelvin resolution in Raman distributed temperature sensing using image processing," Proc. SPIE 9916, 99162A, 2016, doi:10.1117/12.2236934.
[5] X. Qian et al., "Noise level estimation of BOTDA for optimal non-local means denoising," Appl. Opt., 56(16), 4727-4734, 2017.

Nb Katkılı SnS İnce Filmlerin Üretimi ve Karakterizasyonu

Selvihanım KANBUROĞLU[*,1], Meltem DÖNMEZ KAYA[2,3]

[1]*Department of Photonics Science and Engineering, Graduate School of Natural and Applied Sciences, Gazi University, Ankara, Türkiye*
[2]*Photonics Application and Research Center, Gazi University, Ankara, Türkiye*
[3]*Department of Photonics, Faculty of Applied Sciences, Gazi University, Ankara, Türkiye*
*E-mail: kanburoglu06@gmail.com.tr

Özet

Yenilenebilir enerji teknolojilerinin gelişimi, düşük maliyetli, çevre dostu ve yüksek performanslı yarıiletken malzemelere olan ilgiyi artırmaktadır. Bu kapsamda kalay sülfür (SnS); doğada bol bulunan ve toksik olmayan elementlerden oluşması, yaklaşık 1,3 eV bant aralığına ve yüksek optik soğurma katsayısına (~10^4–10^5 cm^{-1}) sahip olması nedeniyle fotovoltaik ve optoelektronik uygulamalar açısından dikkat çeken bir yarıiletken malzemedir. Bununla birlikte, saf SnS ince filmlerde taşıyıcı konsantrasyonu ve hareketliliğinin sınırlı olması ile yapısal kusurlar, malzemenin elektriksel ve optik performansını olumsuz yönde etkileyebilmektedir.

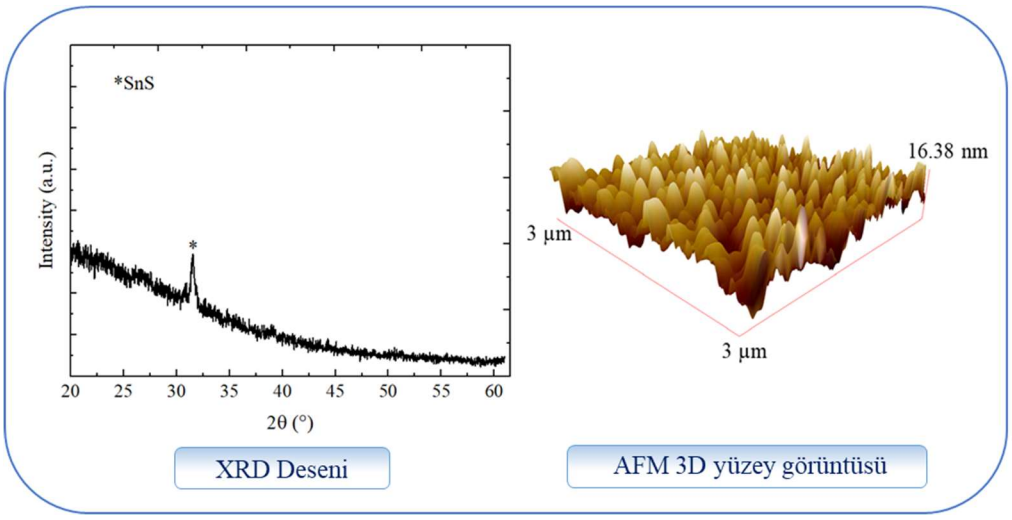

Şekil 1: Nb katkılı SnS ince filme ait XRD deseni ve üç boyutlu AFM yüzey görüntüsü

Bu çalışmada, SnS ince filmlerin yapısal, morfolojik, optik ve elektriksel özelliklerinin geliştirilmesi amacıyla niyobyum (Nb) katkılamasının etkisi araştırılmıştır. Nb katkılı SnS ince filmler, Radyo Frekans (RF) magnetron eş-saçtırma (co-sputtering) yöntemi kullanılarak farklı katkılama koşullarında üretilmiştir. Nb katkısının SnS kristal yapısı, yüzey özellikleri, optik davranışı ve elektriksel özellikleri üzerindeki etkileri sistematik olarak incelenmiştir. XRD analizleri, yapısal doğrulama ortaya koyarken, AFM analizleri homojen bir yüzey morfolojisinin oluştuğunu göstermiştir. Optik karakterizasyon sonucunda ise güneş ışığının etkin soğurulması açısından uygun bir optik bant aralığı elde edilmiştir. Nb:SnS ince filmlerin yapısal analizi, homojen yüzey morfolojisi ve elde edilen uygun optik bant aralığı birlikte değerlendirildiğinde, Nb katkılı SnS ince filmlerin güneş hücrelerinde soğurucu tabaka olarak kullanım açısından umut verici özellikler sergilediği belirlenmiştir.

Anahtar Kelimeler: Kalay sülfür (SnS), Niyobyum (Nb) katkılama, İnce film, RF magnetron saçtırma

Acknowledgements

Bu çalışma, Fotonik Uygulama ve Araştırma Merkezi'nde 2019K12-149045 nolu proje ile CB-SBB tarafından desteklenmektedir.

Referanslar

[1 Hartman, K., Johnson, J. L., Bertoni, M. I., Recht, D., Aziz, M. J., Scarpulla, M. A., & Buonassisi, T. (2011). SnS thin-films by RF sputtering at room temperature. Thin Solid Films, 519(21), 7421-7424.
[2] Patel, M., & Ray, A. (2014). Magnetron sputtered Cu doped SnS thin films for improved photoelectrochemical and heterojunction solar cells. Rsc Advances, 4(74), 39343-39350.

Metilamonyum Kurşun İyodür ($MAPbI_3$) Perovskit İnce Filmlerin Simülasyon Destekli Üretimi ve Optik-Yapısal Özelliklerinin İncelenmesi

Çağdaş Eğin*[1,2], Alihan Kumtepe[1,2], Çağrı Taha Delikanlı[1,2], Çağatay Ezen[1], Özlem Coşkun[1,5], Meriç Çalışkan Arslan[1], Meltem Dönmez Kaya[3,4]

[1] *Kalyon PV R&D Center, Ankara, Türkiye*

[2] *Department of Photonics Science and Engineering, Graduate School of Natural and Applied Sciences, Gazi University, Ankara, Türkiye*

[3] *Photonics Application and Research Center, Gazi University, Ankara, Türkiye*

[4] *Department of Photonics, Faculty of Applied Sciences, Gazi University, Ankara, Türkiye*

[5] *Micro and Nanotechnology Program, Middle East Technical University (METU), Ankara, Türkiye*

*cegin@kalyonpv.com

Özet

Metilamonyum kurşun iyodür ($MAPbI_3$) perovskit ince filmler, yüksek optik soğurma kapasiteleri, ayarlanabilir bant aralıkları ve çözelti tabanlı yöntemlerle kolaylıkla üretilebilmeleri nedeniyle fotovoltaik ve elektro-optik uygulamalarda fotoaktif yarı iletken tabaka olarak önemli bir potansiyele sahiptir. Bu çalışmada, $MAPbI_3$ tabakasının üretim süreci, deneysel çalışmalar öncesinde gerçekleştirilen optik ve sayısal simülasyonlarla desteklenmiş; simülasyon çıktıları doğrultusunda hedeflenen film özelliklerine yönelik üretim parametreleri belirlenmiştir. $MAPbI_3$ perovskit ince filmler, flor katkılı kalay oksit (FTO) cam altlıklar üzerine spin kaplama tekniği kullanılarak iki aşamalı ardışık kaplama (two-step sequential deposition) yöntemiyle üretilmiştir. Simülasyon destekli bir yaklaşımla gerçekleştirilen üretim süreci sonucunda, hedeflenen optik davranışa ve film sürekliliğine sahip $MAPbI_3$ tabakaların elde edilmesi amaçlanmış ve üretim parametrelerinin film özellikleri üzerindeki etkisi ortaya konulmuştur. Üretilen filmlerin kristal yapısı, faz oluşumu ve kristallenme davranışı X-ışını kırınımı (XRD) analizi ile incelenmiştir. Yüzey morfolojisi, tane oluşumu ve film sürekliliği taramalı elektron mikroskobu (SEM) ile değerlendirilirken, yüzey topografyası ve pürüzlülük özellikleri atomik kuvvet mikroskobu (AFM) kullanılarak karakterize edilmiştir. Film kalınlıkları profilometre ile kontrol edilerek, optik özellikler UV-Vis spektrofotometresi ile analiz edilmiş, soğurma davranışı ve optik bant aralığı değerlendirilmiştir. Elde edilen bulgular, $MAPbI_3$ fotoaktif tabakanın ilerleyen aşamalarda oluşturulacak çok katmanlı (stack) cihaz yapısına entegrasyonu açısından önemli bir deneysel temel oluşturmuştur. Ayrıca, filmlerin tandem hücre mimarilerinde katmanlar arası optik uyumun, ışık yönetiminin ve fotoaktif tabaka seçiminin değerlendirilmesine yönelik önemli tasarım girdileri sağlamıştır.

Şekil 1: $MAPbI_3$ perovskit ince filmlerin üretim süreci ve yüzey karakterizasyon görüntüleri.

Anahtar Kelimeler / Keywords: Fotovoltaik, Perovskite, İnce Film, Spin Coating, $MAPbI_3$

Acknowledgements

Bu çalışma, Fotonik Uygulama ve Araştırma Merkezi'nde 2019K12-149045 nolu proje ile CB-SBB tarafından desteklenmektedir.

Referanslar / References

[1] Cho, Y., Jung, H. R., & Jo, W. (2022). Halide perovskite single crystals: growth, characterization, and stability for optoelectronic applications. Nanoscale, 14(26), 9248-9277.

[2] Zhang, L., Zuo, C., & Ding, L. (2021). Efficient MAPbI3 solar cells made via drop-coating at room temperature. *Journal of Semiconductors*, *42*(7), 072201.

High-Brightness 1018 nm Monolithic Fiber Laser with Power Scaling Beyond 500 W

Salih Kağan Kalyoncu*[1], Halil İbrahim Çetin[1], Büşra Mete[1]

[1]*TÜBİTAK BİLGEM, 41470 Kocaeli, Türkiye*

Corresponding author: salih.kalyoncu@tubitak.gov.tr | Presenting author: halilibrahim.cetin@tubitak.gov.tr

Abstract

High-power ytterbium-doped fiber lasers are attractive for industrial, scientific, medical, and defense applications; however, conventional diode pumping at 915–976 nm introduces a comparatively large quantum defect and thermal load. Tandem pumping with high-brightness fiber lasers operating near 1018 nm can reduce this thermal burden and enable efficient core-pumping of multi-kilowatt master oscillator power amplifier systems. Operation at 1018 nm is nevertheless challenging because the required high inversion competes with amplified spontaneous emission and parasitic lasing at longer wavelengths. In this study, the active-fiber length and output-coupler reflectivity are numerically examined to balance pump absorption, wavelength selectivity, conversion efficiency, and ASE suppression.

The optimized monolithic cavity employs approximately 3.5 m of 15/130 µm Yb-doped double-clad fiber, a 99.4% high-reflector FBG, an 11.7% output-coupler FBG, and seven wavelength-stabilized 976 nm pump diodes delivering about 650 W through a 7×1 combiner. A polymer-free cladding power stripper, tightly coiled water-cooled gain fiber, and an angle-cleaved coreless end cap support thermal management, higher-order-mode suppression, and back-reflection control. The system produces 502 W at 1017.9 nm with an approximately 76% slope efficiency, 51.4 dB ASE suppression, 1.7 nm spectral bandwidth, and near-diffraction-limited beam quality of $M^2 \approx 1.15$. The corresponding brightness reaches 36.6 $GW \cdot cm^{-2} \cdot sr^{-1}$, supporting fused-combiner integration for power-scalable tandem-pumped architectures. The underlying study was previously published as a journal article [1] and has not previously been presented at a conference.

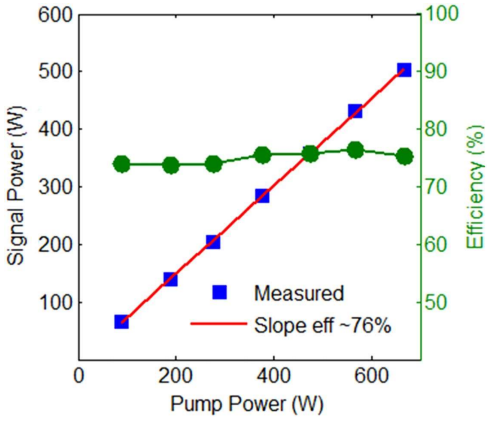

Figure 1: Measured output power and slope efficiency of the 1018 nm monolithic fiber laser (adapted from [1]).

Keywords: ytterbium-doped fiber laser; tandem pumping; 1018 nm laser; ASE suppression; beam quality

Acknowledgements

This work was supported by the Ministry of Development of Türkiye (2014K121010) and TÜBİTAK SAVTAG (113A053).

References

[1] S. K. Kalyoncu and A. Yeniay, "High brightness 1018 nm monolithic fiber laser with power scaling to >500 W," Applied Optics 59(16), 4763–4767 (2020). https://doi.org/10.1364/AO.393043.

[2] S. K. Kalyoncu, "The stability analysis for in-band pumped master oscillator power amplifier," IEEE Photonics Journal 8, 1502208 (2016).

[3] Y. Glick et al., "Single-mode 230 W output power 1018 nm fiber laser and ASE competition suppression," Journal of the Optical Society of America B 33, 1392–1398 (2016).

Viskozite Ölçümü için Mikrosütun Tabanlı Mikroakışkan Sistemlerde Geometrinin Akış Kaynaklı Deformasyon Üzerindeki Etkisinin Analizi

Özlem Koçoğlu[1,2], Ali Haydar Yıldız[1], Rezzan Yardımcı[*1,3], Ahmet Can Erten[*1]
[1] *Department of Electronics and Communication Engineering, Istanbul Technical University*
[2] *Vocatinal School of Biomedical Device Technology Programme, Istanbul Beykent University*
[3] *Department of Biomedical Engineering, Istanbul Yeni Yüzyıl University*
E-mail: yardimci24@itu.edu.tr ve aerten@itu.edu.tr

Özet
Viskozite, akışkanların akmaya karşı gösterdiği iç direnci tanımlayan temel bir reolojik özellik olup endüstriyel ve biyolojik sistemlerde akışkan davranışının karakterizasyonunda yaygın olarak kullanılmaktadır [1]. Mikroakışkan tabanlı viskozimetreler hassas akış kontrolü, hızlı analiz, düşük numune tüketimi ve görüntüleme sistemleriyle kolay entegrasyon gibi önemli avantajlar sağlamaktadır [2]. Özellikle mikrosütun tabanlı mikroakışkan sistemler, akışkan-yapı etkileşimi (Fluid Solid Interation, FSI) sonucunda meydana gelen mekanik davranışın ölçülebilir bir çıktıya dönüştürülmesine olanak sağlayan yaklaşımlar arasında öne çıkmaktadır. Bu çalışmada, daire ve kare geometrisine sahip mikrosütunların belirli bir viskozite ve çeşitli akış hızları altındaki deformasyon davranışları deneysel olarak optik görüntüleme yöntemiyle incelenmiş ve elde edilen bulgular ANSYS CFD (Computational Fluid Dynamics) tabanlı nümerik analizlerle değerlendirilmiştir. Literatürdeki çalışmaların çoğunlukla belirli bir mikrosütun geometrisi için viskozite ve akış hızının etkilerine odaklandığı, farklı mikrosütun geometrilerinin akış kaynaklı mekanik yanıtlarının deneysel ve sayısal yöntemlerin birlikte kullanıldığı karşılaştırmalı bir yaklaşımla yeterince ele alınmadığı görülmektedir [3], [4]. Bu doğrultuda çalışmanın temel amacı, farklı mikrosütun geometrilerinin değişen akış hızındaki deformasyon yanıtlarını karşılaştırmalı olarak değerlendirmektir. Deneysel ölçümler ve nümerik analizlerden elde edilen sonuçlar, akış hızındaki artışın mikrosütun yapılarında meydana gelen deformasyonu artırdığını göstermiştir. Geometriye bağlı yapısal değerlendirmeler ise mikrosütun geometrisinin akışkan-yapı etkileşiminde (FSI) belirleyici bir parametre olduğunu ve oluşan deformasyon davranışını doğrudan etkilediğini ortaya koymuştur.

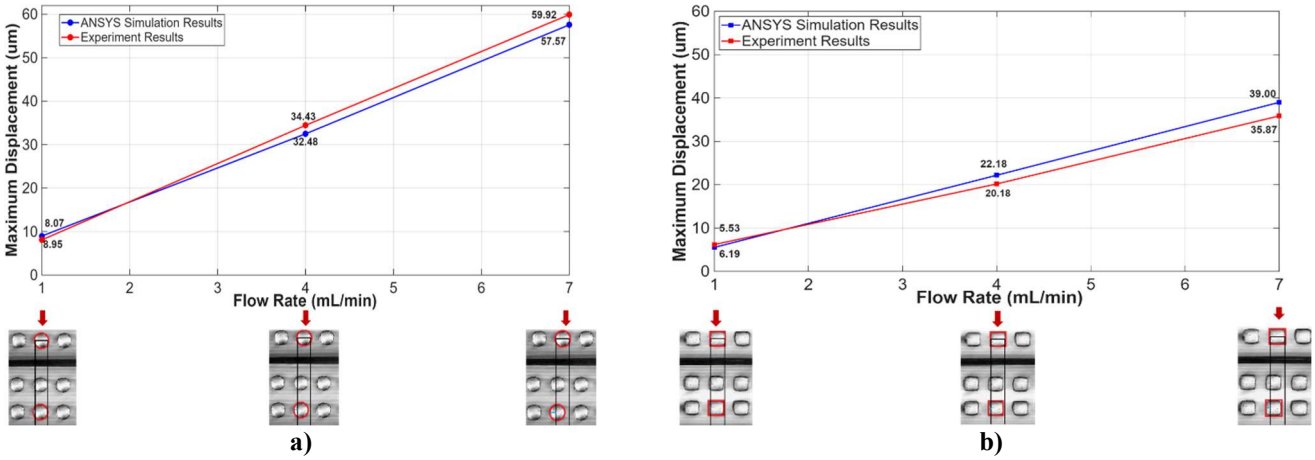

Şekil 1: 5,45 cP viskozitede farklı akış debileri altında mikrosütun deformasyonlarının deneysel ve nümerik olarak karşılaştırılması: (a) dairesel ve (b) kare mikrosütun geometrisi.

Anahtar Kelimeler: Mikroakışkan viskozimetre, mikrosütun yer değiştirmesi, akışkan-yapı etkileşimi (Fluid–Solid Interaction, FSI), hesaplamalı akışkanlar dinamiği (Computational Fluid Dynamics, CFD)

Referanslar
[1] Leblanc, G. E., Secco, R. A., & Kostic, M. (2023). Viscosity measurement. In Mechanical Variables Measurement-Solid, Fluid, and Thermal (pp. 11-1). CRC Press.
[2] Del Giudice, F. (2022). A review of microfluidic devices for rheological characterisation. Micromachines, 13(2), 167.
[3] Mustafa, A., Eser, A., Aksu, A. C., Kiraz, A., Tanyeri, M., Erten, A., & Yalcin, O. (2020). A micropillar-based microfluidic viscometer for Newtonian and non-Newtonian fluids. Analytica chimica acta, 1135, 107-115.
[4] Chang, Y. N., & Yao, D. J. (2026). A Microfluidic Platform for Viscosity Testing of Non- Newtonian Fluids in Engineering and Biomedical Applications. Micromachines, 17(2), 201.

Silisyum Tabanlı Yapılarda Yüzey Mühendisliği ve Al_2O_3 Antireflektif Kaplamaların Optik Performansı

Çağatay Ezen*[1] Alihan Kumtepe[1,2], Çağdaş Eğin[1,2], Çağrı Taha Delikanlı[1,2], Özlem Coşkun[1,5], Meriç Çalışkan Arslan[1,]

[1] Kalyon PV R&D Center, Ankara, Türkiye

[2] Department of Photonics Science and Engineering, Graduate School of Natural and Applied Sciences, Gazi University, Ankara, Türkiye

[3] Photonics Application and Research Center, Gazi University, Ankara, Türkiye

[4] Department of Photonics, Faculty of Applied Sciences, Gazi University, Ankara, Türkiye

[5] Micro and Nanotechnology Program, Middle East Technical University (METU), Ankara, Türkiye

* cezen@kalyonpv.com

Özet

Silisyum tabanlı fotovoltaik ve elektro-optik yapılarda yüzey reflektansı, aktif bölgeye ulaşan foton miktarını sınırlayan temel optik kayıp mekanizmalarından biridir. Hava ile yüksek kırılma indisli silisyum arasındaki optik uyumsuzluk nedeniyle oluşan Fresnel yansımalarının azaltılması, özellikle görünür (VIS) ve yakın kızılötesi (NIR) bölgede ışığın silisyum içerisine daha etkin iletilmesi ve foton yönetiminin iyileştirilmesi açısından önem taşımaktadır. Bu çalışmada, silisyum waferlarda yüzey morfolojisinin düzenlenmesi ve Al_2O_3 antireflektif kaplama uygulanmasının optik performans üzerindeki etkileri incelenmiştir. Parlatılmış (polished) Si waferlar referans olarak kullanılmış, ardından waferlara endüstriyel ıslak kimyasal proses hattında alkali bazlı tekstürleme işlemi uygulanmıştır. Numuneler yaklaşık 80 ± 2 °C'de NaOH esaslı çözeltide 460 s işleme tabi tutulmuş ve ardışık temizleme işlemleriyle kaplamaya hazırlanmıştır. Tekstürlenmiş Si yüzeyler, trimetilalüminyum (TMA) ve H_2O prekürsörleri kullanılarak yaklaşık 150 °C'de atomik tabaka biriktirme (ALD) yöntemiyle Al_2O_3 ile kaplanmıştır. Numune hazırlama ve kaplama süreci, ortam kaynaklı nem, oksijen ve diğer safsızlıkların etkisini en aza indirmek amacıyla kontrollü inert atmosfer sağlayan glovebox koşullarında gerçekleştirilmiştir. Film kalınlığının optik davranış üzerindeki etkisini değerlendirmek amacıyla farklı ALD döngü sayılarında kaplamalar gerçekleştirilmiş ve döngü sayısı 500'e kadar aşamalı artırılmıştır. Parlatılmış Si, tekstürlenmiş Si ve farklı Al_2O_3 kaplama koşullarına sahip tekstürlenmiş Si yapıların optik analizleri gerçekleştirilip dalga boyuna bağlı reflektans spektrumları karşılaştırmalı olarak değerlendirilmiştir.

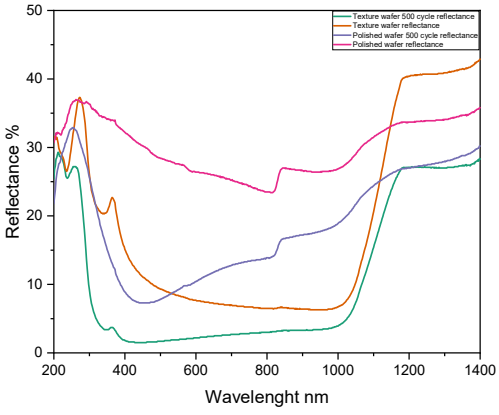

Şekil1: UV-VIS reflektans verileri

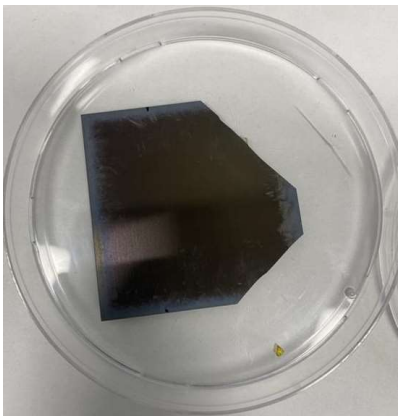

Şekil 2: ALD ile Al_2O_3 kaplanmış silisyum wafer

Anahtar Kelimeler: Silisyum, Al_2O_3, yüzey mühendisliği, ALD, antireflektif kaplama, reflektans, ışık yönetimi, UV degradasyonu

Referanslar

[1] Zhu, L. Q., Li, X., Yan, Z. H., Zhang, H. L., & Wan, Q. (2012). Dual Function of Antireflectance and Surface Passivation of Atomic-Layer-Deposited Films. *IEEE electron device letters*, *33*(12), 1753-1755.

[2] Marques, F. C., Urdanivia, J., & Chambouleyron, I. (1998). A simple technology to improve crystalline-silicon solar cell efficiency. Solar energy materials and solar cells, 52(3-4), 285-292.

Design Optimization of a Graphene-Enhanced Surface Plasmon Resonance Biosensor for Early Detection of Alzheimer's Disease

İsra Deniz Çandır[1,*], Şevval Koç[1]

[1] *Department of Engineering Physics, Faculty of Engineering, Ankara University, Ankara, Türkiye*

**Corresponding author, E-mail: denizcndir@gmail.com*

Özet / Abstract

Alzheimer's disease (AD) pathology initiates decades prior to clinical manifestation, where early monitoring of cerebrospinal fluid amyloid-beta 42 (Aβ_{1-42}) concentrations offers a crucial diagnostic window. Conventional diagnostic modalities such as PET imaging and lumbar puncture remain constrained by cost and invasiveness. Surface Plasmon Resonance (SPR) biosensors present a label-free, real-time, and high-resolution alternative; however, conventional thin-film gold (Au) substrates suffer from sub-optimal refractive index sensitivity and weak biomolecular adsorption via π–π stacking at ultra-low concentrations.

In this work, we propose a computational screening pipeline using the Transfer Matrix Method (TMM) to systematically optimize a graphene-enhanced SPR biosensor in a Kretschmann prism-coupling configuration (BK7 prism / 50 nm Au / N-layer graphene / analyte) at λ = 633 nm. Optical transfer matrix simulations reveal a non-monotonic sensitivity trend where bulk refractive index sensitivity initially increases with graphene layer addition due to evanescent field confinement and enhanced optical density (n = 3.0 + i1.149), but saturates and degrades around N = 8 due to optical absorption damping. By evaluating resonance dip depth (R_{min}) and Figure of Merit (FOM) alongside angular shift sensitivity, our findings identify the trade-off window required to design highly sensitive and resolved biosensors for ultra-low trace Aβ_{1-42} biomarker detection.

Keywords: Surface Plasmon Resonance (SPR), Graphene, Biosensor, Transfer Matrix Method (TMM), Alzheimer's Disease, Amyloid-beta (Aβ_{1-42}).

Acknowledgements: The authors thank Ankara University Department of Engineering Physics for academic and institutional support.

References:

[1] World Health Organization, Dementia Key Facts Sheet (2025).

[2] R. J. Bateman et al., Clinical and Biomarker Changes in Dominantly Inherited Alzheimer's Disease, N. Engl. J. Med. 367, 795–807 (2012).

[3] L. Wu, H. S. Chu, W. S. Koh, and E. P. Li, Highly sensitive graphene-on-gold surface plasmon resonance biosensors, Opt. Express 18, 14395–14400 (2010).

[4] S. J. Byrnes, Multilayer optical calculations, arXiv:1603.02720 (2016).

[5] E. Derin, Ö. Erdem et al., ACS Appl. Mater. Interfaces 17, 64808 (2025).

High-Dynamic-Range 2D LiDAR for Robust Detection of Surfaces with Different Reflectivity

Dr. Azad Ozan Korkan*[1], Ömer Faruk Günaydın[1, 2], Dr. Nurdan Baci[1], Ahmet Taşan[1], Enes Altay Nohutçuoğlu[1], Dr. İsa Kiyat*[1]

[1] TÜBİTAK BİLGEM, Barış Mah. Dr. Zeki Acar Cad. No:1, 41400 Gebze, Kocaeli, Türkiye

[2] Institute of Defence Technologies, Gebze Technical University, Gebze, Kocaeli, Türkiye

azad.korkan@tubitak.gov.tr ; isa.kiyat@tubitak.gov.tr

Abstract

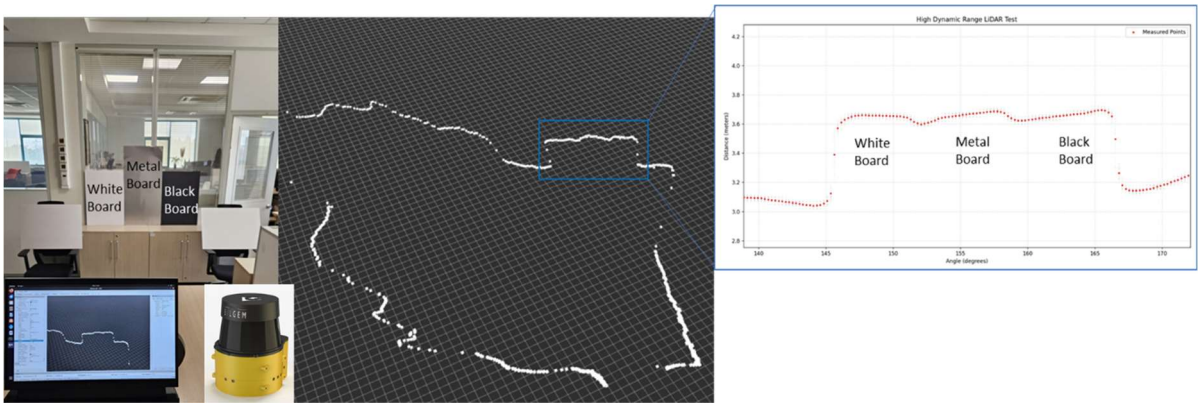

Figure 1: Three different surfaces are placed at the same distance to the 2D LiDAR. It detected each surface at their actual distance even all have highly different optical reflection coeficients.

This work presents the development of a high-dynamic-range (HDR) sensing approach for a 2D LiDAR system, with the main objective of improving measurement robustness when detecting surfaces with different optical properties. In practical environments, LiDAR sensors may encounter dark, metallic, retroreflective, and transparent objects during the operation. These surfaces can generate large variations in the intensity of the received optical signal [1]. In particular, metallic and retroreflective surfaces may produce very strong return signals that can saturate the receiver electronics, while dark or transparent surfaces may result in weak or complex reflections that are more difficult to detect. Therefore, achieving a sufficiently wide dynamic range of echo signal intensity is an important requirement for reliable LiDAR operation.

The LiDAR uses the time-of-flight (ToF) principle. To increase the dynamic range of the system, different methods for controlling the receiver sensitivity are investigated and implemented. These include adjustment of the dedector gain, signal attenuation, and adaptive control of the receiver according to the received signal strength. The main purpose is to prevent saturation for high-intensity optical returns while maintaining sufficient receiver sensitivity for weak signals. Another important aspect is the effect of received optical power on the accuracy of the measured distance. Changes in signal amplitude can introduce timing errors in the detection electronics and consequently affect the calculated ToF. For this reason, calibration and compensation methods are used to reduce amplitude-dependent ranging errors and provide more consistent distance measurements over the extended dynamic range.

The HDR approach aims to improve the overall robustness of the 2D LiDAR when operating in environments containing metallic, retroreflective, transparent, dark, and normally reflective surfaces. This is particularly suitable for industrial and autonomous applications, where objects with highly different reflectivities can be located close to each other. Our work demonstrates how optical receiver design and adaptive signal conditioning can be combined to extend the practical dynamic range and improve the reliability of LiDAR-based distance sensing.

Anahtar Kelimeler / Keywords: 2D LiDAR, High Dynamic Range (HDR), Time-of-Flight (ToF) measurements

Acknowledgements

This work has been done within Hiconnects Project funded by Chips JU program of Horizon Europe and TÜBİTAK.

Referanslar / References

[1] A. O. Korkan and H. Yuksel, "A 32-Channel, Low Resources and High-Precision FPGA Time-to-Digital Converter (TDC) Based on Dynamic Phase Shifting (DPS) for 3-D LiDAR Applications," in IEEE Transactions on Instrumentation and Measurement, vol. 75, pp. 1-14, 2026

Sparse Optical Acquisition for Spatial Spectral Reconstruction in Hyperspectral Microscopy

Edanur Çarbuğa[12], Faruk Aktaş[2], Tuğcan Korak[2], Merve Gülsen Bal Albayrak[2], Ahmet Aslan[1], Semih Yurtseven[1], Hümbet Nasibli[1]

[1]National Metrology Institute, The Scientific and Technological Research Council of Türkiye (TÜBİTAK- UME, Ulusal Metroloji Enstitüsü), PO 54, Gebze, Kocaeli, 41470, Türkiye)

[2]Faculty of Technology, Kocaeli University, İzmit, Kocaeli, 41001, Türkiye

humbet.nasibli@tubitak.gov.tr

Abstract

Hyperspectral microscopy integrates spatially resolved optical imaging with wavelength resolved spectral measurements, enabling characterization of wavelength dependent light matter interactions in biological samples. Variations in absorption, scattering, and reflectance across the spectrum generate characteristic spectral signatures that can improve discrimination of cellular and tissue structures beyond conventional intensity based microscopy. However, sequential raster based acquisition produces large hyperspectral data volumes and relatively long measurement times, which may restrict the spatial area that can be practically examined.

In this study, systematic and stratified random acquisition strategies were investigated to reduce the number of physically acquired hyperspectral measurements while preserving the wavelength dependent optical response, spatial information, and spectral fidelity required for reconstruction. A fixed prostate cancer cell line sample in a single Petri dish was first imaged using complete raster scanning to obtain a reference hyperspectral dataset. Without changing the sample position, partial datasets were subsequently acquired at five sampling ratios ranging from 20% to 60%, using systematic and stratified random sampling with three sampling seeds (42, 111, and 2026). Missing spatial spectral information was reconstructed using nearest neighbor and linear interpolation. The reconstructed hypercubes were compared with the full raster reference using PCA based spatial analysis and spectral similarity metrics, including spectral angle mapper (SAM), R^2, RMSE, spectral correlation, and Euclidean distance.

Across the evaluated sampling conditions, reconstructed datasets showed high agreement with the raster reference, with R^2 values of 0.91–0.95, spectral RMSE of 0.097–0.133, spectral correlation of 0.955–0.978, and mean SAM values of 4.25–6.24°. These results indicate that wavelength dependent spectral characteristics and spatial spectral structure can be successfully preserved after reconstruction over sampling ratios of 20–60%. The proposed framework therefore offers a promising approach for reducing optical acquisition burden while maintaining spectral integrity in biological hyperspectral microscopy.

Keywords: Hyperspectral microscopy; light matter interaction; optical spectroscopy; spectral reconstruction

Acknowledgements: This study was supported by the Health Institutes of Türkiye (TÜSEB) under Project No. 2026-A2 group 54886

References

[1] Nasibov, H. (2024). Evaluation of focus measures for hyperspectral imaging microscopy using principal component analysis. Journal of Imaging, 10(10), 240. https://doi.org/10.3390/jimaging10100240

[2] Holman, E. A., Fang, Y.-S., Chen, L., DeWeese, M., Holman, H.-Y. N., & Sternberg, P. W. (2020). Autonomous adaptive data acquisition for scanning hyperspectral imaging. Communications Biology, 3, 684. https://doi.org/10.1038/s42003-020-01385-3

[3] Zhu, M., Yi, W., Du, J., Zhu, S., Qi, J., Fu, M., Li, L., & Li, X. (2023). Push-broom compressive hyperspectral imaging method based on self-fusion refinement. Optics Communications, 530, 129198. https://doi.org/10.1016/j.optcom.2022.129198

[4] Takizawa, S., Hiramatsu, K., Lindley, M., Gala de Pablo, J., Ono, S., & Goda, K. (2023). High-speed hyperspectral imaging enabled by compressed sensing in time domain. Advanced Photonics Nexus, 2(2), 026008. https://doi.org/10.1117/1.APN.2.2.026008

[5] Hahn, J., Debes, C., Leigsnering, M., & Zoubir, A. M. (2014). Compressive sensing and adaptive direct sampling in hyperspectral imaging. Digital Signal Processing, 26, 113–126. https://doi.org/10.1016/j.dsp.2013.12.001

Modeling and Dosimetric Analysis of Cherenkov Radiation in Radiotherapy Using the Monte Carlo (GATE/Geant4) Method

Secher Sechoglou[1], Nasire Uluç[1,2]
[1]Middle East Technical University, Ankara, 06800, Çankaya, Türkiye
[2]Physics Group, Middle East Technical University, Northern Cyprus Campus, Kalkanli, Turkey
Nasire Uluç, E-mail: nassim.ulu@gmail.com

Abstract
Cherenkov imaging has emerged as a promising modality for real-time in vivo radiotherapy monitoring and dosimetric verification. Although previous studies have demonstrated correlations between absorbed dose and Cherenkov emission, quantitative interpretation of Cherenkov signals remains challenging because optical photon transport is strongly influenced by tissue composition and anatomical heterogeneity. Furthermore, experimental Cherenkov correction factors are currently available only for a limited number of treatment geometries, such as whole-breast irradiation, restricting broader clinical implementation. Here, we present a GATE/Geant4 Monte Carlo framework that incorporates tissue heterogeneity to systematically evaluate surface-detectable Cherenkov emission across clinically representative treatment geometries. The simulations show that tissue optical properties have a limited influence on Cherenkov photon generation, whereas optical transport strongly determines the signal reaching the tissue surface. Validation against published whole-breast irradiation measurements closely reproduced the experimentally reported Cherenkov-to-dose relationship for 6 MV photon beams (R^2 = 0.678 vs. 0.670). Following this benchmarking step, the framework was applied to extremity soft-tissue sarcoma and craniospinal irradiation, treatment geometries for which experimental Cherenkov calibration data are currently unavailable. These simulations show geometry-dependent Cherenkov behavior and the need for appropriate quantitative evaluation metrics across different irradiation configurations. Overall, the proposed framework links tissue heterogeneity, optical transport, and treatment geometry, providing a computational basis for extending quantitative Cherenkov dosimetry beyond experimentally calibrated radiotherapy configurations.

Keywords: Radiotherapy, Radiation dosimetry, Cherenkov Radiation, GATE/Geant4, Monte Carlo Simulations

Acknowledgements
The simulations presented in this work were carried out using the server infrastructure provided by Middle East Technical University (METU).

Referanslar / References
[1] Agostinelli, S., Allison, J., Amako, K., Apostolakis, J., Araujo, H., Arce, P., et al., 2003. Geant4—a simulation toolkit. Nuclear Instruments and Methods in Physics Research Section A 506, 250–303. doi:10.1016/S0168-9002(03)01368-8.
[2] Glaser, A., Zhang, R., Gladstone, D., Pogue, B., 2014. Optical dosimetry of radiotherapy beams using cherenkov radiation: the relationship between light emission and dose. Physics in Medicine and Biology 59, 3789–3811. doi:10. 1088/0031-9155/59/14/3789.
[3] Hachadorian, R., Bruza, P., Jermyn, M., Gladstone, D., Pogue, B., Jarvis, L., 2020. Imaging radiation dose in breast radiotherapy by x-ray ct calibration of cherenkov light. Nature Communications 11, 2298. doi:10.1038/ s41467-020-16031-z.
[4] Hachadorian, R., Bruza, P., Jermyn, M., Mazhar, A., Cuccia, D., Jarvis, L., Gladstone, D., Pogue, B., 2018. Correcting cherenkov light attenuation in tissue using spatial frequency domain imaging for quantitative surface dosimetry during whole breast radiation therapy. Journal of Biomedical Optics 24, 1–10. doi:10.1117/1.JBO.24.7.071609.
[5] Hachadorian, R., Farwell, J., Bruza, P., Jermyn, M., Gladstone, D., Pogue, B., Jarvis, L., 2021. Verification of field match lines in whole breast radiation therapy using cherenkov imaging. Medical Physics 48, 2392–2400.
[6] Jacques, S., 2013. Optical properties of biological tissues: a review. Physics in Medicine & Biology 58, R37–R61. doi:10.1088/0031-9155/58/11/R37.
[7] Zlateva, Y., Muir, B., El Naqa, I., Seuntjens, J., 2019. Cherenkov emission-based external radiotherapy dosimetry: I. formalism and feasibility. Medical Physics 46, 2370–2382. doi:10.1002/mp.13414.

Laboratory-Calibrated Spectral Modeling of a Long-Range BOTDR System

Volkan Türker*[1], Ali Emre Yılmaz[1], Rahmetullah Durgun[1], Fatih Özcan[1], Ekmel Özbay[1,2,3], İbrahim Özdür[4]

[1]*NANOTAM, Bilkent University, Ankara, Türkiye*

[2]*Department of Electrical and Electronics Engineering, Bilkent University, Ankara, Türkiye*

[3]*Physics, Bilkent University, Ankara, Türkiye*

[4]*Department of Electrical and Electronics Engineering, TOBB ETU, Ankara, Türkiye*

volkan.turker@bilkent.edu.tr

Brillouin optical time-domain reflectometry (BOTDR) enables long-range distributed temperature and strain sensing from a single fiber end [1]. For practical system design, however, the measurable range and the quality of the recovered Brillouin spectrum depend on the optical operating point, fiber losses, local discontinuities, and the confidence of the spectral fit. In this study, a laboratory-calibrated numerical spectral model was developed to reproduce the distance- and frequency-dependent response of a BOTDR setup comprising 75 km of G.655 fiber. The aim is to provide a model that can be compared directly with measured spectral maps and used for pre-experiment parameter selection and measurability estimation.

The model jointly accounts for the EDFA operating point, in-pulse power, round-trip fiber attenuation, the connection loss at 50 km, a Lorentzian Brillouin peak, a localized SBS pedestal, and the confidence criteria of the frequency-scanned receiver [2]. Validation was performed at an EDFA current of 60 mA with -19 dBm mean power at the fiber under test (FUT) input, 500 ns pulses, an 800 µs interrogation period, 1,000-frame averaging, polarization control enabled, and a 1 MHz frequency step. Laboratory and simulated data were evaluated on a common frequency-distance grid using identical criteria for Brillouin frequency shift (BFS), full width at half maximum (FWHM), Lorentzian-fit peak intensity, and reliable range. Results were rejected when the spectral-fit SNR was below 3 or the peak contrast was below 0.03 dB. With only a constant 17.659 dB reference offset, the 3D-map RMSE was 0.040 dB, while the BFS, FWHM, and intensity RMSE values were 1.61 MHz, 2.16 MHz, and 1.06 dB, respectively. The last reliable BFS positions were 59.84 km for the laboratory data and 65.41 km for the model.

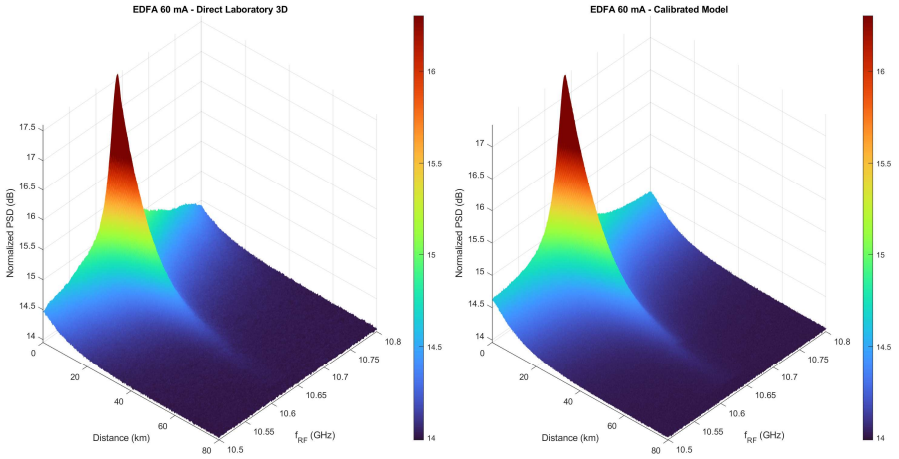

Figure 1: Direct laboratory and calibrated-model 3D Brillouin spectra at the 60 mA operating point.

In conclusion, the laboratory-calibrated model reproduces the measured spectral envelope particularly well over the 0-50 km region and yields comparable BFS, FWHM, and peak-intensity behavior under the validated operating condition. The difference in the last reliable BFS position, together with the change observed around the 50 km fiber transition, indicates that the connection region and distances beyond 60 km require additional direct measurements and calibration. Within the calibrated region, the model can therefore support pre-experiment operating-point selection, reliable-range estimation, and long-range BOTDR measurement planning without replacing experimental verification.

Keywords: BOTDR, Brillouin frequency shift, spectral modeling, distributed fiber sensing, long range

References

[1] X. Bao and L. Chen, "Recent Progress in Distributed Fiber Optic Sensors," Sensors 12, 8601-8639 (2012), doi:10.3390/s120708601.

[2] S. Jin, Z. Yang, X. Hong, and J. Wu, "Analytical Signal-to-Noise Ratio Model on Frequency-Scanned Brillouin Optical Time-Domain Reflectometry," J. Lightwave Technol. 42(16), 5786-5796 (2024).

Dolaşımlı Frekans Kaydırmalı İnterferometre ile DFB Lazer Akustik Sensörlerin Dinamik Demodülasyonu

Mehmet Ziya Keskin*[1], Abdulkadir Yentür [1], Furkan Durmuş[1],İbrahim Tuna Özdür[1]
[1]*Elektrik ve Elektronik Mühendisliği, TOBB Ekonomi ve Teknoloji Üniversitesi, Ankara, Türkiye*
*corresponding author, E-mail: mehmetziya.keskin@etu.edu.tr

Özet

Dağıtık geri beslemeli (DFB) fiber lazerler; elektromanyetik girişim bağışıklığı, yüksek hassasiyetleri ve noktasal algılama kabiliyetleri sayesinde su altı akustik algılama sistemlerinde kritik bir rol oynamaktadır. Harici akustik basınç alanı, fiber çekirdeğindeki foto-elastik etki ve boyutsal gerinim mekanizmaları üzerinden lazerin optik ışıma frekansını modüle eder. Ancak bu frekans sapmalarının tespiti; lazerin içsel $1/f$ faz gürültüsü, çevresel kaynaklı kuadratür sürüklenmeleri ve geleneksel taşıyıcı üretim (PGC) tekniklerinin gerektirdiği yüksek frekanslı aktif modülasyon donanımı karmaşıklığı nedeniyle kısıtlanmaktadır. Bu çalışmada, tek bir 40 MHz akusto-optik modülatör (AOM) ve optik gecikme hattı ($\tau \approx 245$ ns) içeren Dolaşımlı Frekans Kaydırmalı (Recirculating Frequency Shifting) interferometre mimarisi ile pasif çok taşıyıcılı bir sorgulama yaklaşımı sunulmaktadır. Önerilen mimari, optik dolaşım yoluyla 40 MHz temel ve 80 MHz ikinci harmonik taşıyıcılarını ek bir RF sentezleyici gerekmeksizin pasif olarak üretir. Sistemin transfer fonksiyonunun sağladığı ortak mod gürültü bastırma mekanizması, aktif kuadratür stabilizasyon ihtiyacını ortadan kaldırmaktadır. 500 MSPS örnekleme hızında çalışan sayısal I/Q demodülasyon algoritması ve istatistiksel çeşitlilik birleştirme (diversity combining) tekniği ile yüksek frekanslı ilintisiz elektronik gürültü bastırılmış; 1 kHz frekansında 24 μrad/$\sqrt{\text{Hz}}$ faz gürültüsü tabanı elde edilmiştir. Bu değer, $\sim$ 15 Hz/$\sqrt{\text{Hz}}$ eşdeğer frekans gürültüsü seviyesine karşılık gelerek DFB kavitesinin termal tabanına yaklaşmaktadır. Çoklu harmonik yapısı sayesinde donanımsal değişiklik gerektirmeksizin 1 kHz'de $\sim$ 147 dB dinamik aralık elde edilmiş olup, akustik alan seviyesine göre yazılımsal olarak ölçeklenebilen donanım-verimli bir sorgulama çözümü sağlanmıştır.

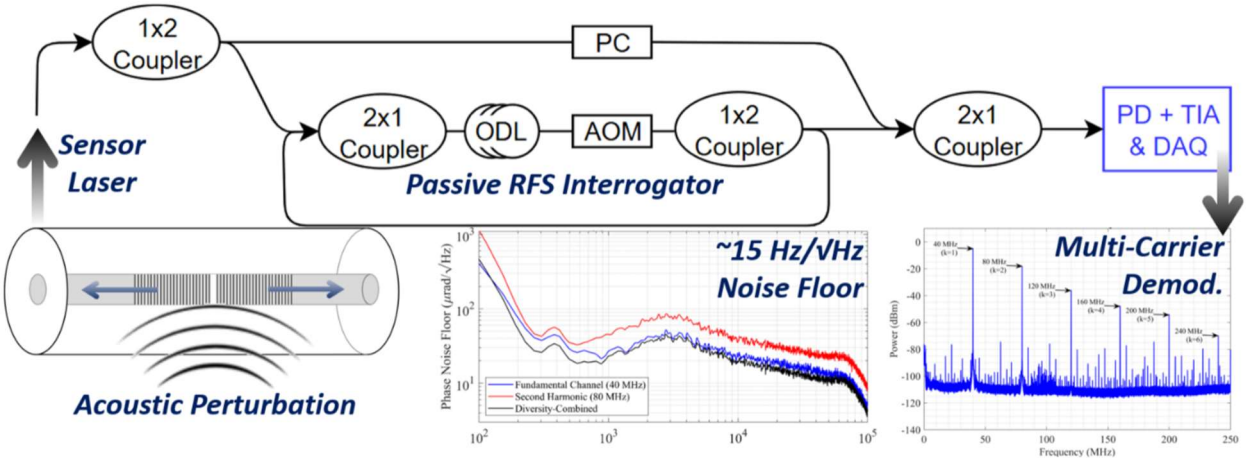

Şekil 1: π faz kaymalı DFB fiber lazer akustik sensörün dolaşımlı frekans kaydırmalı (RFS) interferometrik sorgulama mimarisi: Akustik pertürbasyon altındaki sensör çıkışının tek bir AOM (40 MHz) ve optik gecikme hattı (ODL) içeren pasif RFS döngüsüyle çok taşıyıcılı RF tarağına dönüştürülmesi, eşzamanlı demodülasyonu ve birleştirme yöntemiyle 1 kHz'de elde edilen $\sim$ 15 Hz/$\sqrt{\text{Hz}}$ (24 μrad/$\sqrt{\text{Hz}}$) eşdeğer frekans gürültü tabanı analizi (PC: Polarizasyon Kontrolcüsü, PD-TIA: Fotodedektör ve Trans-Empedans Yükseltici, DAQ: Veri Toplama Birimi).

Anahtar Kelimeler: Akustik algılama; DFB fiber lazerler; frekans kaydırmalı interferometri; çok taşıyıcılı demodülasyon; pasif optik sorgulayıcı; faz gürültüsü analizi.

Referanslar

[1] C. K. Kirkendall and A. Dandridge, "Overview of high performance fibre-optic sensing," J. Phys. D: Appl. Phys., vol. 37, no. 18, pp. R197–R216, 2004, doi: 10.1088/0022-3727/37/18/r01.

[2] G. A. Cranch, G. M. H. Flockhart, and C. K. Kirkendall, "Distributed feedback fiber laser strain sensors," IEEE Sensors J., vol. 8, no. 7, pp. 1161–1172, 2008, doi: 10.1109/JSEN.2008.926876

[3] V. Billault et al., "Coherent optical fiber sensing based on a frequency shifting loop," J. Lightw. Technol., vol. 39, no. 12, pp. 4118–4124, 2021, doi: 10.1109/JLT.2021.3060105.

Optical Design of a Common-Aperture Dual Band SWIR/LWIR Seeker System

İrem Buket Aydın[1], Devrim Anıl[2], Barış Kınacı[3]

[1]Gazi University, Photonics Science and Engineering, Graduate School of Natural and Applied Sciences, Gazi University, 06560 Ankara, Türkiye*

[2]ASELSAN, Microelectronics & Electro-Optics Systems, Ankara, Türkiye, 06750

[3]Gazi University, Faculty of Applied Sciences, Department of Photonics, Gazi University, 06560 Ankara

*İrem Buket Aydın, E-mail: irembuketaydn@yandex.com

Abstract

Multi-band electro-optical imaging is becoming a standard requirement in guided munitions and seeker systems, where target detection and tracking must be maintained across changing atmospheric conditions, operational ranges, and countermeasure environments. Pairing short-wave infrared (SWIR) and long-wave infrared (LWIR) bands within a single seeker head leverages the distinct advantages of each spectral region: SWIR provides superior resolution and enhanced transmission through haze, while LWIR delivers consistent thermal contrast independent of ambient illumination. Furthermore, combining these bands into a single system eliminates the increased volume and mechanical complexity associated with separate optical trains.

This study presents a comprehensive optical design for a dual-band SWIR/LWIR seeker, developed in Zemax OpticStudio. The architecture utilizes a common-aperture, two-mirror Cassegrain-type front group shared by both spectral bands. Subsequently, coordinate breaks and fold mirrors divide the optical path into two independent imaging channels. The SWIR channel consists of a refractive relay constructed from crown and flint glass elements, optimized to align the field of view and image quality with the SWIR detector's pixel pitch. The LWIR channel incorporates ZnSe, germanium, and a diffractive binary surface for athermalization, tailored to an uncooled microbolometer. Both channels are integrated within a compact, shared track length suitable for a constrained seeker envelope.

Performance evaluations, including ray fan, spot diagram, and vignetting analyses, demonstrate that image quality is consistent with the pixel pitch of both detectors across the entire field of view. Vignetting remains highly controlled with no abrupt field cutoff. The finalized design confirms that a shared-aperture, dual-band configuration successfully meets the stringent compactness, field of view, and image quality requirements of next-generation seeker payloads.

Keywords: Common-Aperture Architecture, Catadioptric Optical Design, Zemax OpticStudio Simulation, Dual-Band Seeker, Multi-Spectral Optical Path, SWIR and LWIR, Electro-Optical Imaging

Referanslar / References

[1] Y. Jiang, Q. Xie, E. Qu, et al., "Athermal design of refractive/diffractive hybrid infrared optical system with large relative aperture," in 9th International Symposium on Advanced Optical Manufacturing and Testing Technologies: Micro- and Nano-Optics, Catenary Optics, and Subwavelength Electromagnetics, vol. 10840, SPIE, Jan. 2019, Art. no. 1084018, doi: 10.1117/12.2504864.

[2] M. J. Riedl, Optical Design Fundamentals for Infrared Systems. Washington: SPIE Press, 2001.

Aerosol Jet Printing of Silver-Based Electrodes on Commercial Wound Dressing Substrates

Elif Dilara Güler[1], Nehir Ece Alkan[1], Berkay Şahin[2,3], Berk Serbest[1,2,3], Nihan Akın Sönmez[1,2,3]

[1] Gazi Univ., Fac. of Applied Sci., Dept. of Photonics, 06560 Ankara, Türkiye
[2] Gazi Univ., Grad. Sch. of Nat. & Appl. Sci, Dept. of Photonic Sci. & Eng., 06560 Ankara, Türkiye
[3] Gazi Univ., Photonics App. & Res. Center, 06560 Ankara, Türkiye
***Emails**: edg1969elif@gmail.com (E.D.G.); nehirecealkan05@gmail.com (N.E.A.)*

Abstract

Flexible conductive electrodes are important components of wearable and biophotonic sensor platforms. Printing methods have been increasingly used to integrate conductive and sensing elements into flexible wound-monitoring systems [1]. However, commercial wound dressing materials have different surface, optical, and thermal properties, which can affect printing quality and the electrical performance of printed electrodes. Therefore, the compatibility between conductive inks and wound dressing substrates is important for developing printed smart wound dressing systems.

In this study, silver-based electrodes were printed by Aerosol Jet Printing (AJP) on four commercially available wound dressing substrates, and their printing, optical, and electrical properties were investigated. Silver nanowire (AgNW) ink was first used because of its potential for flexible and transparent electrodes [2]. The optical transmittance of the substrates was measured using UV-Vis spectroscopy before and after printing. AgNW interdigital electrodes were printed using three consecutive passes under the same conditions. The printed patterns were examined by optical microscopy, and electrical measurements were performed. The effect of thermal treatment on the substrates was also investigated. The AgNW-printed electrodes showed no measurable electrical conduction under the investigated conditions. Optical microscopy showed spreading of the AgNW ink on the wound dressing surfaces, resulting in poorly defined and non-uniform electrode patterns. Thermal treatment was applied to improve electrical connectivity, but the thermal sensitivity of the wound dressing materials caused structural degradation at higher temperatures.

Therefore, silver nanoparticle (AgNP) ink was tested as an alternative conductive material. Compared with AgNW ink, AgNP ink produced more uniform and well-defined electrode patterns. After thermal treatment, measurable electrical conduction was obtained from AgNP electrodes printed on two of the four wound dressing substrates. These results showed that both the conductive ink and substrate properties are important for obtaining functional printed electrodes.

Overall, this study provides a preliminary evaluation of conductive ink-substrate compatibility for AJP on commercial wound dressing materials. The results will be used to select a suitable ink-substrate combination for further development of a ZnO-based UV-responsive sensor for smart wound dressing applications.

Keywords: Silver-based ink, Aerosol Jet Printing, wound dressing, flexible electrode, optical transmittance

Acknowledgments: This work was supported by TÜBİTAK (2209-A, Project No: 1919B012517019) and the Presidency of Strategy and Budget of Türkiye (CB-SBB-2019K12-149045). Support from the Photonics Application and Research Center is also gratefully acknowledged.

References:

[1] Farooqui, M., & Shamim, A. (2016). *Low Cost Inkjet Printed Smart Bandage for Wireless Monitoring of Chronic Wounds*. Scientific Reports, 6, 28949.
[2] Serbest, B., Kara, S. G., Alpay, R., Ataşer, T., Kınacı, B., Akın Sönmez, N., & Özçelik, S. (2025). *Aerosol jet printing of flexible transparent conductive silver nanowire electrodes: effects of printing cycles.* Journal of Electronic Materials, 54(2), 1245–1253.

Silver Nanowire Filter Foil SERS Sensors

Ghazanfar Ali Khan[1], Onuralp Cakir[2], Özge Demirtaş[3], Selen Yüksel[1], Valentina Masciotti[4], Doga Doganay[2], Sahin Coskun[5], Sinan Genç[6], Marco Lazzarino[4], Husnu Emrah Unalan[2], Alpan Bek[2]*

[1]Department of Physics, METU, Ankara, 06800, Türkiye
[2]Department of Metallurgical and Materials Engineering, METU, Ankara, 06800, Türkiye
[3]Department of Physical Chemistry II, University of Duisburg-Essen, Essen, 45141, Germany
[4]CNR-IOM Istituto Officina dei Materiali-Consiglio Nazionale delle Ricerche c/Area Scinece Park, Basovizza, Trieste, I-34149, Italy
[5]Department of Metallurgical and Materials Engineering, Eskisehir Osmangazi University, Eskisehir, 26040, Türkiye
[6]Department of Electrical Electronics Engineering, Abdullah Gül University, 38080, Kayseri, Türkiye
corresponding author's E-mail: bek@metu.edu.tr

Abstract

The risks posed by pathogens are of extreme importance due to their potential for catastrophic consequences evidenced by lose of millions of lives and economic losses amounting to trillions of dollars.[1] Despite the pressing need for efficient pathogen detection, conventional identification methods remain labor intensive, time consuming, and incapable of on-site based analysis.[2,3] For that reason, free-standing filter foil (FF) made from silver nanowires (AgNWs) using a simple and scalable vacuum filtration method is developed as a high performance surface enhanced Raman scattering (SERS) active platform for the fast and accurate identification of waterborne pathogens. The fast and scalable fabrication process enables a mechanically robust, free-standing AgNW filter foil (AgNW-FF) with tunable thickness, featuring a three-dimensional (3D) ultrafine AgNW network with nanoscale gaps smaller than most target pathogens. The FFs exhibit an analytical enhancement factor (EF) of 4.5×10^8. The FFs supports the SERS detection for both Gram-negative and Gram-positive bacteria, i.e., *Escherichia coli* and *Staphylococcus aureus* respectively. A microfluidic SERS sensor is derived from the FF. The microfluidic SERS sensor enables the simultaneous collection and SERS detection of Gram-positive bacterium *Staphylococcus epidermidis*.

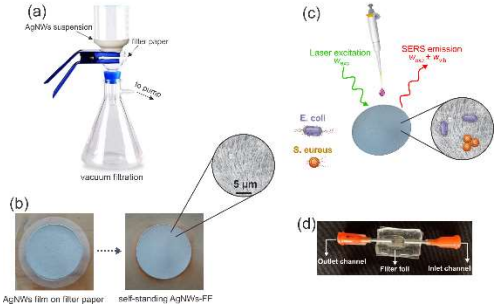

Figure 1: (a) Schematic illustration of the fabrication of the free-standing AgNW-FF through vacuum filtration; (b) photographs of 47 mm diameter AgNWs film on filter paper and AgNW-FF with a corresponding top-view SEM image; (c) schematic illustration of SERS measurements of pathogens using AgNW-FF; (d) digital photograph of the AgNW-FF SERS sensor

Keywords: silver nanowires, vacuum filtration, free-standing silver nanowires filter foil, surface enhanced Raman scattering, pathogens

Acknowledgements

The authors thanks Prof. Ahmet Oral for the Raman spectrometer system. This work was supported by The Scientific and Technological Research Council of Türkiye (TÜBİTAK, Grant Numbers 119N413 and 121N708).

References

1. C.Y. Lee, I. Degani, J. Cheong, R. Weissleder, J.-H. Lee, J. Cheon, H. Lee, Development of integrated systems for on-site infection detection, Acc. Chem. Res. 54 (2021) 3991–4000.
2. P. Rajapaksha, A. Elbourne, S. Gangadoo, R. Brown, D. Cozzolino, J. Chapman, A review of methods for the detection of pathogenic microorganisms, Analyst 144 (2019) 396–411.
3. L. Settanni, A. Corsetti, The use of multiplex PCR to detect and differentiate food-and beverage-associated microorganisms: a review, J. Microbiol. Methods 69 (2007) 1–22.

Low-Cost, Scalable, and Ultrasensitive Flexible SERS Substrates

Ghazanfar Ali Khan[1], Batuhan Balkan[1], Alpan Bek[1]*
[1]Department of Physics, METU, Ankara, 06800, Türkiye
corresponding author's E-mail: bek@metu.edu.tr

Abstract
Evaporation-induced deposition of nanoparticles (NPs) from suspension directly onto pristine filter paper is challenging,[1,2] yet achieving it will lead to a uniform, flexible, reproducible, cost-effective, scalable, and ultrasensitive surface enhanced Raman scattering (SERS) platform suitable for routine SERS analysis. We propose the deposition of silver (Ag) NPs onto the filter paper by a novel double-sided tape assisted evaporation-induced deposition strategy. The method involves affixing a piece of filter paper onto commonly available double-sided tape. The tape securely holds the filter paper and also confines the NPs suspension, preventing it from leaking out during gradual evaporation. The slow evaporation, alongside with electrostatic attraction between Ag NPs and filter paper and the paper's microstructure, induces the uniform deposition of Ag NPs on the filter paper. Feasibility of our platform for swab based sampling is especially appealing in facilitating SERS based detection of pesticides,[3] dye pollutants,[4] and explosives.[5] Our method of Ag NPs deposition on filter paper is simple, cost-effective, scalable, highly sensitivity, reproducible, and stable.

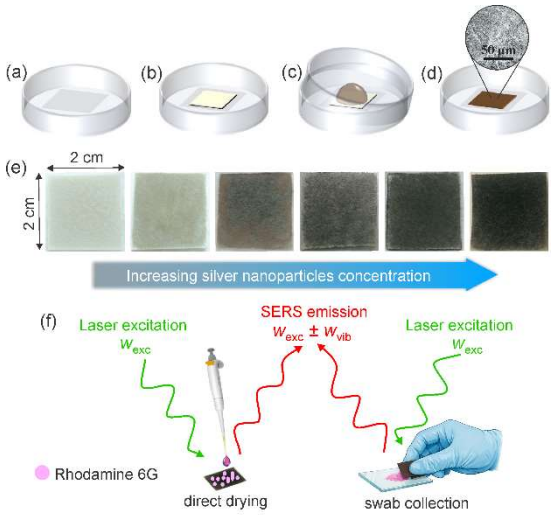

Figure 1: Schematic illustration of the stepwise procedure for the uniform deposition of Ag NPs onto filter paper. (a) Attachment of double-sided tape to a petri dish; (b) placement of the filter paper onto the tape; (c) drop-casting of Ag NPs solution onto the filter paper and evaporation; (d) formation of a uniformly distributed Ag NPs on filter paper resulting from gradual solvent evaporation and NPs sedimentation; (e) photographs images of SERS substrates with 2 × 2 cm dimensions obtained after NPs deposition at different concentrations on filter paper; (f) schematic illustration of SERS measurements on substrates through direct drying and swab collection methods

Keywords: silver nanoparticles; double tape assisted slow evaporation; flexible substrates; surface-enhanced Raman scattering; swab-based SERS sensor

Acknowledgements
The authors thanks Prof. Ahmet Oral for the Raman spectrometer system. This work was supported by The Scientific and Technological Research Council of Türkiye (TÜBİTAK, Grant Numbers 119N413 and 121N708).

References
1. A. Batool, G.A. Khan, W. Ahmed, Seed-mediated growth of highly concentrated silver nanoparticles on a flexible substrate for applications in SERS-based trace detection, Vib. Spectrosc. 123 (2022) 103438.
2. S. He, J. Chua, E.K.M. Tan, J.C.Y. Kah, Optimizing the SERS enhancement of a facile gold nanostar immobilized paper-based SERS substrate, RSC Adv. 7 (2017) 16264–16272.
3. M. Lee, K. Oh, H.-K. Choi, S.G. Lee, H.J. Youn, H.L. Lee, D.H. Jeong, Subnanomolar sensitivity of filter paper-based SERS sensor for pesticide detection by hydrophobicity change of paper surface, ACS Sensors 3 (2018) 151–159.
4. G.A. Khan, F. Anjum, M.A. Ghanem, W. Ahmed, Enhanced SERS Detection of Toxic Dyes Using Gold–Silver Core-Shell Nanoparticles, ChemistrySelect 10 (2025) e05303.
5. G.A. Khan, Ö. Demirtaş, A.K. Demir, Ö. Aytekin, A. Bek, A.S. Bhatti, W. Ahmed, Fabrication of flexible, cost-effective, and scalable silver substrates for efficient surface enhanced Raman spectroscopy based trace detection, Colloids Surfaces. A, Physicochem. Eng. Asp. 619 (2021).

Etched Nanoworms for Sensitive SERS Detection of Acrylamide

Ghazanfar Ali Khan[1], Alpan Bek[1*]
[1]Department of Physics, METU, Ankara, 06800, Türkiye
corresponding author's E-mail: bek@metu.edu.tr

Abstract
Nanomaterials with high concentration of surface defects such as necks, kinks, or bends, are excellent hot-spots for surface-enhanced Raman scattering (SERS).[1] These defects are abundant in smaller one dimensional wavy nanoparticles (NPs).[2] However, they typically can smoothen out within the larger particles, attenuating their SERS activity. At the same time deliberately arresting growth at the ideal stage to possess these defects for optimal SERS activity poses a formidable challenge.[2] Herein, we report an alternative approach that involves the oxidative etching of polycrystalline Au-Ag nanoworms (NWs) which generates high-surface area rich in defects, thereby significantly enhancing their SERS activity. The structural changes were thoroughly characterized and correlated with the enhancement in SERS activity. Under optimized conditions, the etched NWs allowed the detection of acrylamide, a hazardous and toxic compound found in processed food. Remarkably, the etched NWs exhibit excellent detection sensitivity towards acrylamide and achieved a detection limit of 1 ppb concentration.

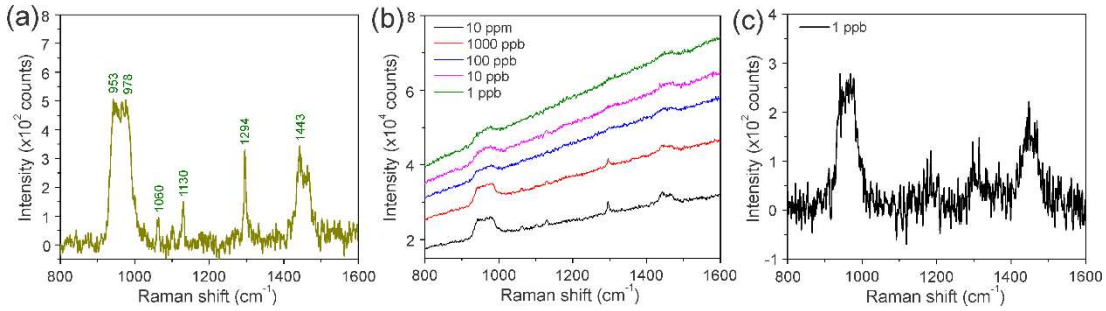

Figure 1: (a) SERS spectrum of acrylamide using etched NWs; (b) SERS spectra of acrylamide at varying concentrations acquired using the etched NWs; (c) SERS spectrum of acrylamide acquired at a concentration of 1 ppb using etched NWs.

Keywords: nanoworms; surface defects; etched nanoworms; surface-enhanced Raman scattering; acrylamide

Acknowledgements
The authors thanks Prof. Ahmet Oral for the Raman spectrometer system. This work was supported by The Scientific and Technological Research Council of Türkiye (TÜBİTAK, Grant Numbers 119N413 and 121N708).

References
1. H.I. Khan, G.A. Khan, S. Mehmood, A.D. Khan, W. Ahmed, Gold nanoworms: Optical properties and simultaneous SERS and fluorescence enhancement, Spectrochim. Acta - Part A Mol. Biomol. Spectrosc. 220 (2019). https://doi.org/10.1016/j.saa.2019.05.016.
2. X. Huang, Z. Zhao, Y. Chen, C.-Y. Chiu, L. Ruan, Y. Liu, M. Li, X. Duan, Y. Huang, High Density Catalytic Hot Spots in Ultrafine Wavy Nanowires , Nano Lett. 14 (2014) 3887–3894. https://doi.org/10.1021/nl501137a.

Surfactant-Free Percolated Silver Nanostructures on Filter Paper for SERS Applications

Ghazanfar Ali Khan[1], Alpan Bek[1]*
[1]Department of Physics, METU, Ankara, 06800, Türkiye
corresponding author's E-mail: bek@metu.edu.tr

Abstract
Hollow noble metal nanostructures have drawn significant attention due to their remarkable potential across various applications.[1] Although typically synthesized in solution, many applications require them onto substrates.[1] Of particular intrigue is the innovative fabrication of these nanostructures directly on filter paper. Filter paper has been utilized as a versatile substrate due to its natural porosity, low-cost, flexibility, biocompatibility, and biodegradability. The porous, oxygen-rich cellulose fibers aid in the rapid concentration of target analytes, thereby improving the efficiency of sample collection on the substrate, especially important for SERS.[2,3] So far numerous techniques have been employed to directly grow nanostructures on filter paper which include drop casting, chemical reduction approach, immersion deposition, thermal deposition, and inkjet printing.[4] However, all these methodologies are primarily focused on the growth of solid nanostructures on the filter paper. We propose a simple, fast, cost-effective method of the surfactant-free synthesis of percolated silver nanostructures directly on filter paper. In particular, the fabricated substrates possess ultrasensitive surface enhanced Raman scattering (SERS) properties.

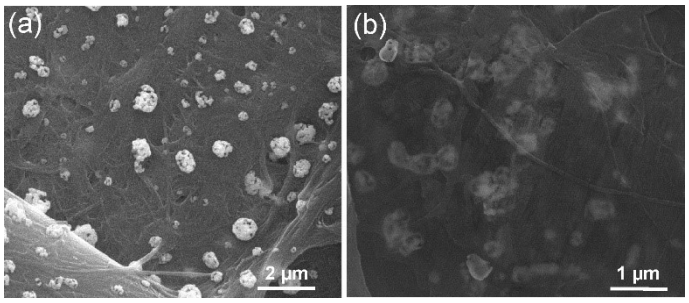

Figure 1: SEM images of percolated silver nanoparticles both (a) on the surface; and (b) inside the filter paper.

Keywords: percolated nanostructures; filter paper, surface-enhanced Raman scattering; flexible SERS substrates, trace level SERS identification

Acknowledgements
The authors thanks Prof. Ahmet Oral for the Raman spectrometer system. This work was supported by The Scientific and Technological Research Council of Türkiye (TÜBİTAK, Grant Numbers 119N413 and 121N708).

References
1] X. Wang, J.I. Feng, Y. Bai, Q. Zhang, Y. Yin, Synthesis, properties, and applications of hollow micro-/nanostructures, Chem. Rev. 116 (2016) 10983–11060.
[2] G.A. Khan, Ö. Demirtaş, A.K. Demir, Ö. Aytekin, A. Bek, A.S. Bhatti, W. Ahmed, Fabrication of flexible, cost-effective, and scalable silver substrates for efficient surface enhanced Raman spectroscopy based trace detection , Colloids Surfaces. A, Physicochem. Eng. Asp. 619 (2021). https://doi.org/10.1016/j.colsurfa.2021.126542.
[3] G.A. Khan, O.Ö. Demirtaş, A. Bek, A.S. Bhatti, W. Ahmed, Facile fabrication of Au-Ag alloy nanoparticles on filter paper: Application in SERS based swab detection and multiplexing, Vib. Spectrosc. (2022) 103359. https://doi.org/https://doi.org/10.1016/j.vibspec.2022.103359.
[4] A. Vicente, A. Araújo, M.J. Mendes, D. Nunes, M.J. Oliveira, O. Sanchez-Sobrado, M.P. Ferreira, H. Águas, E. Fortunato, R. Martins, Multifunctional cellulose-paper for light harvesting and smart sensing applications , J. Mater. Chem. C, Mater. Opt. Electron. Devices 6 (2018) 3143–3181. https://doi.org/10.1039/c7tc05271e.

Investigation of Optical Beam Splitter and RF Shielding Properties of ZnO/Ag/ZnO Structure

Oğuzhan Özdoğru*[1], Akın Bacıoğlu[1]
[1]*Department of Physics Engineering, Hacettepe University, Ankara, Türkiye*
corresponding author, E-mail: oguzhanozdogru@hacettepe.edu.tr

Abstract

Interaction of canopy, windows and optical elements, such as lenses, beam splitters and polarizers of electro-optic systems, where are used in aeronautics with electromagnetic waves, has become a critical design parameter. In TCO/metal/TCO or dielectric/metal/dielectric (DMD) multi layered structures, transparency of metal oxides used in top and bottom layers is combined with high electrical conductivity of metal ultra thin films [1]. Silver (Ag) ultra thin films are critical in transparent electromagnetic interference (EMI) shielding windows and optoelectronic applications thanks to their high electrical and thermal conductivity [2].

In this work, optical trasmittance of ZnO(30nm)/Ag(1nm)/ZnO(30nm) and Ag(1nm)/ZnO(30nm) structures on glass substrate produced by thermal evaporation system resulted in %45(±2) and %60(±2), respectively between 500-1100 nm (Figure 1). In this range, the structures are candidates for optical beam splitters thanks to having constant optical transmittance. Two different ZnO/Ag/ZnO structures having 2 nm and 10 nm silver layers are produced on 4 x 4 inches Corning 1737F glass substrate. ZnO/Ag10/ZnO structure showed reflective properties in visible region and ZnO/Ag2/ZnO has an %18(±1) optical transmittance between 700-1100 nm (Figure 2). The optical transmittance experienced a significant reduction as the thicknesses of bottom ZnO layer decreased and the thickness of silver layer increased.

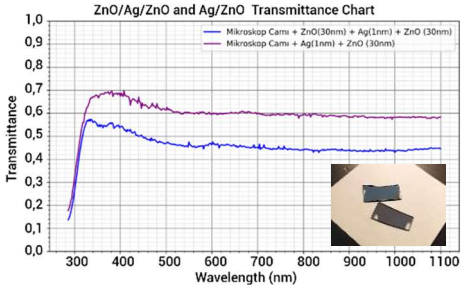

Figure 1: Optical transmittance and picture of ZnO/Ag/ZnO and Ag/ZnO samples

Transmitted microwave amplitude has measured as voltage by using horn antenna and receiver operating at 10 GHz (X-Band) wavelength. ZnO/Ag/ZnO structures on Corning glass have diminished transmitted microwave amplitude to %0,2 (±0,1) of Corning glass itself as shown in Figure 2. A standing wave pattern isn't obtained with ZnO/Ag/ZnO structure, on the contrary of Corning glass, thanks to the destructive interference of coating. ZnO/Ag10/ZnO structure, reflective in visible region, and ZnO/Ag2/ZnO having optical transmittance, exhibit the same RF shielding performance, which is promising for optoelectronic applications requiring optical transmittance without reducing RF shielding performance. Consequently ZnO/Ag/ZnO structure has been offering RF shielding properties by decreasing the microwave transmittance of Corning glass sample to %0,2, besides its beam splitter properties.

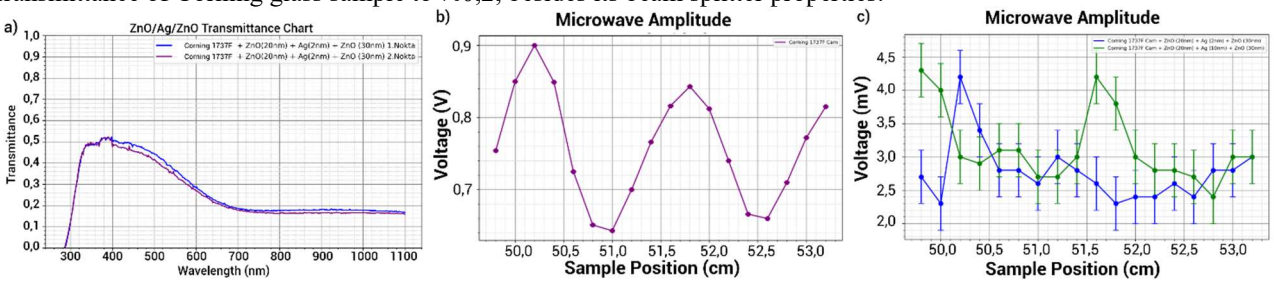

Figure 2: a) Optical transmittance of ZnO/Ag/ZnO structure on Corning substrate, b) Microwave transmittance of Corning 1737F glass, c) Microwave transmittance of ZnO/Ag/ZnO structures on Corning 1737F glass substrate

Keywords: Optical Beam Splitter, EMI Shielding, Thermal Vapor Deposition
Acknowledgements
This work was supported by TÜBİTAK 2209-A program under project number 1919B012454348.

References

[1] Raaif, M., El-Hossary, F.M., El-Moula, A.A.A. et al. A comparative study of the optical, electrical, and wettability properties of amorphous and nanocrystalline ITO/Cu/ITO multilayer thin films prepared by DC pulsed magnetron sputtering. Appl. Phys. A 131, 603 (2025). https://doi.org/10.1007/s00339-025-08717-2
[2] Wang, D., Qu, Z., Wang, Y., Liu, J., & Wang, Q. (2022). Effects of Al-doping concentration on the structure and electromagnetic shielding properties of transparent Ag thin films. Optical Materials, 113353. https://doi.org/10.1016/j.optmat.2022.113353

SDR Tabanlı Adaptif Modülasyonlu Optik Haberleşme Sistemi

Beyhan Özer*[1], Rabia Edeviyye Dağdeviren[1], Burak Şişman[1], Murat Can Karakoç[2]
[1] *Elektrik-Elektronik Mühendisliği, Erzurum Teknik Üniversitesi, Erzurum, Türkiye*
[2] *Elektrik-Elektronik Mühendisliği, Ankara Yıldırım Beyazıt Üniversitesi, Ankara, Türkiye*
corresponding author: Beyhan Özer, E-mail: beyhan.ozer39@erzurum.edu.tr

Özet / Abstract

Işık kullanarak kablosuz veri ileten ve değişen ortam koşullarına göre haberleşme yöntemini otomatik olarak uyarlayan yazılım tanımlı radyo (software-defined radio, SDR) tabanlı bir optik haberleşme sistemi geliştirilmesi amaçlanmaktadır. Verici tarafta bilgisayar ortamında oluşturulan dijital veri, SDR yardımıyla BPSK, QPSK veya 16-QAM modülasyonlarından biri kullanılarak işlenecek; elde edilen sinyal uygun sürücü devresi üzerinden bir LED veya lazer kaynağının ışık şiddetine aktarılacaktır. Karşı tarafta fotodiyot, ışık şiddetindeki değişimleri elektriksel sinyale dönüştürecek ve alınan veri SDR üzerinden çözülecektir **[1]**. Çalışmanın temel özelliği, sistemin kanal kalitesini SNR ve BER gibi performans ölçütleriyle değerlendirmesi ve uygun modülasyon türünü otomatik olarak seçmesidir **[2]**. Kanal koşulları iyi olduğunda daha yüksek veri hızı sağlayan 16-QAM, orta seviyede QPSK, sinyal kalitesinin düştüğü durumlarda ise daha dayanıklı olan BPSK kullanılacaktır. Deneysel çalışmalarda verici ile alıcı arasındaki mesafe, açı, ortam ışığı ve optik hattaki engeller değiştirilerek sistemin davranışı incelenecektir. Son aşamada adaptif modülasyon kullanan sistem ile sabit modülasyon kullanan sistem; BER, SNR, veri hızı ve bağlantı sürekliliği açısından karşılaştırılacaktır. Böylece SDR'nin yazılımsal esnekliği ile optik haberleşmenin avantajları birleştirilerek değişken kanal koşullarına otomatik uyum sağlayabilen, güvenilir ve verimli bir haberleşme yapısının ortaya konması hedeflenmektedir.

Anahtar Kelimeler / Keywords: SDR, görünür ışık haberleşmesi, adaptif modülasyon, BPSK, QPSK, 16-QAM, SNR, BER.

Referanslar / References

[1] R. Martinek, L. Danys, and R. Jaros, "Visible Light Communication System Based on Software Defined Radio: Performance Study of Intelligent Transportation and Indoor Applications," *Electronics*, vol. 8, no. 4, Art. no. 433, 2019, doi: 10.3390/electronics8040433.
[2] A. Costanzo, V. Loscri, and M. Biagi, "Adaptive Modulation Control for Visible Light Communication Systems," *Journal of Lightwave Technology*, vol. 39, no. 9, pp. 2780–2789, 2021, doi: 10.1109/JLT.2021.3056177.

Perovskit Güneş Hücrelerinde TiO2 Üretim Yöntemlerinin Cihaz Performansına Etkisi

Çağrı Taha Delikanlı*[1,2], Alihan Kumtepe[1,2], Çağdaş Eğin[1,2], Çağatay Ezen[1], Özlem Coşkun[1,5], Tuğçe Ataşer[2,3,4], Meriç Çalışkan Arslan[1,6]

[1] Kalyon PV R&D Center, Ankara, Türkiye
[2] Department of Photonics Science and Engineering, Graduate School of Natural and Applied Sciences, Gazi University, Ankara, Türkiye
[3] Photonics Application and Research Center, Gazi University, Ankara, Türkiye
[4] Department of Photonics, Faculty of Applied Sciences, Gazi University, Ankara, Türkiye
[5] Micro and Nanotechnology Program, Middle East Technical University (METU), Ankara, Türkiye
[6] Polymer Science and Technology Program, Middle East Technical University (METU), Ankara, Türkiye
** ctdelikanli@kalyonpv.com*

Özet

Küresel ölçekte giderek artan enerji talebi ve fosil yakıt kullanımının yol açtığı çevresel sorunlar, yenilenebilir enerji kaynaklarına olan talebi hızla arttırmaktadır. Bu doğrultuda, temiz ve sürdürülebilir enerji üretimi sağlayan fotovoltaik teknolojilerin geliştirilmesine yönelik çalışmalar hız kazanmıştır. Fotovoltaik teknolojiler arasında son yıllarda önemli bir gelişme gösteren perovskit güneş hücreleri, düşük üretim maliyeti, çözelti bazlı üretim olanakları ve güç dönüşüm verimlerinde sağlanan gelişmeler doğrultusunda son yıllarda önemli bir araştırma konusu haline gelmiştir.

Bu çalışma kapsamında, düzlemsel n-i-p mimarisine sahip perovskit güneş hücrelerinin üretimi ve cihaz performanslarını optimizasyonu amaçlandı. Tasarlanan cihaz mimarisi Şekil 1 (a) ve 1(b)'de görüldüğü gibi; FTO/TiO_2/$MAPbI_3$/PTAA/Ag katmanlarından şeklindedir.

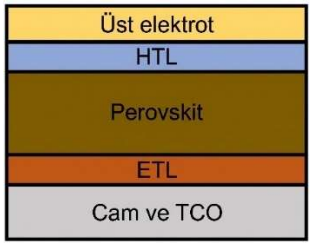

Şekil 1a-) n-i-p hücre mimarisi

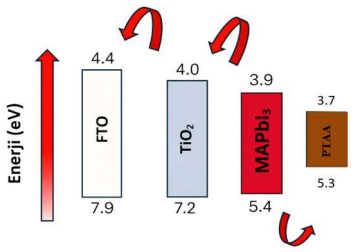

Şekil 1b-) Kullanılacak olan perovskit güneş hücresi mimarisi

Bu çalışmada elektron taşıma tabakası (ETL) olarak kullanılan TiO_2'nin farklı kaplama yöntemleriyle üretilmesinin perovskit güneş hücrelerinin performansı üzerindeki etkisi incelendi. Aynı TiO_2 solüsyon reçetesi kullanılarak filmler; dönerek kaplama, sprey kaplama ve doktor blade yöntemleriyle FTO kaplı cam altlıklar üzerine kaplandı. TiO_2 elektron taşıma tabakasının oluşturulmasının ardından, aktif $MAPbI_3$ perovskit tabakası ve PTAA delik taşıma tabakası standart spin coating yöntemi kullanılarak kaplandı. Son olarak, gümüş (Ag) üst kontaklar aerosol jet baskı tekniği kullanılarak basıldı ve perovskit güneş hücrelerinin üretimi tamamlandı.

Üretilen TiO_2 filmlerinin morfolojik, optik, yapısal ve elektriksel özellikleri AFM, profilometre, SEM, UV-Vis spektroskopisi, XRD ve dört uçlu prob (Four-point Probe) teknikleri kullanılarak incelendi. Elde edilen sonuçlar doğrultusunda, farklı TiO_2 kaplama tekniklerinin perovskit güneş hücrelerinin performansı üzerindeki etkisi değerlendirildi.

Anahtar Kelimeler / Keywords: Perovskit Güneş Hücreleri, n-i-p Mimarisi, TiO2 Kaplama Yöntemleri.

Teşekkürler:
Bu çalışma, Türkiye Cumhuriyeti Cumhurbaşkanlığı Strateji ve Bütçe Başkanlığı tarafından 2019K12-149045 proje numarasıyla desteklenmiştir.

Angular Scattering-Based Composition Estimation of Binary Microplastic Mixtures

Batuhan Can[1], Esma Nur Karadag[1], Ibrahim Hancer[1], Nazlican Celik[1,2], and Sinan Genc[1,2*]

[1] Department of Electrical-Electronics Engineering, Abdullah Gül University, 38080, Kayseri, Türkiye

[2] Department of Physics, Middle East Technical University, 06800, Ankara, Türkiye

sinan.genc@agu.edu.tr

Abstract

Microplastic pollution in aquatic environments is a growing global threat. While optical scattering methods can detect and size individual particles [1], characterizing the relative fraction of each size population in a mixture remains an open problem. Existing approaches focus on monodisperse samples [2,3]. We address the binary mixture case: given a PS4 (4 μm) + PS8 (8 μm) polystyrene suspension, can a simple optical measurement determine the PS8 fraction?

A collimated 520 nm laser beam illuminates a cuvette containing the PS4+PS8 suspension. The far-field angular scattering pattern forms on a diffuse screen placed 6.5 cm from the cuvette exit face and is captured by a Raspberry Pi camera in dark-room conditions. For each sample, 86 radial lines (5°–90°, 1° steps) are drawn from the detected beam center, yielding a 101-point angular intensity profile per image [2]. A 25th-degree polynomial fit is applied to suppress noise, and interference ring angles are extracted via local maxima.

Samples were prepared at 21 PS8 concentration levels (0%–100%, 5% steps) with 20 replicates each, yielding 420 profiles in total. Analysis reveals that PS8-dominant mixtures exhibit well-resolved Mie interference rings at ~11° and ~25°, while PS4-dominant mixtures show monotonic forward-scattering decay, consistent with Mie scattering theory [3]. A Ridge regression model trained on the angular intensity profiles is evaluated under a One-Percentage-Out (OPO) cross-validation protocol [4,5], in which all replicates of one concentration level are withheld during training, directly assessing generalization to unseen compositions. The model achieves an overall MAE of 3.5% across all 21 concentration levels.

These results demonstrate that static image-based angular scattering, without mechanically scanned detectors, provides sufficient information to resolve binary microplastic mixture composition at the 5% concentration step level using a low-cost optical platform.

Keywords: angular light scattering, microplastics, binary mixture, Mie scattering, ridge regression, OPO cross-validation.

Acknowledgements

This work was supported by METU DOSAP B program.

References

[1] Koelmans, A.A. et al. (2019). Microplastics in freshwaters and drinking water: Critical review and assessment of data quality. Water Research, 155, 410–422. https://doi.org/10.1016/j.watres.2019.02.054

[2] Genc, S., Icoz, K., Erdem, T. (2023). Numerical analysis and experimental verification of optical scattering from microplastics. R. Soc. Open Sci., 10, 230586. https://doi.org/10.1098/rsos.230586

[3] Bohren, C.F., Huffman, D.R. (1983) *Absorption and Scattering of Light by Small Particles*. Wiley. https://doi.org/10.1016/j.watres.2019.02.054

[4] Genc, S., Erdem, T., Icoz, K. (2024). Size, material type, and concentration estimation for micro-particles in liquid samples. Sensors and Actuators A: Physical, 370, 115265. https://doi.org/10.1016/j.sna.2024.115265

[5] Saur, L. et al. (2026). Classification of microplastic particles in water using polarized light scattering and machine learning methods. Journal of Hazardous Materials Advances, 23, 101343. https://doi.org/10.1016/j.hazadv.2026.101343

Thermal Annealing-Induced Changes in Spatially Resolved Surface Absorption

Pervin Tüzün[*1,2], Mevlüt Karabulut[2], Zehra Uğan[1], Zehra Nur Çetintaş[1], Bai Zhongxuan[3], Yuanan Zhao[3,5], Humbet Nasibli[1]

[1]National Metrology Institute, The Scientific and Technological Research Council of Türkiye (TÜBİTAK- UME), Gebze, Kocaeli, 41470, Türkiye)

[2]Department of Physics, Gebze Technical University, Gebze, Kocaeli, 41400, Türkiye

[3]Precision Optical Manufacturing and Testing Center, Shanghai Institute of Optics and Fine Mechanics, Shanghai, 201800, China

[4]Laboratory of Thin Film Optics, Shanghai Institute of Optics and Fine Mechanics, Shanghai, 201800, China

[5]State Key Laboratory of Ultra-intense Laser Science and Technology, Shanghai, 201800, China

corresponding author: pervin.tuzun@bursiyer.tubitak.gov.tr

Abstract

Thermal annealing is an effective approach for reducing optical absorption in thin-film coatings and improving their optical performance. In this study, the effect of thermal annealing on the absorption characteristics of Ta_2O_5 and SiO2 optical coatings was investigated at 275 nm using both one-dimensional absorption scans and two-dimensional surface absorption mapping. The measurements were performed using Photothermal Common-Path Interferometry (PCI), enabling sensitive characterization of low optical absorption and its spatial distribution over the coating surface. The one- and two-dimensional measurements were performed to investigate the spatial homogeneity of absorption and to assess the local changes induced by annealing. The resullts revealed a pronounced decrease in absorption following thermal treatment. For Ta_2O_5 coatings, the measured absorption decreased by approximately 68–87%, depending on the coating and deposition conditions, whereas the reduction observed for SiO_2 coatings ranged from approximately 24–53%. The observed reduction in absorption is attributed to thermally activated modifications within the coating, including relaxation of structural defects and internal stresses, removal or reduction of absorbing impurities and volatile species, and structural densification of the thin-film material. The comparison of one- and two-dimensional measurements provides complementary information on both the magnitude and spatial distribution of the absorption reduction. These results demonstrate the significant role of thermal annealing in improving the optical quality of Ta_2O_5/SiO_2 coatings and highlight PCI as a prominent technique for evaluating spatially resolved absorption changes in optical thin films.

Keywords: Photothermal common-path interferometry / thermal annealing / linear absorption / 2D absorption map

Acknowledgements

This study was conducted within the scope of the TÜBİTAK project 224N066 (Lida-FM) and the Bureau of International Cooperation, Chinese Academy of Sciences (Grant No. 111GJHZ2024025MI).

Synthesis And Performance Evaluation Of Anisotropic Silver Coated NanoWorms for SERS Based Trace Detection Of Crystal Violet and Ammonium Nitrate

Zeynep Cantürk, Ghazanfar Ali Khan, Alpan Bek
Department of Physics, Middle East Technical University, 06800, Ankara, Türkiye

Abstract
Silver (Ag) coated nanostructures (NSs) hold significant potential for trace molecule detection using surface-enhanced Raman scattering (SERS) spectroscopy due to their excellent plasmonic characteristics. Nevertheless, the impact of Ag coating on nanoworms (NWs), especially in the context of SERS applications, is still not well studied. In this research, we present a highly anisotropic Ag shell on NWs that demonstrates exceptional SERS sensitivity. The undulating shape of the NWs, along with the optimized reaction conditions during the seeded growth method, facilitated the creation of a highly anisotropic Ag shell on NWs without leading to secondary nucleation within the growth solution. Finite element simulations indicated that these Ag coated NWs (Ag@NWs) provide superior field enhancement compared to the NWs, and they also exceed the performance of smoother Ag ellipsoids when in aggregate form. A strong comparison of the SERS capabilities between NWs and Ag@NWs was established using crystal violet. The Ag@NWs exhibited an experimental enhancement factor that is 3.5 times greater than that of NWs, achieving detection limits of ten picomolar for crystal violet and ten micromolar for ammonium nitrate. These findings indicate that an anisotropic Ag shell can greatly enhance the SERS performance of NWs, making it an engineered ultrasensitive nanomaterial suitable for quantitatively detecting trace levels of analytes.

Keywords: SERS, Raman spectroscopy, FDTD simulations, gold nanoparticles.

Acknowledgements

The authors would like to thank TÜBİTAK for supporting this work under Grant No. 123M819, ODTÜ Central Laboratory for providing the TEM images, and ODTÜ GÜNAM for providing access to their facilities. Z.C. also acknowledges TÜBİTAK for support under Grant No. 124N875. G.A.K. acknowledges ALLCHEMY KIMYA SAN. TIC. A.Ş. for financial support.

References

[1] J. Zheng et al., *Chem. Rev.* 121 (2021) 13342–13453.
[2] Y. Qi et al., *J. Alloys Compd.* 776 (2019) 934–947.
[3] P. B. Johnson and R. W. Christy, *Phys. Rev. B* 6 (1972) 4370–4379.
[4] Shibu, E. S. *et al.*, Chem. Mater. 21 (2009) 3773–3781.
[5] Lin, S. *et al.*, J. Alloys Compd. 805 (2019) 318–326.
[6] Pham, M. K. *et al.*, Anal. Methods 15 (2023) 5239–5249.
[7] Khan, G. A. *et al.*, Colloids Surf. A 619 (2021) 126542.
[8] Khan, G. A. *et al.*, Vib. Spectrosc. 120 (2022) 103359.

Design, MOCVD Growth and Characterization of 885 nm InGaAs/AlGaAs Quantum-Well Laser Diodes for Nd:YAG Pumping

Samir Tariverdiev[1]*, Gamze Yolcu[1,2], Ilkay Demir[1,3]
[1]Sivas Cumhuriyet University Nanophotonics Research and Application Center-CÜNAM, 58140 Sivas, Türkiye
[2]Department of Department of Metallurgical and Materials Engineering, Sivas Cumhuriyet University, 58140 Sivas, Türkiye
[3]Department of Nanotechnology Engineering, Sivas Cumhuriyet University, 58140 Sivas, Türkiye
*samirtariverdiyev@cumhuriyet.edu.tr

Semiconductor laser diodes operating around 885 nm are promising pump sources for Nd:YAG solid-state lasers due to their potential for reduced quantum defect, lower thermal load, and improved pumping efficiency compared with conventional 808 nm excitation.

In this work, an InGaAs/AlGaAs quantum-well laser diode structure designed for emission near 885 nm was investigated through numerical modeling, MOCVD epitaxial growth, and electro-optical characterization. The laser design was optimized by considering the quantum-well composition and thickness, carrier confinement, optical mode distribution, strain, and the surrounding AlGaAs waveguide and barrier layers.

The designed structure was grown by MOCVD on a GaAs substrate and subsequently processed into edge-emitting laser devices. The experimental results were compared with numerical calculations in order to evaluate the effects of quantum-well composition, thickness, strain, interface quality, and epitaxial growth conditions on the emission wavelength and device performance.

The results demonstrate the feasibility of a combined design–epitaxy–characterization approach for the development and further optimization of 885 nm InGaAs/AlGaAs laser diodes for Nd pumping applications.

Keywords: *laser diode, epitaxy, quantum well, MOCVD, Nd:YAG pumping*

Acknowledgment:
This work is supported by TÜBİTAK under the 1001 Scientific and Technological Research Projects Support Program, Project No. **125F147**, entitled **"Nd Katı Hal Lazer Uygulamaları İçin Kademeli 88x nm Lazer Diyot Tasarımı, Epitaksiyel Büyütülmesi ve Aygıt Üretimi"**, for the project period **01.06.2026–01.06.2029.**

Mg_4FGeO_6:Mn Coatings for Optical Fluorescence Surface Thermometry

Ömer F. Kadı[1,4], Yadi Zhao[2], Pervin Tüzün[1], Yuanan Zhao[2,3], Mevlüt Karabulut[4], Humbet Nasibli*[1]

[1]National Metrology Institute, The Scientific and Technological Research Council of Türkiye (TÜBİTAK UME), Gebze, Kocaeli, 41470, Türkiye)

[2]Laboratory of Thin Film Optics, Shanghai Institute of Optics and Fine Mechanics, Shanghai, 201800, China

[3]State Key Laboratory of Ultra-intense Laser Science and Technology, Shanghai, 201800, China

[4]Department of Physics, Gebze Technical University, Gebze, Kocaeli, 41400, Türkiye

corresponding author, E-mail: humbet.nasibli@tubitak.gov.tr

Abstract

Surface temperature is a key parameter in many industrial and scientific processes, yet it is difficult to measure accurately. Contact thermometers disturb the surface and cannot follow moving objects, while infrared thermometers depend on surface emissivity and ambient radiation. In phosphor thermometry, a phosphor-coated surface is optically excited and the temperature is derived from the spectral or temporal characteristics of the luminescence after calibration [1]. This non-contact technique is largely independent of emissivity, making it suitable for harsh environments, moving objects and fast transient processes [2, 3].

In this work, Mg_4FGeO_6:Mn was characterized as a thermographic phosphor using three methods: single-band peak wavelength shift, two-band intensity ratio and luminescence decay time. The phosphor, mixed with a high-temperature binder, was spray-coated onto graphite and stainless-steel substrates and calibrated in a three-zone furnace against an ITS-90-traceable thermocouple [4]. For the two time-integrated methods, the coating was excited with a 385 nm LED and its emission spectrum was recorded with a fibre-coupled spectrometer from room temperature to 100 °C. For the decay-time method, it was excited with 355 nm Nd:YAG pulses and the luminescence decay was imaged with a high-speed camera at 40,000 fps from room temperature to 400 °C.

The optical characteristics of Mg_4FGeO_6 were investigated using three phosphor thermometry approaches: peak-shift, intensity-ratio, and decay-time methods. Particular attention was given to its fluorescence characteristics, including the temperature-dependent shifts of the emission peaks near 659 nm and 631 nm, their intensity ratio, and the fluorescence decay time. Measurements were performed from room temperature to 400 °C to assess the temperature sensitivity and applicability of the phosphor for LED-illuminated phosphor thermometry. The measurement results, temperature sensitivities, and associated uncertainty analysis are presented and discussed, demonstrating the feasibility of Mg_4FGeO_6 as a candidate material for LED-excited phosphor thermometers.

Keywords: phosphor thermometry; Mg_4FGeO_6:Mn; decay-time; intensity ratio; peak-shift; high-speed imaging

Acknowledgements

This study is conducted in the scope of the TÜBİTAK ARDEB 2568 for Grant No 224N066 and the Key Foreign Cooperation Projects of the Bureau of International Cooperation of the Chinese Academy of Sciences (111GJHZ2024025MI).

Referanslar / References

[1] Ö.F. Kadı et al., TEMPMEKO & ISHM 2025, Reims, France, 2025.
[2] G. Sutton, S. Korniliou, A. Andreu, D. Wilson, Int J Thermophys 43 (2022) 36.
[3] G. Machin et al., Nuclear Engineering and Design, 371 (2021) 110939.
[4] Ö.F. Kadı et al., 42nd Int. Physics Congress of the Turkish Physical Society (TFD-42), Bodrum, Türkiye, 2026.

Laser-induced damage threshold of SiO2/HfO2 high-reflectors at 355 nm under atmospheric and vacuum conditions (s- and p-polarizations)

Pervin Tüzün[*1,2], Mevlüt Karabulut[2], Ömer Faruk Kadı[1], Mengxia Wang[3], Weili Zhang[4], Kun Shuai[3], Semih Yurtseven[1], Can Gözönünde[1], Yuxin Leng[5], Yuanan Zhao[3,5], Humbet Nasibli[1]

[1]National Metrology Institute, The Scientific and Technological Research Council of Türkiye (TÜBİTAK- UME), Gebze, Kocaeli, 41470, Türkiye)

[2]Department of Physics, Gebze Technical University, Gebze, Kocaeli, 41400, Türkiye

[3]Precision Optical Manufacturing and Testing Center, Shanghai Institute of Optics and Fine Mechanics, Shanghai, 201800, China

[4]Laboratory of Thin Film Optics, Shanghai Institute of Optics and Fine Mechanics, Shanghai, 201800, China

[5]State Key Laboratory of Ultra-intense Laser Science and Technology, Shanghai, 201800, China

corresponding author: pervin.tuzun@bursiyer.tubitak.gov.tr

Abstract

This study investigates ultraviolet (UV) laser-induced damage of high-reflectivity (HR) optical coatings at 355 nm under both vacuum and air conditions. The laser-induced damage threshold (LIDT) and damage morphology were examined for both p- and s-polarized multi-pulse irradiations using 2-inch mirrors at 45° incidence fabricated in the same deposition batch. Each mirror was divided, with one half tested in air and the other in vacuum, and configurations reversed for companion samples to ensure consistency. Damage morphologies were systematically characterized relative to environmental conditions. Results show that LIDT is consistently lower in vacuum than in air, with a more pronounced reduction for p-polarization. The decrease in LIDT under vacuum is attributed to enhanced propagation of laser-induced nanoparticles due to the absence of plasma shielding, along with coating dehydration. In air, nanoparticles accumulate near the damage crater due to plasma shielding, whereas in vacuum they disperse across a larger area, acting as secondary damage precursors and further reducing LIDT.

Keywords: SiO2/HfO2High-reflective coatings / 355 nm / Vacuum dehydration / Polarization / Damage morphology / Damage precursors / Plasma shielding

Acknowledgements

TimeThis study is conducted in the scope of the “TÜBİTAK BİDEB 2214-A - International Research Fellowship Programme for PhD Students” scholarship. This research was supported by the Scientific and Technological Research Council of Türkiye (TÜBİTAK) ARDEB 2568 for Grant No 224N066 and the Key Foreign Cooperation Projects of the Bureau of International Cooperation of the Chinese Academy of Sciences (111GJHZ2024025MI).

Koherent Fiber LiDAR Mimarisinde Costas Kodlu Dalga Formu Uygulaması

Furkan Durmuş*[1], İbrahim Tuna Özdür[1]
[1]*Elektrik ve Elektronik Mühendisliği Bölümü, TOBB Ekonomi ve Teknoloji Üniversitesi, Ankara*
*corresponding author, E-mail: fdurmus@etu.edu.tr

Özet

Koherent LiDAR sistemleri, geri dönen optik sinyalin genlik ve faz bilgisinin algılanmasına olanak sağlaması nedeniyle yüksek hassasiyetli menzil ve hız ölçümü, atmosferik algılama ve uzaktan hedef tespiti gibi uygulamalarda yaygın olarak kullanılmaktadır. Costas frekans kodlu dalga biçiminin koherent LiDAR mimarisinde uygulanması ve darbe sıkıştırma metodu deneysel olarak incelenmiştir. Costas kodlaması, toplam darbe süresini ve darbe enerjisini korurken alt darbelerin farklı frekanslara bölünmesi sayesinde geniş etkin bant genişliği ve uygun korelasyon özellikleri sağlamaktadır [1]. Deneysel sistemde sekiz elemanlı Costas dizisi kullanılmış; toplam darbe süresi 4 μs, alt darbe süresi 0.5 μs ve frekans adımı 2 MHz olarak belirlenmiştir. Bu parametrelerle yaklaşık 16 MHz etkin bant genişliği elde edilmiş, teorik sıkıştırılmış darbe süresi 62.5 ns ve darbe sıkıştırma oranı yaklaşık 64 olarak hesaplanmıştır.

Koherent LiDAR alıcısından elde edilen sinyaller matched-filtreleme işlemlerine tabi tutulmuştur. Matched-filtre çıkışında Costas ve klasik burst dalga biçimleri −3 dB ana lob genişliği bakımından karşılaştırılmıştır. Costas dalga biçimi için yaklaşık 57.7 ns, burst dalga biçimi için ise 2.36 μs ana lob genişliği ölçülmüş ve Costas çıktısının yaklaşık 41 kat daha dar olduğu görülmüştür. Ayrıca Costas eşleşmiş filtre çıktısında tepe yan lob oranı (PSLR) yaklaşık −14.9 dB olarak ölçülmüştür. Elde edilen sonuçlar, RF darbe sıkıştırma yöntemlerinin koherent lazer radar sistemlerine uygulanabildiğini gösteren önceki çalışmalarla uyumlu olarak [2], Costas kodlamasının koherent LiDAR sistemlerinde darbe sıkıştırma ve yüksek zamansal ayrım açısından etkili bir yaklaşım olduğunu göstermektedir.

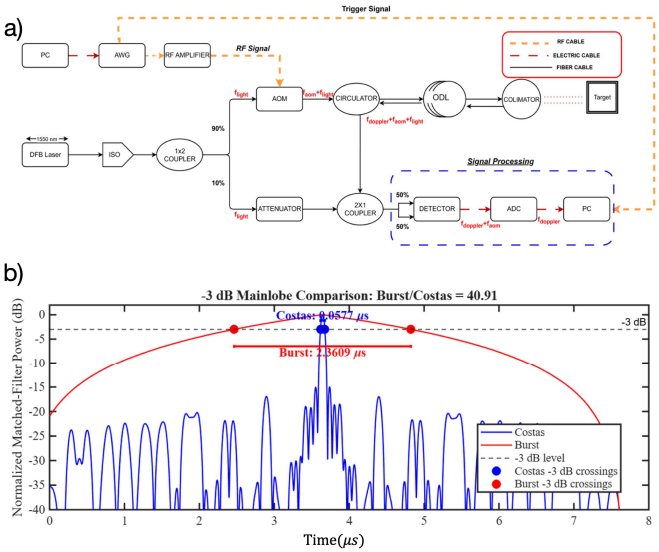

Şekil 1: Costas kodlu koherent LiDAR sisteminin deneysel uygulaması ve darbe sıkıştırma analizi: (a) Koherent Lidar sistem mimarisi (AWG: Arbitrary Waveform Generator, ISO: Isolator, ODL: Optical Delay Line, DFB: Distributed Feedback, ADC: Analog to Digital Converter, PC: Personal Computer) (b) Costas ve Burst matched filtre ana lob karşılaştırması.

Anahtar Kelimeler: PSLR, -3 dB ana lob genişliği, matched-filtre, Koherent fiber Lidar, Costas, darbe sıkıştırma metodu, darbe sıkıştırma oranı, frekans atlaması.

Referanslar:

[1] J. P. Costas, "A Study of a Class of Detection Waveforms Having Nearly Ideal Range–Doppler Ambiguity Properties," *Proceedings of the IEEE*, vol. 72, no. 8, pp. 996–1009, 1984, doi: 10.1109/PROC.1984.12967.
[2] C. Allen, Y. Cobanoglu, S. K. Chong, and S. Gogineni, "Development of a 1310-nm, Coherent Laser Radar with RF Pulse Compression," in *Proc. IEEE IGARSS 2000*, pp. 1784–1786, 2000, doi: 10.1109/IGARSS.2000.857345.

Substrate-Dependent Correlation Between Raman Signatures and Terahertz Conductivity in Single-Layer Graphene

Fatma Feyza Sadıkoğlu[1,2], Yusuf Samet Aytekin[2], Hakan Altan[3], Okan Esentürk[1,2]
[1] Micro and Nanotechnology Program, Graduate School of Natural and Applied Sciences, Middle East Technical University (METU), Ankara, Türkiye
[2] Laser Spectroscopy Group, Department of Chemistry, Middle East Technical University (METU), Ankara, Türkiye
[3] Department of Physics, Middle East Technical University (METU), Ankara, Türkiye
feyza.sadikoglu@metu.edu.tr

Transferred single-layer graphene (SLG) is highly sensitive to its supporting substrate, which can modify both Raman signatures and charge-carrier dynamics through charge transfer, strain, residual polymers, and surface heterogeneity. Here, CVD-grown SLG transferred onto PET, PDMS, and a PDMS+PMMA blend was investigated using 532 nm Raman spectroscopy and fluence-normalized 800 nm optical pump-THz probe spectroscopy. Raman spectra were collected from 25 points on each sample and evaluated through Lorentzian fitting of the G and 2D bands. The substrates produced distinct changes in peak position, linewidth, and I(2D)/I(G). PDMS+PMMA exhibited the highest average I(2D)/I(G) (1.88), close to the commonly used single-layer-like value of approximately 2 [2]. PET showed the narrowest 2D band, whereas PDMS displayed the broadest and most blue-shifted 2D band. Despite these differences, the single-Lorentzian 2D profiles remained consistent with an SLG-like Raman response, showing that I(2D)/I(G) alone is insufficient for layer assignment on polymer substrates. All samples showed positive differential THz transmission with sub-picosecond rise times, consistent with reported photoinduced THz behavior in monolayer graphene [3]. Importantly, the Raman and THz measurements exhibited the same substrate-dependent trend, PDMS+PMMA > PET > PDMS, supporting a qualitative correlation between the Raman signatures and photoinduced THz response. The combined results indicate that substrate-induced doping, strain, interfacial residues, and spatial heterogeneity, rather than layer number alone, influence both the spectroscopic and terahertz responses.

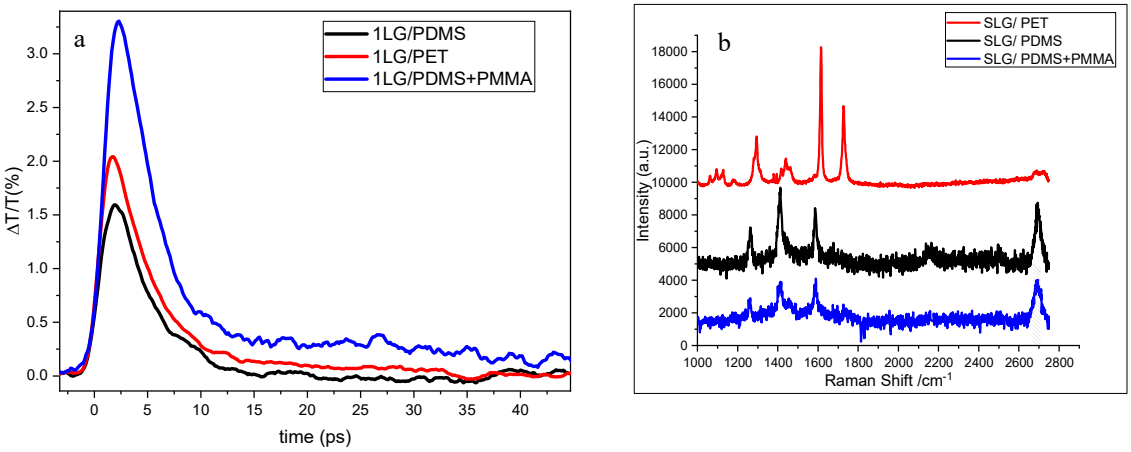

Figure 1: (a) Fluence corrected 800 nm pump Terahertz probe spectra (b) 532 nm Raman spectra of single graphene samples grown on PET, PDMS, PMMA+PDMS

Anahtar Kelimeler / Keywords: Single-layer graphene; Raman spectroscopy; terahertz spectroscopy; substrate effects; charge-carrier dynamics

Acknowledgements
We thank Lisheshar W. Ibrahim, Seval Kinden, and Nihan Perkgöz Koşku from the Department of Electrical and Electronics Engineering, Eskişehir Technical University, for providing the samples used in this study.

Referanslar / References
[1] R. J. Dolleman et al., 'Optomechanics for Thermal Characterization of Suspended Graphene,' Phys. Rev. B 96, 165421 (2017).
[2] S. Kar et al., 'Tuning Photoinduced Terahertz Conductivity in Monolayer Graphene: Optical-Pump Terahertz-Probe Spectroscopy,' Phys. Rev. B 90, 165420 (2014).

Time-Resolved CW-ODMR with Ensemble Diamond NV Center

Tuna Özdür[1], Baha Gencay Işıkdoğan[1], Muhammed Bilgin[2,3], Serkan Ateş[1]
[1]Faculty of Engineering and Natural Sciences, Sabanci University, İstanbul 34956, Türkiye
[2]Nanomagnetics Instruments Inc, 06530, Ankara,
[3]Department of Physics, Middle East Technical University, 06800, Ankara, Türkiye
tuna.ozdur@sabanciuniv.edu
serkan.ates@sabanciuniv.edu

Abstract
Solid-state point defects with active electronic spins are key building blocks for next-generation quantum technologies. For example, quantum sensing utilizes electronic spins to detect weak magnetic fields for various applications in biological and physical sciences. Among several platforms, nitrogen-vacancy (NV) center in diamond has emerged over the past two decades as the benchmark platform for such sensing, owing to its accessible spin–photon coupling via optically detected magnetic resonance (ODMR) [1]. On the other hand, NV centers serve as the reference standard for novel spin-active defects in other materials such as hexagonal boron nitride (hBN) [2]. In this work, we report optical characterization of ensemble NV centers using a photoluminescence spectroscopy, probing their electronic spin state using microwave antenna and reading out spin information optically. We will present our investigations on linewidth and contrast change of ODMR signal under various continuous-wave and pulsed excitation conditions as non-gated/gated CW-ODMR. Building on this characterization, we outline our ongoing extension of the apparatus toward time-resolved pulsed protocols like pulsed ODMR, Rabi oscillations, and Ramsey interferometry for coherent spin control, with the eventual goal of applying the same methodology to spin defects in hBN [3].

Keywords: Spin Active Defects, NV center, ODMR, Spin-photon Interaction, Quantum Technologies, Quantum Sensing

Acknowledgement: We thank Rümeysa Salcı and Leyla Çolakerol from Gebze Technical University for the NV center sample used in this work.

References

[1] Maze, J. R., P. L. Stanwix, J. S. Hodges, et al. 2008. “Nanoscale Magnetic Sensing with an Individual Electronic Spin in Diamond.” Nature 455 (7213): 644–47. https://doi.org/10.1038/nature07279.
[2] Gottscholl, Andreas, Matthias Diez, Victor Soltamov, et al. 2021. “Spin Defects in hBN as Promising Temperature, Pressure and Magnetic Field Quantum Sensors.” *Nature Communications* 12 (1): 4480. https://doi.org/10.1038/s41467-021-24725-1.
[3] Stern, Hannah L., Carmem M. Gilardoni, Qiushi Gu, et al. 2024. “A Quantum Coherent Spin in Hexagonal Boron Nitride at Ambient Conditions.” *Nature Materials* 23 (10): 1379–85. https://doi.org/10.1038/s41563-024-01887-z.

Moderate-Resolution FTIR Spectroscopy for Relative-Value Spectroscopic Gas Thermometry

Can GÖZÖNÜNDE[1], Ahmet Harun ATAĞ[1,2], Eren DEMIREL[1,2], Semih YURTSEVEN[1], Humbet NASIBLI[1,*]

[1]National Metrology Institute, The Scientific and Technological Research Council of Türkiye (TÜBİTAK UME), Gebze, Kocaeli, 41470, Türkiye)
[2] Yıldız Technical University, Istanbul, Türkiye

corresponding author, E-mail: can.gozonunde@tubitak.gor.tr ; humbet.nasibli@tubitak.gov.tr

Abstract

This work demonstrates the potential of moderate-resolution Fourier-transform infrared (FTIR) spectroscopy for relative-value spectroscopic gas thermometry (RVSGT), exploiting the temperature-dependent optical response of molecular absorption bands. Carbon monoxide (CO) spectra were measured over 296–333 K using a 0.5 cm^{-1}-resolution FTIR spectrometer and a 20 m multipass optical cell containing CO at near-atmospheric pressure. The broadband rotational–vibrational spectrum was analysed using two complementary optical retrieval approaches: full-spectrum forward fitting based on HITRAN spectroscopic data and a Boltzmann-plot method based on the population distribution among transitions with different lower-state energies.

Particular attention was given to the interaction between molecular absorption features and the optical instrument line shape (ILS). Because the ILS was substantially broader than the intrinsic absorption lines, instrumental convolution significantly altered the measured spectral profiles and concealed the true optical depth, particularly under optically thick conditions. Direct integration of the measured absorption features consequently produced temperature biases of several kelvin, despite apparently good spectral fits. Incorporating the measured ILS into the transmission-based forward model, together with a free absorber-column scale factor, effectively accounted for the convolution and saturation effects while reducing dependence on absolute optical intensity, path length, and gas concentration.

Temperature retrievals obtained from both optical estimators agreed with SI-traceable contact thermometry within the combined expanded uncertainty (k = 2). The results demonstrate that individual molecular transitions need not be spectrally resolved to extract reliable temperature information from a broadband molecular spectrum. Moderate-resolution FTIR therefore offers a practical and comparatively simple optical route to spectroscopic thermometry, complementary to high-resolution laser-based techniques. The work further emphasizes the importance of accurate ILS characterization and molecular spectroscopic data for achieving improved optical accuracy and traceability.

Keywords: gas thermometry; infrared spectroscopy; Carbon monoxide; Boltzmann-plot method; instrument line shape

Acknowledgements
The project “Primary Spectrometric Thermometry for Gases” (22IEM03-PriSpecTemp) has received funding from the European Partnership on Metrology, co-financed from the European Union’s Horizon Europe Research and Innovation Programme and by the Participating States.

Referanslar / References

[1] Tempmeko
[2] G. Li and V. Ebert, Ro-vibrational spectroscopic gas thermometry (RVSGT): A new primary method for gas thermometer calibrations, Meas. Sci. Technol., 2021
G. Machin et al., Nuclear Engineering and Design, 371 (2021) 110939.
[3] G. Li, et al., "PriSpecTemp: Primary spectrometric thermometry for gases," European Partnership on Metrology Project 22IEM03, EURAMET Publishable Summary (2023–2026).

Terahertz Metasurfaces for Integrated Sensing and Communication in 6G Networks

Mohamad Ahmad Said[1*], Cumali Sabah[1]
[1]*Department of Electrical and Electronics Engineering, Middle East Technical University Northern Cyprus Campus, Kalkanlı, Guzelyurt, TRNC / Mersin 10, Türkiye*
[*]mohamad.said@metu.edu.tr

Abstract

Next-generation 6G wireless systems require sophisticated hardware platforms which allow seamless Integrated Sensing and Communications (ISAC) using shared-hardware approaches, reconfigurable intelligent surfaces, and holographic transmit arrays [1]. Here, we present a reconfigurable all dielectric terahertz metasurface for simultaneous refractive index sensing and active frequency tuning. Our design is built using asymmetric lithium niobate ($LiNbO_3$) cylindrical dimers placed on a quartz substrate where the metasurface supports ultra-high quality-factor quasi-bound states in the continuum that are manifested as sharp Fano resonances in the terahertz transmission spectrum [2]. In order to investigate the structural and electromagnetic performance of the proposed architecture, finite-element method simulations are performed. The sensing results show a slight shift in the resonance frequency from 4.2594 THz to 4.2584 THz when the surrounding analyte refractive index increases from 1.00 to 1.10, which results in a linear refractive index sensitivity with well-defined transmission modulation depths. Additionally, we use the electro-optic properties of $LiNbO_3$ and apply an external voltage bias ranging from -50 V to $+50$ V that induces a controlled refractive index perturbation, resulting in the dynamic tuning of the resonance frequency across a total span of 3.6 GHz with a tuning efficiency of 36 MHz/V. Ultimately, our findings establish the proposed $LiNbO_3$ metasurface as a versatile technology suitable both for terrestrial 6G ISAC architectures and as a dual-functional payload for Martian and lunar micro-rovers, enabling simultaneous high-speed terahertz data telemetry and real-time subsurface material characterization in extreme environments.

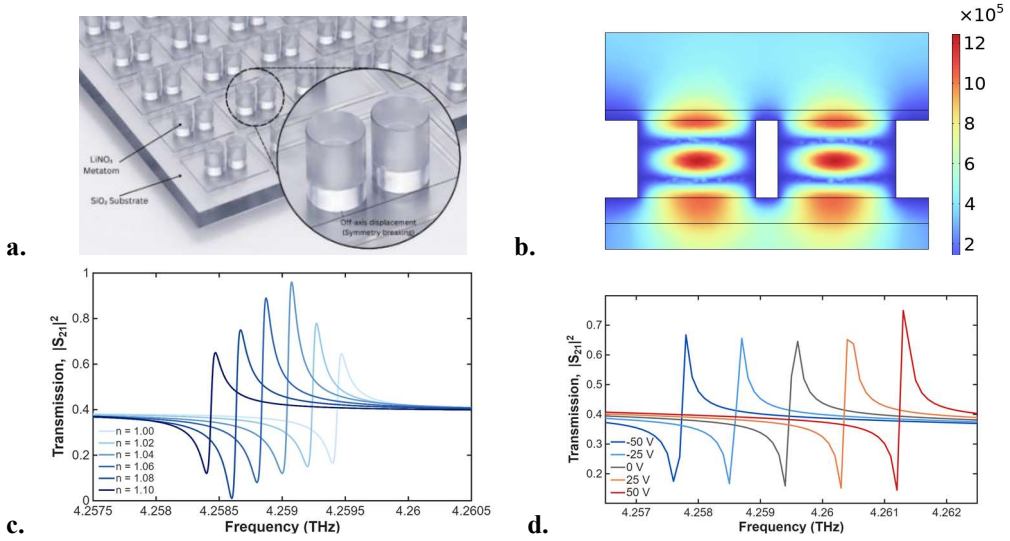

Figure 1: a. Schematic of the $LiNbO_3$ dimer metasurface. **b.** Cross-sectional E-field magnitude distribution ($> 10^6$ V/m) at 4.2594 THz. **c.** Refractive index sensing spectra ($n_{\text{analyte}} = 1.00$–$1.10$). **d.** Voltage-tuning spectra (-50 V to $+50$ V).

Keywords: Terahertz metasurfaces; integrated sensing and communications (ISAC); 6G networks; lithium niobate; quasi-bound states in the continuum; electro-optic tuning; planetary exploration

Acknowledgement: The authors gratefully acknowledge the Office of Research Coordination and Support at Middle East Technical University Northern Cyprus Campus (METU-NCC) for funding this research under Scientific Research Project FEN-25-D-1.

References

[1] A. Magbool, V. Kumar, Q. Wu, M. Di Renzo and M. F. Flanagan, "A Survey on Integrated Sensing and Communication With Intelligent Metasurfaces: Trends, Challenges, and Opportunities," in *IEEE Open Journal of the Communications Society*, vol. 6, pp. 7270-7318, 2025, doi: 10.1109/OJCOMS.2025.3594049.
[2] X. Yu, F. Li, T. Lang, J. Qin, and X. Ma, "Ultrasensitive tunable terahertz lithium niobate metasurface sensing based on bound states in the continuum," *Photonics Research*, vol. 11, no. 12, pp. 2168–2178, 2023.

Investigation of Interface Effects in InGaAs/InAlAs Quantum Cascade Laser Structures

Nisa Nur YENER[1], Merve Nur KOÇAK[1,3], İlkay DEMİR[1,2*]

[1]Nanophotonics Application and Research Center (CÜNAM), Sivas Cumhuriyet University, 58140 Sivas, Türkiye

[2] Department of Nanotechnology Engineering, Sivas Cumhuriyet University, 58140 Sivas, Türkiye

[3]Department of Metallurgy and Materials Engineering, Sivas Cumhuriyet University, 58140 Sivas, Türkiye

corresponding author, E-mail: idemir@cumhuriyet.edu.tr

Abstract

Quantum cascade lasers (QCLs) are highly sensitive to the thickness, composition, and interface properties of the nanometer-scale layers forming the quantum wells and barriers in the active region. Therefore, precise control of the superlattice period and interface quality in InP-based InGaAs/InAlAs structures is essential for the epitaxial growth of QCL heterostructures [1,2]. In this study, two InGaAs/InAlAs superlattice structures grown on InP substrates by MOVPE were compared. The number of interfaces was increased by using thinner superlattice periods, and the effect of this modification on structural quality, surface morphology, and vibrational properties was investigated. The structures were characterized by high-resolution X-ray diffraction (HRXRD), atomic force microscopy (AFM), and Raman spectroscopy. HRXRD results showed that superlattice periodicity was maintained in both structures and that the epitaxial growth was consistent with the intended design [3]. AFM analysis revealed low surface roughness and a well-defined surface morphology, while Raman spectroscopy identified the characteristic vibrational features of the InGaAs/InAlAs heterostructures [4,5]. Considering the results from all characterization techniques, the structural and morphological integrity of the superlattices was preserved despite the increased number of interfaces. These findings highlight the importance of interface control in determining the epitaxial quality of InGaAs/InAlAs-based QCL superlattices and provide useful insight into the controlled MOVPE growth of such heterostructures.

Keywords: Quantum cascade laser; InGaAs/InAlAs superlattice; interface engineering; MOVPE; structural characterization

Acknowledgements

This work is based on results obtained during the ongoing Ph. D. thesis of Merve Nur Koçak, titled “Development of Short- and Mid-Wavelength Quantum Cascade Lasers”. Merve Nur Koçak is supported by the YÖK (Council of Higher Education) 100/2000 Ph. D. Scholarship Program and The Scientific and Technological Research Council of Turkey (TÜBİTAK) 2211/A Program. This study supported by The Scientific Research Project Fund of Sivas Cumhuriyet University, Turkey under the project number MRK-2024-004 and The Scientific and Technological Research Council of Turkey (TUBITAK) under the project number 22AG074.

References

1] J. Faist, F. Capasso, D. L. Sivco, C. Sirtori, A. L. Hutchinson, and A. Y. Cho, “Quantum Cascade Laser,” *Science*, **264**(5158), 553–556 (1994). DOI: 10.1126/science.264.5158.553.

[2] Y. Huang, J.-H. Ryou, R. D. Dupuis, C. Pflügl, F. Capasso, K. Sun, A. M. Fischer, and F. A. Ponce, “Optimization of growth conditions for InGaAs/InAlAs/InP quantum cascade lasers by metalorganic chemical vapor deposition,” *Journal of Crystal Growth*, **316**(1), 75–80 (2011). DOI: 10.1016/j.jcrysgro.2010.12.028.

[3] S. Elagöz and İ. Demir, “Growth of InGaAs/InAlAs Superlattices by MOCVD and Precise Thickness Determination via HRXRD,” *Gazi University Journal of Science*, **29**(4), 947–951 (2016).

[4] Y. Hu, L. Wang, F. Liu, J. Zhang, J. Liu, and Z. Wang, “Micro-Raman study on chirped InGaAs–InAlAs superlattices,” *physica status solidi (a)*, **210**(11), 2364–2368 (2013). DOI: 10.1002/pssa.201330002.

[5] A. G. Milekhin *et al.*, “Vibrational spectroscopy of InAlAs epitaxial layers,” *Journal of Applied Physics*, **104**, 073516 (2008). DOI: 10.1063/1.2980344.

Schottky Transport Characteristics of InGaAs MSM Photodetectors with Barrier and Digital Graded Superlattice Layers

Dudu Hatice Unal[1,2], Preeti Goswami[3], Govind Gupta[3,4], Ilkay Demir[1,5]*

[1]Sivas Cumhuriyet University Nanophotonics Application and Research Center-CÜNAM, 58140 Sivas, Türkiye.
[2]Department of Optical Engineering, Sivas Cumhuriyet University, 58140 Sivas, Türkiye.
[3]CSIR-National Physical Laboratory, Dr K.S. Krishnan Road, New Delhi 110012, India.
[4] Academy of Scientific and Innovative Research, Ghaziabad, Uttar Pradesh 201002, India.
[5] Department of Nanotechnology Engineering, Sivas Cumhuriyet University, 58140 Sivas, Türkiye.
E-mail:idemir@cumhuriyet.edu.tr

Abstract

Metal-semiconductor-metal (MSM) photodetectors are attractive for infrared detection due to their simple structure, low capacitance, and high-speed operation potential [1]. InGaAs has found extensive application in the field of SWIR detection; however, its comparatively low Schottky barrier height has been observed to result in increased carrier injection and dark current, thereby exerting a limiting effect on device performance [1,2]. Consequently, it is imperative to enhance the Schottky barrier height in order to effectively suppress the dark current in InGaAs MSM photodetectors.

In this study, the Schottky contact properties and their effects on dark current were comparatively investigated for InAlAs barrier layers and InGaAs/InAlAs digitally graded superlattice (DGSL) layers, in conjunction with a slightly In-enriched InGaAs absorption layer. In order to this end, the MSM-1 structure, comprising solely an InGaAs absorption layer; the MSM-2 structure, to which an InAlAs barrier layer was added; and the MSM-3 structure, in which a DGSL was inserted between the barrier and absorber layers, were evaluated. The results obtained from the dark I–V characteristics were used to determine the Schottky barrier height, which was found to be approximately 0.26 eV for MSM-1, 0.33 eV for MSM-2, and 0.44 eV for MSM-3. The ideality factors were found to be close to 1 for all structures.

The observation that the ideality factors were obtained near 1 indicates that carrier transport is consistent with the thermionic emission mechanism. Furthermore, it was determined that the reverse saturation current decreased significantly with an increase in the barrier height, and that the lowest dark current was obtained in the MSM-3 structure containing DGSL. The results obtained demonstrate that the InAlAs barrier and DGSL layers limit carrier injection by increasing the Schottky barrier height and provide an effective approach for suppressing dark current in InGaAs MSM photodetectors.

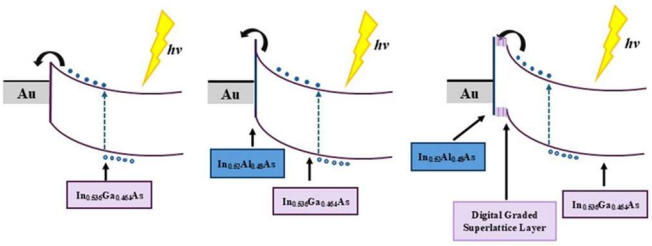

Figure 1: MSM PDs band diagram of MSM under reverse bias condition; a) MSM-1, b) MSM-2, and c) MSM-3.

Keywords: Metal-Semiconductor-Metal photodetector; Schottky barrier height; barrier layer; digital graded superlattice layer

Acknowledgements

The authors acknowledge the usage of the Sivas Cumhuriyet University Nanophotonics Research and Application Center facilities. This work was supported by the Scientific Research Project Fund of Sivas Cumhuriyet University under the project number M-2022-843. Additionally, this study was carried out with the support of the COST Action CA20116 (OPERA – European Network for Innovative and Advanced Epitaxy) through networking, collaboration, and scientific exchange activities.

References

[1] Unal, D. H., & Demir, I. (2023). InGaAs-based MSM photodetector: researching absorption layer, barrier layer, and digital graded superlattice layer with 3D simulation. Results in Optics, 13, 100581.
[2] Shi, L., Chen, K., Zhai, A., Li, G., Fan, M., Hao, Y., ... & Cui, Y. (2021). Status and outlook of metal–inorganic semiconductor–metal photodetectors. Laser & Photonics Reviews, 15(1), 2000401.
[3] Asar, T., Özçelik, S., & Özbay, E. (2014). Structural and electrical characterizations of InxGa1-xAs/InP structures for infrared photodetector applications. Journal of Applied Physics, 115(10).

Savunma Sanayiinde Kullanılan Kızılötesi Bantlar: SWIR, MWIR, LWIR ve Çok Bantlı Sistemlerin Karşılaştırmalı İncelenmesi

Kerem Güdek[*1]
[1]*Department of Photonics, Gazi University, Ankara, Türkiye*
gudekkerem@gmail.com

Özet

Kızılötesi (IR) görüntüleme sistemleri, pasif olarak çalışabilmeleri ve yetersiz aydınlatma şartlarında bile görüntü üretebilmeleri nedeniyle savunma sanayiinde kullanılan elektro-optik sistemlerin en önemli unsurlarından biri haline gelmiştir. Keşif, gözetleme, hedef tespiti ve takibi gibi görevlerde karşımıza çıkan bu sistemlerin performansı, sensör özelliklerine ek olarak kullanılan dalga boyuna, hedefin fiziksel ve termal özelliklerine, hedef ile arka plan arasındaki kontrasta ve atmosferik koşullara bağlıdır. Bu yüzden kızılötesi spektrumun farklı bölgelerinde çalışan sistemlerin birlikte değerlendirilmesi, elektro-optik sistemleri anlamak için gerekli bir adımdır [1].

Kısa Dalga Kızılötesi (SWIR), Orta Dalga Kızılötesi (MWIR) ve Uzun Dalga Kızılötesi (LWIR) bantları birbirinden farklı çalışır. SWIR bandı çoğunlukla yansıyan ışınımdan yararlanır ve belirli malzeme özelliklerinin ayırt edilebilmesinde etkilidir. MWIR ve LWIR bantları ise hedeflerin yaydığı termal ışınımdan yararlanarak gece ve sınırlı görüş koşullarında tespit yapılmasına olanak tanır. Atmosferik geçirgenlik, gözlem mesafesi, hedef ile arka plan arasındaki kontrast ve sistemin boyut-ağırlık-güç (SWaP) gereksinimleri her bandın performansını doğrudan etkileyen unsurlardır [2].

Bu çalışma kapsamında SWIR, MWIR ve LWIR bantlarının fiziksel yapısı, atmosfer içerisindeki davranışı, algılama özellikleri ve savunma sanayiindeki kullanım uygulamaları incelenmiştir. Değerlendirmeler; hava, kara ve deniz platformlarında kullanılan keşif, gözetleme ve hedef algılama sistemlerine odaklanmaktadır. Gece koşullarında insan ve araç tespiti, yüksek sıcaklığa sahip olayların algılanması, kamuflajlı hedeflerin belirlenmesi, arama-kurtarma faaliyetleri ve deniz gözetlemesi gibi farklı senaryolar üzerinden bantların kullanım özellikleri ele alınmıştır. Ayrıca tek bantlı sistemlerin yanında, farklı spektral bölgelerden elde edilen bilgilerin birlikte kullanıldığı çok bantlı ve füzyon tabanlı yaklaşımlara da yer verilmiştir.

Literatür ve farklı uygulama senaryoları birlikte incelendiğinde elde edilen sonuçlar şu şekilde özetlenebilir. SWIR, MWIR ve LWIR bantları birbirinin alternatifi olmaktan ziyade, farklı görev ve çevresel koşullara yönelik avantajlar sunan spektral bölgelerdir. SWIR yansıma ve malzeme ayrımının önemli olduğu görevlerde avantajlıdır. MWIR yüksek sıcaklığa sahip hedefleri ve ani termal olayları yakalamada güçlüdür. LWIR ise ortam sıcaklığına yakın hedefleri gözlemlemek için önemli bir seçenektir. Tek bantlı çözümler, maliyet ve sistem karmaşıklığındaki avantajlarının yanı sıra uygun SWaP özellikleri sayesinde birçok görev için yeterli performans sunabilmektedir. Birden fazla spektral verinin birlikte değerlendirilmesini gerektiren görevlerde ise çok bantlı sistemler öne çıkmakta ve hedeflerin algılanması ile sınıflandırılmasında avantaj sağlayabilmektedir. Bu avantajlara karşılık, sistem maliyetinde ve güç tüketiminde artış meydana gelmekte; optik ve dedektör yapısı karmaşıklaşırken veri işleme ve kalibrasyon gereksinimleri de artmaktadır. Bu nedenle, kızılötesi sistemlerde tek bir spektral bandın her uygulama ve koşul için en uygun seçenek olarak değerlendirilmesi doğru değildir. Bu çalışma, farklı kızılötesi bantları ve tek/çok bantlı görüntüleme yaklaşımlarını bir arada ele alan bütüncül bir literatür çerçevesi sunmayı ve elektro-optik sistemler alanındaki çalışmalara katkı sağlamayı amaçlamaktadır.

Anahtar Kelimeler: savunma teknolojileri, kızılötesi spektral bantlar, SWIR, MWIR, LWIR, elektro-optik sistemler

Referanslar

[1] Rogalski, A., & Chrzanowski, K. (2014). Infrared devices and techniques (Revision). Metrology and Measurement Systems, 21(4), 565–618.
[2] Silva, B. D., Kala, H., Dell, J. M., Zawierta, M., & Faraone, L. (2025). Low-SWaP solutions for adaptive multi-spectral infrared imaging. Journal of Electronic Materials, 54, 8335–8349.

Power, Phase, and Photonics: Investigation of RF-Sputtered Ga_2O_3 Thin Films

Hicret Hopoğlu [1, 2], Ebru Şenadım Tüzemen[1, 2, *]

[1] Department of Physics, Faculty of Science, Sivas Cumhuriyet University, 58140 Sivas, Türkiye

[2] Sivas Cumhuriyet University Nanophotonics Application and Research Center-CÜNAM, 58140 Sivas, Türkiye

*Corresponding author, E-mail: esenadim@cumhuriyet.edu.tr

Abstract

Gallium oxide (Ga_2O_3) is a promising ultra-wide-bandgap semiconductor for solar-blind ultraviolet photodetectors and transparent optoelectronic applications due to its wide optical band gap and high transparency. In this study, Ga_2O_3 thin films were deposited on sapphire and silicon substrates at room temperature by radio-frequency (RF) magnetron sputtering using different RF powers ranging from 60 to 120 W. Selected samples were subsequently annealed at 850 °C to investigate the influence of thermal treatment on their structural and optical properties. X-ray diffraction measurements showed that the as-deposited films exhibited an amorphous structure, whereas annealing promoted the formation of crystalline β-Ga_2O_3. UV–Vis measurements revealed high optical transmittance of approximately 85–95% in the visible region. The optical band gap decreased with increasing RF power and was determined to be in the ranges of 4.59–5.18 eV and 4.58–5.10 eV using the derivative and Tauc methods, respectively. Spectroscopic ellipsometry measurements were analyzed using the Cauchy dispersion model. The refractive index exhibited normal dispersion and generally decreased with increasing RF power. After annealing, an increase in the refractive index was observed, which was associated with film densification and improved structural ordering. In addition, film thickness increased systematically with RF power but decreased after annealing. These findings demonstrate that RF sputtering power and post-deposition annealing can effectively tune the optical properties of Ga_2O_3 thin films, highlighting their potential for UV photodetector and transparent optoelectronic applications.

Keywords: Ga_2O_3 thin films, RF magnetron sputtering, spectroscopic ellipsometry, refractive index, optical band gap, UV photodetector

Acknowledgements

This study was supported by the Scientific and Technological Research Council of Türkiye (TÜBİTAK) under the 2211-A Domestic PhD Scholarship Program and by the Scientific Research Project Fund of Sivas Cumhuriyet University under project number F-2025-736.

References

[1] S. J. Pearton et al., "A review of Ga_2O_3 materials, processing, and devices," Applied Physics Reviews, 5, 011301 (2018).

[2] S. Li et al., "The influence of sputtering power on the structural, morphological, and optical properties of β-Ga_2O_3 thin films," Journal of Alloys and Compounds, 753, 186–191 (2018).

[3] S. Mobtakeri et al., "Gallium oxide films deposition by RF magnetron sputtering: A detailed analysis on the effects of deposition pressure and sputtering power and annealing," Ceramics International, 47, 1721–1727 (2021).

Numerical Investigation of an Environmentally Friendly Ti-O-Zn-S Buffer Layer for CIGS Solar Cells

Abdulrhman ALKRDY[1,2], M. Enes ÇOBAN[1,2], İsmail ALTUNTAŞ[1,2*], İlkay DEMİR[1,2]

[1] *Nanophotonics Application and Research Center (CÜNAM), Sivas Cumhuriyet University, Sivas, Türkiye*

[2] *Department of Nanotechnology Engineering, Sivas Cumhuriyet University, Sivas, Türkiye*

corresponding author, E-mail: ialtuntas@cumhuriyet.edu.tr

Abstract

The rapid increase in global energy demand, together with the environmental consequences of fossil-fuel consumption, has increased interest in renewable energy technologies. Among these, photovoltaic (PV) systems have emerged as an important option for sustainable electricity generation because they directly convert solar energy into electrical power [1].

Among PV technologies, thin-film based-Cu(In,Ga)Se_2 (CIGS) is particularly attractive because of its direct and composition-tunable band gap of approximately 1.0–1.7 eV and high absorption coefficient exceeding 10^5 cm^{-1} [2]. As a result, efficient light absorption can be achieved using only about 1–3 µm of CIGS absorber, compared with approximately 150–200 µm thick crystalline-Si wafers. CIGS devices also offer high efficiency and compatibility with lightweight and flexible substrates [3].

However, conventional CIGS devices commonly employ CdS as the buffer layer. Although CdS provides favorable electronic properties and suitable band alignment with the CIGS absorber, cadmium (Cd) is toxic and raises significant environmental, health, and waste-management concerns. Furthermore, the relatively narrow band gap of CdS leads to parasitic absorption of short-wavelength photons, reducing the amount of incident light reaching the CIGS absorber and thereby limiting the photocurrent and overall device efficiency [4].

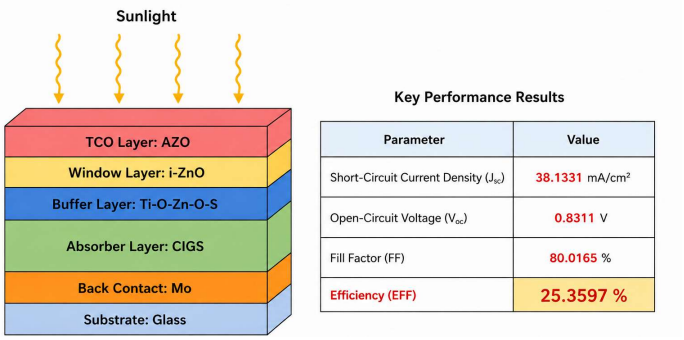

Figure 1: Proposed CdS-free CIGS solar-cell structure and corresponding simulated photovoltaic performance.

Therefore, this work investigates Ti–O–Zn–O–S (TiZnOS) as an environmentally friendly, Cd-free buffer layer for CIGS solar cells using SILVACO ATLAS. The device structure and buffer-layer parameters were numerically optimized by evaluating their effects on the open-circuit voltage (Voc), short-circuit current density (Jsc), fill factor (FF), and power-conversion efficiency. Under the optimized conditions, the TiZnOS-based CIGS solar cell achieved a Voc of 0.83V, a Jsc of 38.13 mA/cm², an FF of 80.02%, and a maximum efficiency of 25.36%. In comparison, the conventional CdS-based CIGS cell exhibited an efficiency of 25.10% under same conditions. These results indicate that TiZnOS is a promising Cd-free buffer material capable of supporting high-performance Cd-free CIGS solar cells.

Keywords: CIGS, TiZnOS, Cd-free buffer layer, thin-film solar cells, SILVACO ATLAS

Acknowledgements

This study is supported by the Scientific Research Project Fund of Sivas Cumhuriyet University, Türkiye, BAP-M-2025-879.

References

[1] S. Chu and A. Majumdar, “Opportunities and challenges for a sustainable energy future,” Nature, vol. 488, pp. 294–303, 2012. doi: 10.1038/nature11475.

[2] J. Ramanujam and U. P. Singh, “Copper indium gallium selenide based solar cells – a review,” Energy & Environmental Science, vol. 10, pp. 1306–1319, 2017. doi: 10.1039/C7EE00826K.

[3] T. Feurer, P. Reinhard, E. Avancini, B. Bissig, J. Löckinger, P. Fuchs, R. Carron, T. P. Weiss, J. Perrenoud, S. Stutterheim, S. Buecheler, and A. N. Tiwari, “Progress in thin film CIGS photovoltaics – Research and development, manufacturing, and applications,” Progress in Photovoltaics: Research and Applications, vol. 25, pp. 645–667, 2017. doi: 10.1002/pip.2811.

[4] D. Hariskos, S. Spiering, and M. Powalla, “Buffer layers in Cu(In,Ga)Se_2 solar cells and modules,” Thin Solid Films, vols. 480–481, pp. 99–109, 2005. doi: 10.1016/j.tsf.2004.11.118.

SiH_4 Flow-Dependent Structural, Electrical, and Optical Response of MOCVD-Grown n-$Al_xGa_{1-x}As$/GaAs

N. MAMERİA[1,2], G. YOLCU[*2,3], İ. DEMİR[1,2]

[1]Department of Nanotechnology Engineering, Sivas Cumhuriyet University, 58140 Sivas, Türkiye
[2]Sivas Cumhuriyet University Nanophotonics Resea
rch and Application Center-CÜNAM, 58140 Sivas, Türkiye
[3]Department of Department of Metallurgical and Materials Engineering, Sivas Cumhuriyet University, 58140 Sivas, Türkiye
corresponding author, E-mail: gamzeyolcu@cumhuriyet.edu.tr

Abstract
$Al_xGa_{1-x}As$/GaAs epitaxial structures are widely employed in optoelectronic and photonic devices due to the strong dependence of their electronic and optical properties on alloy composition and doping conditions [1]. In particular, SiH_4 is commonly used as a silicon donor precursor for n-type doping of AlGaAs layers grown by metal-organic chemical vapor deposition (MOCVD), while the electrical activation of Si can vary considerably with Al composition and growth conditions [2]. In this study, the influence of SiH_4 flow rate on the structural and electrical characteristics of MOCVD-grown n-type $Al_xGa_{1-x}As$/GaAs epitaxial layers was investigated. Four samples grown using SiH_4 flow rates of approximately 30, 15, 5, and 2.5 sccm were examined. Structural properties and alloy composition were evaluated by high-resolution X-ray diffraction (HRXRD) [3], whereas carrier type, electron concentration, and mobility were determined by Hall effect measurements system (HEMS), optical characterization was performed by spectroscopic ellipsometry. HRXRD analysis revealed systematic variations in the position of the AlGaAs (004) diffraction peak relative to the GaAs substrate peak. Despite the nominally constant group-III precursor flow rates, the Al mole fraction extracted from HRXRD fitting varied from approximately 0.62 to 0.70 across the investigated SiH_4 flow conditions, with the highest Al mole fraction obtained at the lowest SiH_4 flow rate. Hall measurements showed n-type conductivity for all samples. The electron concentration was approximately 5.4×10^{17} cm^{-3} at a SiH_4 flow rate of 30 sccm, increased slightly to approximately 6.2×10^{17} cm^{-3} at 15 and 5 sccm, and then decreased markedly to approximately 2.1×10^{17} cm^{-3} at 2.5 sccm. The corresponding electron mobilities were approximately 917, 1098, 857, and 1634 $cm^2/V{\cdot}s$ for SiH_4 flow rates of 30, 15, 5, and 2.5 sccm, respectively, with the highest mobility obtained at the lowest SiH_4 flow rate. These variations in carrier concentration and mobility reflect the complex dependence of Si donor behavior on alloy composition and growth conditions in AlGaAs . Overall, the combined HRXRD and Hall effect results reveal a clear relationship between the investigated SiH_4 flow conditions, Al composition, and electrical transport properties of n-$Al_xGa_{1-x}As$ epitaxial layers.

Keywords: AlGaAs, MOCVD, SiH_4 flow rate, HRXRD, HEMS

Acknowledgements
This study was carried out within the scope of Project No. **125F147**, entitled **"Graded 88x nm Laser Diode Design, Epitaxial Growth, and Device Fabrication for Nd:YAG Solid-State Laser Applications."**

References
[1] E. Mobini, D. H. G. Espinosa, K. Vyas, and K. Dolgaleva, "AlGaAs Nonlinear Integrated Photonics," *Micromachines*, 13(7) (2022) 991. DOI: 10.3390/mi13070991.
[2] G. Yolcu, İ. Demir, "MOVPE Growth and Doping Optimization of n-$Al_xGa_{1-x}As$ Layers for Laser Diode Applications," *Cumhuriyet Science Journal*, 46(2) (2025) 390–395. DOI: 10.17776/csj.1672625.
[3] M. Gonzalez, G. Rozas, L. Salazar Alarcon, M. Simonetto, A. Bruchhausen, G. Zampieri, A. Baruj, F. Prado, and H. Pastoriza, "Comprehensive analysis of the composition determination in epitaxial $Al_xGa_{1-x}As$ films: A multitechnique approach," *Materials Science in Semiconductor Processing*, 123 (2021) 105469. DOI: 10.1016/j.mssp.2020.105469.

TCAD Analysis of Guard-Ring Configurations in Planar InGaAs/InP SPADs

R. Delvia[1, 2], İ. Demir[2,3], and M. Köksal[1, 2] *

[1]*Department of Physics, Faculty of Sciences, Sivas Cumhuriyet University, 58140 Sivas, Türkiye*

[2]*Sivas Cumhuriyet University Nanophotonics Application and Research Center-CÜNAM, 58140 Sivas, Türkiye*

[3]*Department of Nanotechnology Engineering, Sivas Cumhuriyet University, 58140 Sivas, Türkiye*

corresponding author, E-mail: riskadelvia.318@gmail.com

Abstract

Since the introduction of the concept of the light quantum in 1905, the growing need to detect extremely weak optical signals has accelerated the development of single-photon detectors, which form the foundation of technologies such as quantum communication, LiDAR, and precision optical sensing. [1]. Among these detector types, InGaAs/InP-based single-photon avalanche diodes (SPADs) exhibit high performance, particularly in the near-infrared region at a wavelength of 1550 nm. This superiority stems from the combination of the high photon absorption efficiency of InGaAs layer and the strong avalanche multiplication capability provided by InP Layer [1,2]. However, the performance of planar InGaAs/InP SPADs is directly dependent on the electric field distribution at the lateral p+ junction. The curvature formed at the junction boundaries due to the geometry resulting from Zn diffusion causes the electric field to become excessively concentrated at the edges. This field concentration causes early edge breakdown before the central main amplification region has reached the required avalanche threshold. Therefore, the guard ring design plays a critical role in preventing early breakdown and ensuring a stable avalanche mechanism [2,3].

In this work, the influence of guard-ring configuration on the electrical behavior of a planar SAGCM InGaAs/InP SPAD was systematically investigated using two-dimensional Silvaco ATLAS TCAD simulations. Three device configurations, as shown in Figure 1, were compared: (a) Gaussian diffusion, (b) floating guard ring (FGR), and (c) combined attached–floating guard-ring (AGR–FGR) configuration, while maintaining identical epitaxial structures, doping concentrations, diffusion parameters, and operating conditions. Electric-field distributions and reverse current–voltage characteristics under dark and illuminated conditions were evaluated to determine how different junction-termination geometries influence edge-field localization and avalanche behavior. The comparative simulation results indicate that guard-ring configuration influences the spatial electric-field distribution and avalanche characteristics of the device, providing numerical guidance for selecting an appropriate guard-ring architecture prior to device fabrication.

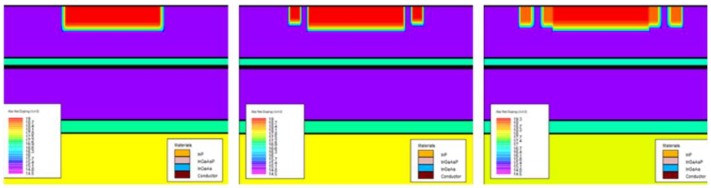

(a) **(b)** **(c)**

Figure 2. Planar InGaAs/InP SPAD configurations: (a) Gaussian diffusion, (b) FGR, and (c) combined AGR–FGR.

Keywords: InGaAs/InP; SPAD; Guard-Ring Configuration; TCAD Simulation; Electric-Field Distribution

Acknowledgements

This work is based on results obtained during the ongoing M.Sc. thesis of Riska Delvia, titled "Zinc Diffusion in III–V Semiconductor Materials: MOCVD-Based Implementation and Simulation-Based Analysis of Its Effects on SPAD Structure".

References

[1] Wang, L., Ye, Y., Kong, D., Bai, T., Yao, X., Yuan, S., ... & Xia, M. (2025). Advances and perspectives in single photon detectors: principles, materials, cooling systems, and applications. Advanced Optical Materials, 13(19), 2500138.

[2] Huang, G. (2024). 1550 nm wavelength single photon avalanche diodes: design rules of double Zn diffusion and floating guard rings for premature edge breakdown suppression in planar InGaAs/InP SPADs (Doctoral dissertation, University of Sheffield).

[3] Chen, Y. C., Yan, R. H., Huang, H. C., Nieh, L. H., & Lin, H. H. (2023). Guard ring design to prevent edge breakdown in double-diffused planar InGaAs/InP avalanche photodiodes. Materials, 16(4), 1667.

Development of NiO/Ga_2O_3 Heterostructures for Solar-Blind UV Photodetector Applications: The Effect of Ga_2O_3 Film Thickness

E. E. Bulut[1, 2], E. Şenadım Tüzemen[1, 2,*]

[1] Department of Physics, Faculty of Science, Sivas Cumhuriyet University, 58140 Sivas, Türkiye

[2] Sivas Cumhuriyet University Nanophotonics Application and Research Center-CÜNAM, 58140 Sivas, Türkiye

*Corresponding author, E-mail: esenadim@cumhuriyet.edu.tr

Abstract

Gallium Oxide (Ga_2O_3) has emerged as a promising material for solar-blind UV photodetector applications today, thanks to its wide bandgap, high optical transmittance, and superior chemical and thermal stability. In this study, Sapphire/NiO/Ga_2O_3 heterostructures were fabricated at different Ga_2O_3 film thicknesses using the RF magnetron sputtering method. During the deposition process, film thicknesses were precisely controlled using a quartz crystal microbalance (QCM). While the thickness of the NiO layer was kept constant at 250 nm, the thicknesses of the Ga_2O_3 layers were adjusted to 150, 200, and 250 nm, respectively. The structural and optical properties of the resulting thin films and heterostructures were systematically investigated. The characterization results revealed that variations in Ga_2O_3 film thickness have a significant effect on the optical properties of the heterostructures. These results indicate that film thickness is a key design parameter for optimizing the performance of solar-blind UV photodetectors based on NiO/Ga_2O_3 heterojunctions. This study provides important insights into the development of NiO/Ga_2O_3 heterostructures, produced via the RF magnetron sputtering method, for solar-blind UV photodetector applications.

Keywords: RF magnetron sputtering, Gallium oxide (Ga_2O_3), Nickel oxide (NiO), Solar-blind UV photodetector

Acknowledgements

This work was supported by the TUBITAK-1005 under Project Number 125F302.

References

[1] H. Hopoğlu et al., "Investigating the optical, electronic, magnetic properties and DFT of NiO films prepared using RF sputtering with various argon pressures," Physica B: Condensed Matter, 661, 414937 (2023).

[2] K. Tang et al., "NiO/Ga_2O_3 heterojunction for transparent and flexible solar-blind UV photodetector application," Physica B: Condensed Matter, 713, 417366 (2025).

[3] M. Amari et al., "A self-powered and flexible deep ultraviolet photodetector based on NiO/Ga_2O_3 heterojunction and employing stable MXene electrodes", Sensors and Actuators A: Physical 373, 115360 (2024).

Phase-Engineered Symmetry Breaking in Bulk Silicon With Composite Optical Vortices

Rana Asgari Sabet[1], Ufuk Can Bozkurt[1], Beliz Doğukaya[1], Alperen Saltık[1], Onur Tokel[1,2*]
[1]Department of Physics, Bilkent University, Ankara 06800, Türkiye
[2]National Nanotechnology Research Center, Bilkent University, Ankara 06800, Türkiye
*corresponding author, E-mail: otokel@bilkent.edu.tr

Abstract

Volumetric laser writing inside silicon enables the fabrication of buried microstructures and photonic devices while preserving the material's surface [1, 2]. At wavelengths within silicon's transparency window, tightly focused nanosecond laser pulses can drive nonlinear absorption and localized material modification in the bulk, enabling micro- and nanoscale features to be written beneath the intact surface. However, conventional scalar vortex beams, characterized by a helical phase and orbital angular momentum, generally produce rotationally symmetric focal intensity distributions, limiting direct control over asymmetric and chiral modification geometries. Composite vortex beams (CVBs), formed by superposing vortex fields with different topological charges, provide an additional degree of freedom for tailoring the transverse intensity distribution [3]. Here, we use holographically generated CVBs with controlled handedness to write planar-chiral structures within bulk silicon. The CVBs are generated using a spatial light modulator (SLM) digitally interleaving two vortex phase functions with a binary checkerboard mask. Radial phase modulation is incorporated into each vortex phase, enabling control over the resulting multi-lobed intensity distribution and its handedness [4]. The phase functions encoded on the two interleaved masks are $\Phi_1(r,\theta) = m\theta + \frac{(m-l)}{2}\nu r$, and $\Phi_2(r,\theta) = l\theta + \frac{(l-m)}{2}\nu r$, where r and θ are the radial and azimuthal coordinates, m and l are the topological charges, and ν is a modulation parameter. The magnitude |m-l| determines the azimuthal lobe multiplicity, whereas the sign of ν determines the handedness of the intensity distribution. For (m,l)=(2,-2) and (3,-3), the resulting four- and six-lobed focal distributions produce corresponding four- and sixfold laser-written morphologies (**Fig. 1a**). Reversing the sign of ν generates mirror-image structures with opposite handedness (**Fig. 1b**). These results demonstrate phase-only control over both rotational symmetry and handedness in subsurface structures**.** This approach expands the geometrical control available in volumetric laser processing and enables handed microstructures to be generated without requiring a multi-arm interferometer.

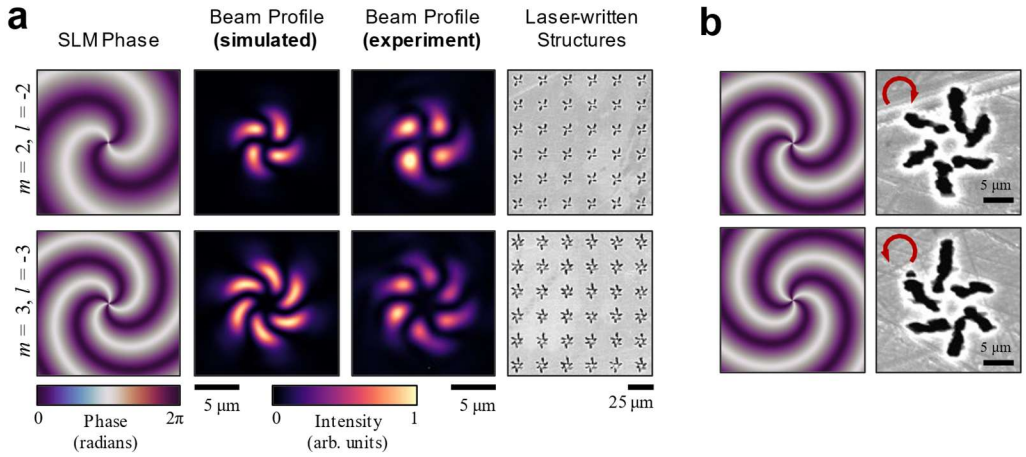

Figure 1. a Applied SLM phase masks, simulated and experimental focal transverse beam profiles, and scanning electron microscope images of the resulting structures for CVBs formed by the superposition of vortex beams with topological charges m and l and ν = 0.01. The pulse energies used for each topological charge pair (m, l) are: 3 µJ for (2, -2), and 5 µJ for (3, -3). **b** Mirror image pair of structures generated by CVBs of (m=3, l=-3) and opposite handedness (ν = ± 0.01).

Keywords: Vortex Beams, Topological Charge, Chirality, Laser Writing, Silicon Photonics

Acknowledgements: The authors acknowledge support from TÜBİTAK 1001 project No.: 121F387.

Referanslar / References

[1] Tokel, O. *et al*. In-chip microstructures and photonic devices fabricated by nonlinear laser lithography deep inside silicon. *Nat. Photonics* 11, 639–645 (2017).
[2] Asgari Sabet, R., Ishraq, A., Saltık, A., Bütün, M. & Tokel, O. Laser nanofabrication inside silicon with spatial beam modulation and anisotropic seeding. *Nat. Commun.* 15, 5786 (2024).
[3] Maleev, I. D. & Swartzlander, Jr., G. A. Composite optical vortices. *J. Opt. Soc. Am. B* 20, 1169 (2003).
[4] Li, J., Yan, J., Jiang, L., & Qu, L. Chiral Lithography with Vortex Non-diffracted Laser for Orbital Angular Momentum Detection. *Laser Photon. Rev.* 18, (2024).

Layer-Selective Laser Nanofabrication within Silicon-on-Insulator Platform

Rana Asgari Sabet[1,2], Enis Furkan Uçar[1,2], Onur Tokel[1,2*]
[1]Department of Physics, Bilkent University, Ankara 06800, Türkiye
[2]National Nanotechnology Research Center, Bilkent University, Ankara 06800, Türkiye
*corresponding author, E-mail: otokel@bilkent.edu.tr

Abstract

Silicon-on-insulator (SOI) platforms comprising a device layer, buried oxide (BOX), and a silicon handle substrate, form the basis for conventional silicon photonics and a growing range of electronic, optoelectronic, and quantum technologies. Established SOI nanofabrication, however, remains confined to the near-surface device layer, leaving the vertical extent of both layers largely inaccessible for further functionality. Direct writing into these buried volumes at selected depths could enable layer-selective, three-dimensional (3D) architectures within a standard SOI stack. Achieving this requires optical energy to traverse multiple interfaces and be deposited selectively within the targeted silicon layer without modifying the intervening layers. In transparent semiconductors, this balance is governed by nonlinear propagation and absorption, which can both inhibit and localize internal energy deposition [1].

Building on previous demonstrations of direct micro- and nanofabrication in bulk silicon using Gaussian and Bessel beams [2,3], we demonstrate layer-selective volumetric nanofabrication in SOI using nanosecond pulses at 1.55 µm, where both silicon and the BOX are linearly transparent. A spatial light modulator generates a Bessel beam that is focused at prescribed depths in the SOI stack, while the sample is translated in three dimensions. Under device-side illumination and with the polarization parallel to the scan direction, transverse scanning writes planar nanostructure arrays at selected depths *selectively* in the device or handle layer. Cross-sectional scanning electron microscopy (SEM) following brief etching reveals buried nanostructures at multiple depths throughout the 155-µm-thick device layer and within the 1-mm-thick handle layer (**Fig. 1**). These results demonstrate independent depth addressability across the SOI stack and establish Bessel-beam writing as a route toward embedded 3D functionality without wafer bonding or layer removal.

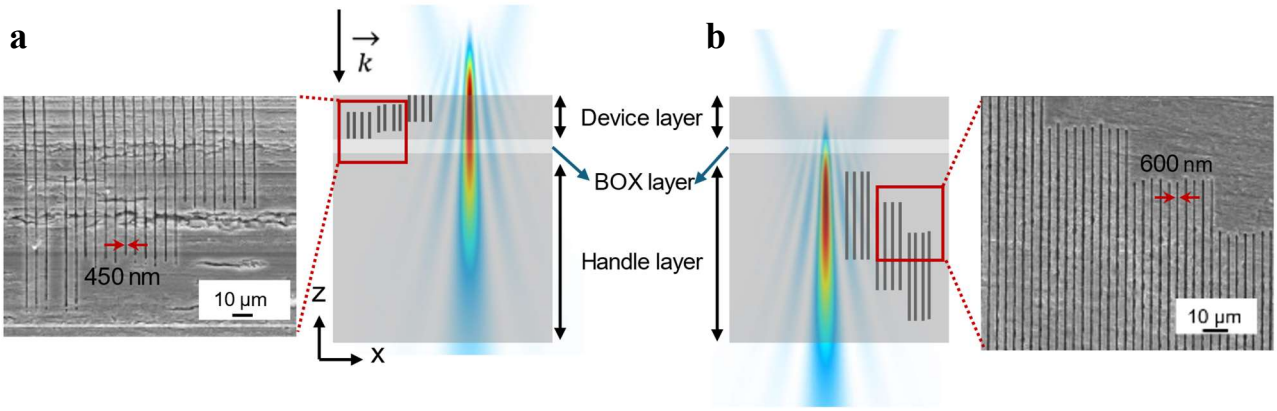

Figure 1. Laser nanofabrication in the SOI platform using a Bessel beam. **(a)** Nanofabrication in the device layer of SOI. SEM image of nanostructures at varying depths buried in the device layer of 155 µm. The average feature size is measured to be 450 ± 60 nm. **(b)** Nanofabrication in the handle layer of SOI. SEM image of completely buried nanostructures in the handle layer of 1 mm. BOX layer of thickness 1 µm does not preclude the nano-structuring. Device and handle layers are p-type/Boron-doped, with 1-5 Ω.cm resistivity.

Keywords: Silicon On Insulator (SOI), Laser Nanofabrication, Bessel Beam, 3D modifications.

Acknowledgments: TUBITAK 2247-A National Outstanding Researchers Program Project No:123C530

Referanslar / References

[1] Chambonneau, M., Blothe, M., Fedorov, V.Y. et al. Extreme optical nonlinearities unveiled by ultrafast laser filamentation in semiconductors. *Nat. Commun.* 17, 1701 (2026).

[2] Tokel, O. et al. In-chip microstructures and photonic devices fabricated by nonlinear laser lithography deep inside silicon. *Nat. Photonics* 11, 639–645 (2017).

[3] Asgari Sabet, R., Ishraq, A., Saltık, A., Bütün, M. & Tokel, O. Laser nanofabrication inside silicon with spatial beam modulation and anisotropic seeding. *Nat. Commun.* 15, 5786 (2024).

Integrated Metasurfaces for efficient portable Raman Spectroscopy

Deniz Atmaca*[1], Junyeop Lee[2], Mizan Karavar[1], Alpan Bek[1], Hamza Kurt[2]
[1] *Department of Physics, Middle East Technical University, 06800, Ankara, Türkiye*
[2] *Korea Advanced Institute of Science and Technology (KAIST), Daejeon, Republic of Korea*
deniz.atmaca@metu.edu.tr

Özet / Abstract

Conventional diffraction gratings in portable Raman spectrometers suffer from polarization dependence and limited Raman spectrometers capable of high-sensitivity, high-resolution measurements are typically large benchtop instruments, limiting their use in on-site, field-based analysis. Achieving a portable Raman spectrometer requires shrinking the optical components, and conventional diffraction gratings—bulky and inherently polarization-sensitive—are a key bottleneck. Metasurfaces, arrays of subwavelength nanostructures that tailor the amplitude, phase, and polarization of light within an ultrathin, planar footprint, offer a compact alternative. To address this, we developed an inverse-designed metasurface diffractive element as a compact, polarization-independent, broadband replacement, integrated into a Czerny–Turner portable spectrometer architecture. An open-box prototype combining the metasurface, laser, CCD-based detector, and control electronics was assembled and functionally tested. A custom automated angular-resolved scatterometry setup was built to characterize the metasurface's diffraction across angle and polarization. The metasurface achieves 61% diffraction efficiency, meeting the ≥60% target, and exhibits multi-order diffraction, with polarization independence observed at higher diffraction orders. Design optimization to extend this polarization independence to the fundamental order is ongoing.

Anahtar Kelimeler / Keywords: Metasurfaces, Raman spectroscopy, portable spectrometer, polarization independence

Acknowledgements

The authors gratefully acknowledge the financial support from the Scientific and Technological Research Council of Türkiye (TÜBİTAK) under Grant No. 124N875.

Referanslar / References

[1] K. C. Bantz et al., “Recent progress in SERS biosensing,” Phys. Chem. Chem. Phys., vol. 13, no. 24, p. 11551, 2011, doi: 10.1039/c0cp01841d.
[2] A. Kudelski, “Analytical applications of Raman spectroscopy,” Talanta, vol. 76, no. 1, pp. 1–8, Jun. 2008, doi: 10.1016/j.talanta.2008.02.042.
[3] J. Kim, B. Neseli, J. -Y. Kim, J. Yoon, H. Yoon, H. -H. Park, and Hamza Kurt, “Inverse design of on-chip optical response predictor enabled by deep neural network,” Opt. Express vol. 31, no 2, pp. 2049-2060, 2023, doi:10.1515/nanoph-2019-0474.
[4] J. F. Kelly, T. A. Blake, B. E. Bernacki, and T. J. Johnson, “Design Considerations for a Portable Raman Probe Spectrometer for Field Forensics,” Int. J. Spectrosc., vol. 2012, pp. 1–15, Sep. 2012, doi: 10.1155/2012/938407.

Desing and Simulation-Based Photometric Assessment of Integrated Front Fog and Cornering Functions Using a Single Freeform Optic

Kaan TURAN[1,2], Fatih GÖREN[2]

[1]*Kocaeli University, Department of Electro-Optical Systems Engineering, Kocaeli, Türkiye*
[2]*FARBA Automotive Inc., Gebze/Kocaeli, Türkiye*
corresponding author, E-mail: kaan.turan@farba.com.tr

Abstract

Integrating multiple automotive front-lighting functions within limited packaging space requires precise control of luminous flux and compliance with photometric regulations. This study presents a single-piece polycarbonate (PC) freeform lens designed to combine front fog and cornering functions within one optical element. The lens geometry was developed in Ansys Speos using non-sequential ray tracing and iterative surface optimization, considering the LED emission distribution, material refractive properties, installation axis, packaging constraints, and prescribed angular targets. The front fog distribution was designed to cover −45° to +45°, whereas the cornering region extended from +30° to +60°, with +30° to +45° serving as a shared transition zone. Simulation-based photometric evaluation indicated compliance with the relevant control points of UN Regulation No. 149, which consolidates the requirements previously specified in UN Regulations Nos. 19 and 119. The combined distribution provided continuous lateral coverage of 45° inboard and 60° outboard, together with comparatively uniform road illumination extending to approximately 60 m. These results demonstrate the feasibility of integrating two distinct lighting functions using a single freeform optic. The proposed architecture can reduce component count, packaging volume, and alignment interfaces while maintaining application-specific photometric performance, offering a compact solution for multifunctional automotive front-lighting systems. Unlike rotationally symmetric lenses, freeform surfaces provide spatially varying curvature and enable local control of ray direction [1]. In this study, a single polycarbonate (PC) freeform lens was developed to generate both front fog and cornering distributions within the available packaging volume. The non-sequential optical model incorporated the LED radiation pattern, PC refractive properties, source-to-lens distance, vehicle installation axis, and mechanical boundaries. Two angular targets were defined: −45° to +45° for the front fog function and +30° to +60° for the cornering function. The region between +30° and +45° was treated as a shared transition zone to support both functions and prevent abrupt intensity variations. The initial lens geometry was constructed from the available package envelope and subsequently optimized in Ansys Speos. Local surface regions were iteratively modified to redirect the incident flux toward the prescribed angular zones [2,3]. The optimization criteria included luminous-intensity compliance at regulatory test points, horizontal coverage, distribution continuity, road-illumination uniformity, optical efficiency, and stray-light suppression. Surface smoothness, minimum wall thickness, edge thickness, local curvature, and injection-molding feasibility were evaluated simultaneously. The final geometry therefore represented a compromise among photometric performance, compact packaging, and manufacturability while enabling two lighting functions to be realized with a single optical component.

Keywords: Freeform optics, automotive lighting, front fog lamp, cornering lighting, photometric optimization, non-sequential ray tracing.

a) b) c)

Figure 1: a) Freeform optic designed with Ansys Speos design program b) Freeform optic realistic render image c) Coverage from approximately −45° to +60° for the combined front fog and cornering functions

Acknowledgements

The authors acknowledge FARBA Automotive Inc. for its support of this study

References

[1] C.-C. Sun, C.-S. Wu, Y.-S. Lin, Y.-J. Lin, C.-Y. Hsieh, S.-K. Lin, T.-H. Yang, Y.-W. Yu, Review of optical design for vehicle forward lighting based on white LEDs, Optical Engineering 60(9), 091501 (2021).
[2] H. Wang, X. Li, P. Ge, Design of an optical lens combined with a total internal reflection (TIR) freeform surface for a LED front fog lamp, Optics & Laser Technology 88, 11–16 (2017).
[3] H. Wu, X. Zhang, P. Ge, Design method of a light emitting diode front fog lamp based on a freeform reflector, Optics & Laser Technology 72, 125–133 (2015).

Improving SERS Sensitivity Using Metal Nanoparticles in Textured Silicon Cavities

Okan Atiker, Zeynep Cantürk, Ghazanfar Ali Khan, Alpan Bek

Department of Physics, Middle East Technical University, 06800, Ankara, Türkiye

Abstract

Raman spectroscopy is widely used in many fields to identify molecules or materials such as pollution monitoring, narcotics detection, and food safety analysis. Because Raman spectroscopy conventionally produces inherently weak signals, surface enhancement techniques are employed to improve detection sensitivity, which are called surface-enhanced Raman spectroscopy (SERS). Over the past decades, many strategies have been developed to improve SERS substrates and to increase Raman enhancement factors. One of these approaches is surface texturing through various etching processes, while another one is using metal nanoparticles such as silver or gold to generate plasmonic enhancement.

In this study, we aim to fabricate SERS substrates using the photochemical etching method and metal-assisted photochemical etching. In addition, the incorporation of metal nanoparticles onto these cavity surfaces is investigated to further improve the plasmonic enhancement. For this purpose, Au nanoworms (AuNWs) were incorporated onto Ag-coated textured Si surfaces, and Raman measurements were performed using crystal violet (CV) as the analyte at 532 nm. The experimental SERS response of the hybrid substrate was compared with Ag-coated textured Si and AuNWs on flat Si. A significant improvement in the EF was observed for the hybrid substrate, reaching 2.09×10^7, corresponding to a 3.5-fold improvement compared with Ag-coated textured Si and a 3.34-fold improvement compared with AuNWs on flat Si. Furthermore, 3D FDTD simulations of the experimental configurations showed that combining AuNWs with the Ag-coated cavity provides the highest local electromagnetic field enhancement. The simulations predicted a 3.44-fold improvement for the hybrid configuration, which is in close agreement with the experimentally observed 3.5-fold enhancement. These results show that combining surface texturing with metal nanoparticles provides an effective strategy to further improve SERS sensitivity.

Keywords: SERS, Raman spectroscopy, photochemical etching, FDTD simulations, gold nanoparticles.

Acknowledgements

The authors would like to thank TÜBİTAK for supporting this work under Grant No. 123M819, ODTÜ Central Laboratory for providing the TEM images, and ODTÜ GÜNAM for providing access to their facilities. Z.C. also acknowledges TÜBİTAK for support under Grant No. 124N875. G.A.K. acknowledges ALLCHEMY KIMYA SAN. TIC. A.Ş. for financial support.

References

[1] J. Zheng et al., *Chem. Rev.* 121 (2021) 13342–13453.
[2] Y. Qi et al., *J. Alloys Compd.* 776 (2019) 934–947.
[3] Akbıyık *et al.*, *Adv. Optical Mater.* **10**, 2200114 (2022). — Photochemical Si texturing / SERS substrate
[4]G. A. Khan, A. Bek, J.-F. Masson, and W. Ahmed, *Colloids Surf. A* **713**, 136451 (2025). — Au–Ag NW synthesis and controlled $HAuCl_4$ etching.
[5] P. B. Johnson and R. W. Christy, *Phys. Rev. B* 6 (1972) 4370–4379.
[6] E. D. Palik (Ed.), *Handbook of Optical Constants of Solids*, Academic Press.
[7] Khan, G. A. *et al.*, Colloids Surf. A 619 (2021) 126542.
[8] Khan, G. A. *et al.*, Vib. Spectrosc. 120 (2022) 103359.

Inverse Design of Heat-Reflecting Multilayer Coatings for Vehicle Glazing via a Physics-Informed Data-Driven Tandem Neural Network

Furkan ÇÖZELİ[*1], İsa HATİPOĞLU[1,2]

[1]*Photonics Science and Engineering, Graduate School of Natural and Applied Sciences, Gazi University, Ankara, Türkiye*

[2]*Department of Photonics, Faculty of Applied Sciences, Gazi University, Ankara, Türkiye*

*Corresponding author, E-mail: cozelifurkan117@gmail.com

Abstract

Solar heat gain through vehicle glazing raises cabin temperature and air-conditioning load, while ECE R43 sets a minimum light transmittance for glazing in the driver's field of vision [2]. A heat-reflecting coating must therefore transmit visible light efficiently (VLT, 380-780 nm) while rejecting most near-infrared solar energy (SER, 780-2500 nm). Five-layer dielectric/metal/dielectric/metal/dielectric (DMDMD) stacks with thin silver films can satisfy both requirements, but their design is a challenging inverse problem: discrete material choices and continuous thicknesses must be optimized together, and conventional optimization is restarted for every new target. In this study, we develop a physics-informed, data-driven tandem neural network that designs DMDMD coatings directly from a target spectrum, using SiO_2, TiO_2, Si_3N_4 and Al_2O_3 as dielectrics and silver as the metal. A training set of 500,000 stacks was generated with the transfer matrix method (TMM) and cross-validated against RCWA; the two agree to within MSE $\approx 1.05\times10^{-16}$. Spectral weighting follows ISO 9050 and the AM1.5G spectrum of ASTM G173 [3,4]. A forward surrogate provides differentiable structure-to-spectrum prediction while the inverse network returns layer materials and thicknesses from the target spectrum; band-weighted spectral losses, direct VLT and SER losses, cycle consistency and Gumbel-Softmax sampling embed the physics, and candidates are re-ranked and refined by the exact TMM. The trained network meets the target metrics within ±0.01, recovers the critical silver thickness with 0.6 nm mean absolute error and proposes manufacturable designs within milliseconds; a representative Si_3N_4/Ag/Al_2O_3/Ag/TiO_2 stack (35/15/105/14/25 nm) attains 88.8% VLT, 94.4% SER and 53.0% TSER.

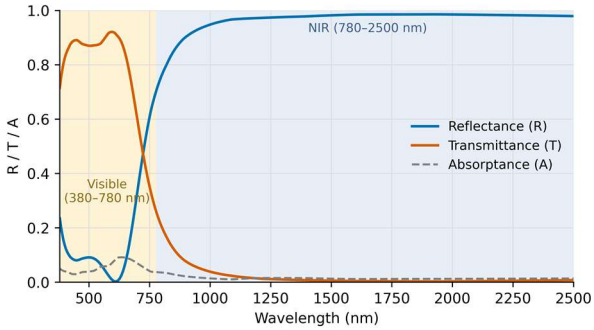

Figure 1: Computed reflectance (R), transmittance (T) and absorptance (A) spectra of the selected Si_3N_4/Ag/Al_2O_3/Ag/TiO_2 (35/15/105/14/25 nm) stack.

For comparison, the TiO_2/Ag/TiO_2/Ag/TiO_2 metafilm (32/15/69/15/28 nm) of Wu et al. [1] was recomputed with the same TMM and optical constants. The proposed design rejects a larger share of near-infrared and total solar energy (94.4% vs. 92.1% SER; 53.0% vs. 51.3% TSER) at a comparable visible transmittance (88.8% vs. 89.7%), indicating that the tandem network offers a practical route to rapid, specification-driven design of solar-control coatings.

Keywords: inverse design, tandem neural network, physics-informed learning, thin film, solar control coating, DMDMD

References

[1] B. Wu, Y. Ren, X. Huang, M. Chen, Y. Li, J. Li, Y. Kou, X. Wu, "Transparent metafilms for enhanced thermal regulation in energy-efficient windows," Nanophotonics 14(22), 3645-3656 (2025).

[2] UNECE Regulation No. 43, Uniform provisions concerning the approval of safety glazing materials and their installation on vehicles (2019).

[3] ISO 9050:2003, Glass in building - Determination of light transmittance, solar direct transmittance and total solar energy transmittance.

[4] ASTM G173-03 (2020), Standard Tables for Reference Solar Spectral Irradiances: Direct Normal and Hemispherical on 37 Degree Tilted Surface.

Magnetically Actuated Composite Vocal Fold Phantom for CT/TA Muscle Mimicry

O. Tavlı[1], K. Erdil[1,2,*], A.K. Dağıstanlı[2], Y.D. Gökdel[1], O. Ferhanoğlu[2]
[1]Electrical and Electronics Engineering, Istanbul Bilgi University, 34060, Türkiye
[2]Electronics and Communication Engineering, Istanbul Technical University, 34469, Türkiye
*erdil21@itu.edu.tr

Abstract

We present a magnetically actuated vocal fold phantom phonation system capable of reproducing longitudinal tension modulation to mimic cricothyroid (CT) and thyroarytenoid (TA) muscle activation. We first formulate the electromagnetic force model and describe how the resulting artificial muscle activation alters longitudinal stiffness, transverse stiffness, and vibratory behavior. Vocal fold phantoms are fabricated using room temperature vulcanizing (RTV) silicone mixed with Fe powder and cast in 3D-printed molds. Leveraging gravity during curing, the Fe powder is concentrated near the transverse surface closest to the actuation coil, enhancing magnetic responsiveness while maintaining tissue-like mechanical properties. Finite-element simulations are used to investigate how longitudinal loading modifies vibratory modes and dynamics, and the analytical and simulation results are validated experimentally using laser Doppler vibrometry (LDV) and knife-edge optical sensing. Magnetic actuation enabled longitudinal elongations up to 2.0 mm, providing a tunable phonation frequency range of 127–191 Hz with a response time of 41–44 ms, consistent with simulation and with physiologically observed laryngeal muscle activation timescales. Repeatability testing over 10 hours revealed only ±95 µm standard deviation in elongation, demonstrating the reliability and stability of both the actuator and the phantom. These results establish a tunable, muscle-mimicking testbed for controlled investigations of tension-dependent phonatory mechanics and for validating computational laryngeal models, supporting future laryngological research.

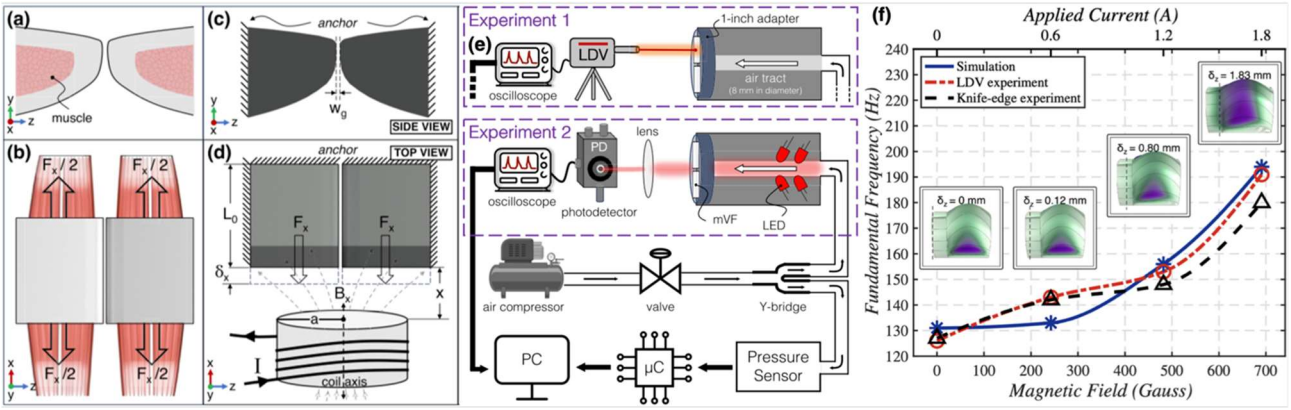

Figure 1: FIGURE 1. Overview of the magnetically actuated vocal fold phantom platform. (a) Side-view and (b) top-view schematics of the human vocal folds, showing the muscular forces (F_x) along the longitudinal direction. (c) Side view and (d) top view of the fabricated phantom, indicating the anchored regions, key geometric parameters, and the coil generating the applied magnetic field (B_x). The x, y, and z axes denote the longitudinal, vertical, and transverse directions of the vocal fold, respectively. (e) Experimental setups used to quantify self-oscillation as a function of magnetic force: LDV (Experiment 1) and knife-edge sensing (Experiment 2). (f) Self-oscillation frequency of the phantom versus magnetic field strength and drive current; insets show the FEM-simulated longitudinal displacement at each field, with vertical dashed lines marking the initial vocal fold length. [1]

Keywords: Biomechanical modeling, composite vocal fold phantom, finite element analysis, magnetic actuation, muscle mimicry, phonation mechanics, self oscillation, soft tissue biomechanics, tension modulation, tunable vocal fold model.

Acknowledgment: This work was supported by TÜBİTAK under Project 125E231.

References:

[1] Tavli, O., Erdil, K., Dagistanli, A. K., Gokdel, D., & Ferhanoglu, O. (2026). Magnetically Actuated Composite Vocal Fold Phantom for CT/TA Muscle Mimicry. IEEE Access.

A Portable and Low-Cost Spirometer with Knife-Edge Optical Detection

Sena Ulgaz*[1], Ömer Gökalp Akcan[1,3], Berkay Yılmaz[2], Onur Ferhanoglu[1], Yiğit Dağhan Gökdel[2]

[1]Department of Electronics and Communication Engineering, Istanbul Technical University, 34467, Istanbul, Türkiye.

[2]Department of Electrical and Electronics Engineering, Istanbul Bilgi University, 34060, Türkiye.

[3]Advanced Vocational Studies, Big Data Analytics, Istanbul Bilgi University, 34387, Istanbul, Türkiye.

Corresponding author, E-mail: akcan21@itu.edu.tr

Abstract

We present a portable, low-cost optical spirometer that addresses moisture-induced degradation observed in our previous graphite-coated disposable airflow sensor. The system removes electrical sensing elements from the airflow path and uses knife-edge optical detection. A red LED array inside an SLA-printed tube illuminates a compliant double-leaf sensor. Airflow-induced deflection progressively unblocks the beam, which is collected by a convex lens and focused onto a photodetector for electrical recording and computer-based post-processing.

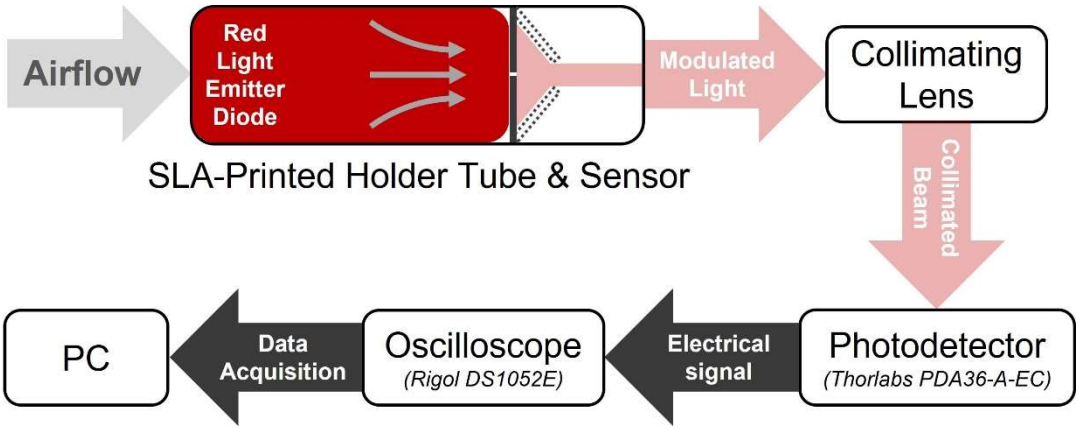

Figure 1: Block diagram of the light-intensity-based air pressure measurement setup.

The sensor comprises two semicircular leaves with a radius of 9.5 mm and thickness of 0.6 mm, separated by a 1.4 mm initial gap and supported by 3 mm cantilever beams. FEM analysis at 11.732 kPa yielded a maximum deflection of 7.22 mm while avoiding plastic deformation in typical spirometry pressure ranges. Controlled airflow tests from 0 to 700 kPa showed a linear response up to 160 kPa with 0.04 V/kPa sensitivity ($R^2 = 0.995$, RMSE = 0.1431). Forced exhalation and inhalation tests with four participants produced distinct respiratory profiles, supporting the system's potential for moisture-resistant, scalable, disposable respiratory monitoring. The optical geometry places the sensor 6 cm from the LED array, followed by a 9 cm propagation distance to the convex lens and a 3.5 cm lens-to-photodetector spacing. The double-leaf sensor is SLA printed using Anycubic Tough Resin Ultra-Gray ($E = 1.35$ GPa, $\rho = 1118$ kg/m^3). Above 160 kPa, nonlinear mechanical deformation and photodetector saturation reduce linearity. Future work will focus on ray-tracing optimization, testing with a larger number of subjects, and compact electronics integration for real-time portable healthcare applications [1]

Keywords: Spirometer, Optical sensing, Knife-edge optics, MEMS airflow sensor, Disposable sensors.

References

[1] S. Ulgaz, Ö. G. Akcan, B. Yılmaz, O. Ferhanoglu, and Y. D. Gökdel, "A Portable and Low-Cost Spirometer with Knife-Edge Optical Detection," EUROSENSORS 2026, (accepted).

Graphitic Polyimide-AuNP Substrates for Fluorescence-Quenched SERS

***Nil Su Gen*[1], *Dogac Tuzel*[1], *Ghazanfar Ali Khan*[1], *Sinan Genc*[1,3], *Sumeyye Kina*[2], *Alpan Bek*[1], *Kamil Cinar**[2]**

[1] *Department of Physics, Middle East Technical University, 06800, Ankara, Türkiye*
[2] *Department of Physics, Gebze Technical Universtiy, 41400, Kocaeli, Türkiye*
[3] *Department of Elextrical-Electronics Engineering, Abdullah Gül Universtiy, 38080, Kayseri, Türkiye*
kcinar@gtu.edu.tr

Abstract
Surface-enhanced Raman spectroscopy (SERS) is a widely used, non-destructive method for molecular identification, yet its application is often limited by the intrinsic weakness of Raman scattering and by fluorescence that can completely mask the Raman peaks [1]. Fluorescence is commonly avoided by shifting to longer excitation wavelengths, but since the Raman intensity scales as $I \propto \lambda^{-4}$, this sacrifices signal, moving from 532 nm to 1064 nm alone reduces the intensity roughly 16-fold. In this work, we instead suppress fluorescence at the substrate level by forming a graphitic surface on a polyimide (Kapton) tape with a short-pulse laser, a cheap and simple alternative to the many delicate steps that SERS substrate preparation usually requires. The graphitic regions quench fluorescence through charge- and energy-transfer mechanisms, while colloidally synthesized gold nanoparticles (AuNPs) provide strong electromagnetic enhancement at their absorption peak [2,3].

Spherical AuNPs were synthesized through the reduction of chloroauric acid ($HAuCl_4$) with ascorbic acid, and drop-cast onto both pristine and graphitic polyimide films [4]. The AuNP absorption peak (~520-526 nm) overlaps well with the 532 nm excitation, ensuring near-optimal plasmonic enhancement. The highly fluorescent dye Rhodamine 6G (R6G, quantum yield $\varphi \approx 0.9$ was deliberately chosen as the test analyte to probe the fluorescence-quenching performance under a worst-case scenario.

While AuNPs alone leave the R6G fluorescence strong enough to mask the Raman peaks, and the graphitic surface alone cannot enhance them, the combination of the two fully suppresses the fluorescence background and renders the Raman peaks clearly visible. The peak positions remain unchanged, and although the chemical interaction between R6G and the graphitic surface slightly lowers the peak intensities (~25% reduction), the signal-to-noise ratio improves from 9.2 to 12.1 (~32% increase) on the graphitic substrate. The low-cost fabrication operates under ambient conditions and is compatible with flexible, in-field SERS, showing potential for portable Raman sensing [5].

Keywords: SERS, Raman spectroscopy, fluorescence quenching, polyimide, gold nanoparticles.

Acknowledgements
The authors gratefully acknowledge the financial support from the Scientific and Technological Research Council of Türkiye (TÜBİTAK) under Grant No. 123M819.

References
[1] P. L. Stiles, J. A. Dieringer, N. C. Shah, R. P. Van Duyne, Surface-enhanced Raman spectroscopy, Annu. Rev. Anal. Chem. 1 (2008) 601–626.
[2] B. Sharma, R. R. Frontiera, A.-I. Henry, E. Ringe, R. P. Van Duyne, SERS: Materials, applications, and the future, Mater. Today 15 (2012) 16–25.
[3] S. A. Maier, Localized surface plasmons, in Plasmonics: Fundamentals and Applications, Springer-Verlag US, 2007, pp. 65–88.
[4] A. E. F. Oliveira, A. C. Pereira, M. A. C. Resende, L. F. Ferreira, Gold nanoparticles: A didactic step-by-step of the synthesis using the Turkevich method, mechanisms, and characterizations, Analytica 4 (2023) 250–263.
[5] X. Zhou et al., A highly-efficient, stable and flexible Kapton tape-based SERS chip, Mater. Chem. Front. 5 (2021).

Development of an Incubator-Integrated Electrochemical Platform for Cell-Based Analysis

Belguzar Karadag[1,2], Fatma Kurul[1,2], Meryem Beyza Avci[1,2,3], Seda Nur Topkaya[1,2], Arif E. Cetin[*1,2,3,4]

[1]Izmir Biomedicine and Genome Center, Balcova, Izmir 35340, Türkiye
[2]Izmir International Biomedicine and Genome Institute, Dokuz Eylul University, Balcova, Izmir 35340, Türkiye
[3]Department of Biophysics, Faculty of Medicine, Dokuz Eylul University, Izmir 35340, Türkiye
[4]Department of Electrical and Electronics Engineering, Istanbul Atlas University, Kagithane, Istanbul 34408, Türkiye

*corresponding author, E-mail: arifengin.cetin@ibg.edu.tr

Abstract

Electrochemical analysis methods are critical in studying cellular behavior due to their high sensitivity and versatility. However, challenges in maintaining physiological conditions during electrochemical measurements can affect data accuracy [1]. In this study, an incubator-integrated electrochemical analysis platform was developed to bridge the gap between conventional cell culture and electrochemical testing environments while maintaining *in vivo*-like conditions. The platform integrates a microfluidic module for cell-electrode interactions, an incubator module for controlled culture conditions, and a measurement module consisting of a screen-printed electrode (SPE) and potentiostat for real-time monitoring. A sample preparation device was also developed to enhance cell adhesion and minimize electrode surface degradation. The platform was evaluated using MCF-7 breast cancer cells to investigate cell adhesion, proliferation, and electrochemical responses at different cell densities. Furthermore, the applicability of the platform for drug efficacy assessment was investigated using a standard cancer drug. The results showed that the platform was able to distinguish different cell densities, monitor cell proliferation, and evaluate the efficacy of cancer drugs based on drug-induced electrochemical responses.

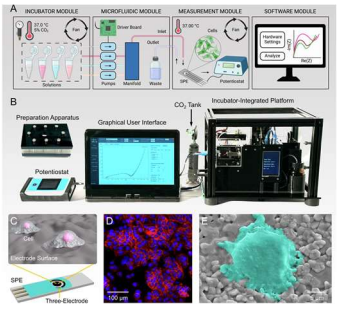

Figure 1: A Schematic representation and **B** photographic image of the electrochemical analysis platform integrated into the incubator, together with the sample preparation apparatus. **C** Schematic representation illustrating cells attached to the surface of the three-electrode configuration within the SPE. **D** Confocal laser scanning microscopy image showing MCF-7 cells stained with phalloidin and DAPI following 24 h of incubation on the SPE surface, with an initial cell density of 2.5 x 10^5 cells/mL. **E** SEM image of an MCF-7 cell attached to the electrode surface, displayed in false color (cyan).

Keywords: Electrochemical biosensor, screen-printed electrode, cancer cell monitoring, drug response

Acknowledgements
A.E.C. acknowledges The Scientific and Technological Research Council of Türkiye (TÜBİTAK) (Project No. 122E384).

References
[1] F. Kurul, M. B. Avci, H. B. Acar, S. N. Topkaya, and A. E. Cetin, "Incubator-integrated electrochemical analysis platform for cell-based studies," *npj Biosensing*, vol. 2, p. 6, 2025, doi: 10.1038/s44328-025-00030-5.

Axicon-Generated Bessel Beams for Subsurface Nanostructuring of Silicon

Bora Ünlü[1], Danyal Karadağ[1], Onur Tokel[1,2]
[1]Department of Physics, Bilkent University, Ankara, Türkiye
[2]UNAM – National Nanotechnology Research Center, Ankara, Türkiye
E-mail: otokel@bilkent.edu.tr

Abstract

Micro- and nanofabrication of semiconductors underpins modern electronics, computing, and artificial intelligence technologies. Conventional semiconductor fabrication methods are predominantly surface-based, creating a need for techniques capable of structuring bulk silicon. Direct laser writing offers a promising route toward this goal [1,2]. However, strong nonlinear propagation in silicon impedes localized deposition of optical energy deep within the material. Bessel beams can mitigate this limitation because their narrow central lobe remains quasi-invariant over an extended axial range [2]. Here, we demonstrate controlled subsurface nanostructuring in silicon using Bessel beams generated by a low-cost refractive axicon and relayed through a 4*f* optical system (Fig. 1), avoiding the need for an expensive infrared spatial light modulator (SLM). Using a refractive axicon with a physical angle of 1°, we fabricate arrays of buried nanoplanes with feature sizes as small as 100 nm (Fig. 1). The refractive axicon imparts a continuous, radially varying phase profile without spatial sampling or interpixel phase coupling intrinsic to pixelated SLMs, thereby limiting optical power redistribution into parasitic diffraction orders [3]. These results establish continuous-phase axicon beam shaping as a simple and cost-effective strategy for nanoscale three-dimensional laser patterning inside silicon.

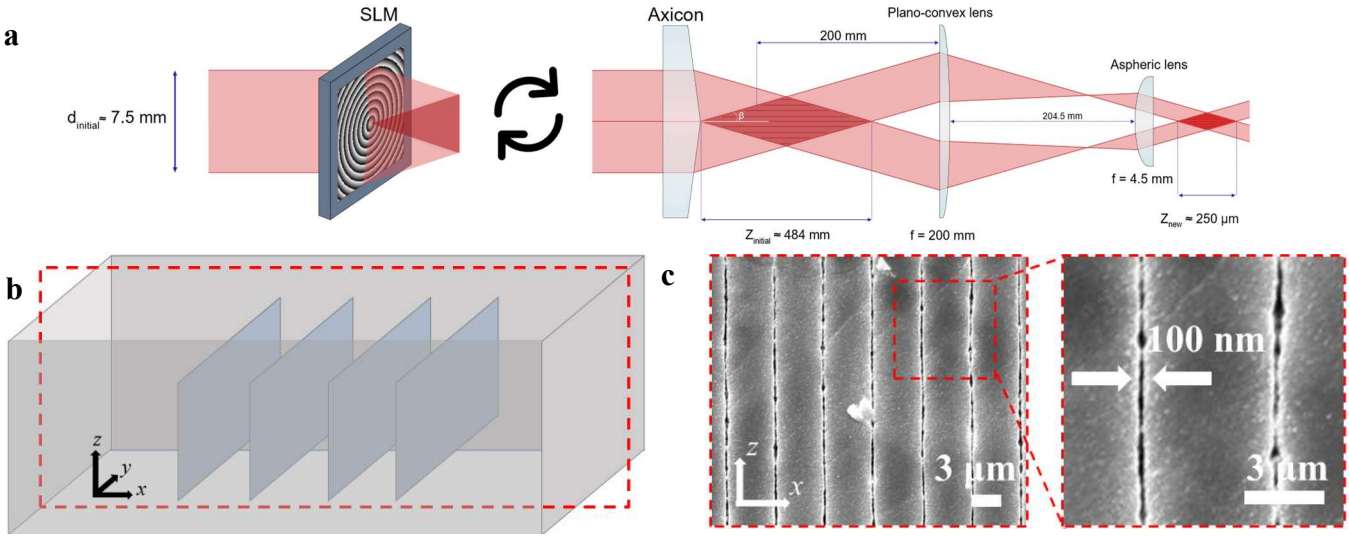

Figure 1. (a) Optical configuration for generating an axicon-based Bessel beam and demagnifying its Bessel zone using a 4*f* relay comprising a plano-convex lens ($f_1 = 200$ mm) and an aspheric lens ($f_2 = 4.5$ mm). **(b)** Schematic of nanoplanes inside Si. **(c)** Cross-sectional SEM images of fabricated nanoplanes, with feature sizes of 100 nm.

Keywords: Refractive axicons; Bessel beams, Laser nanofabrication, 3D nanostructuring.

Acknowledgements. The authors acknowledge support from TÜBİTAK 2209 project no: 1919B012558613.

References

[1] Asgari Sabet, R., Ishraq, A., Saltik, A. *et al.* Laser nanofabrication inside silicon with spatial beam modulation and anisotropic seeding. *Nat. Commun.* **15**, 5786 (2024).

[2] Li, ZZ., Fan, H., Wang, L. *et al.* Super-stealth dicing of transparent solids with nanometric precision. *Nat. Photon.* **18**, 799, (2024).

[3] Lingel, C., Haist, T. & Osten, W. Optimizing the diffraction efficiency of SLM-based holography with respect to the fringing field effect. *Appl. Opt.* **52,** 6877 (2013).

Development and Quantitative Characterization of a Multimodal Visible/Mid-IR Optoacoustic Imaging Platform

Utku Yerlikaya[1], Tuğba Güvercin[1], Eren Şakircan Hacıoğlu[1], Nasire Uluç*[1,2]
[1]*Department of Physics, Middle East Technical University, 06800, Ankara, Türkiye*
[2]*Physics Group, Middle East Technical University, Northern Cyprus Campus, Kalkanlı, Türkiye*
corresponding author, E-mail: nasire.uluc@metu.edu.tr

Özet / Abstract

Photoacoustic (optoacoustic) imaging combines wavelength-dependent optical absorption contrast with ultrasonic detection, enabling label-free interrogation of endogenous absorbers and molecular composition [1–3]. Here, we present a configurable dual-regime optoacoustic platform integrating a 532 nm Q-switched laser and a tunable mid-infrared quantum cascade laser (QCL, 905–1185 cm^{-1}), together with synchronized scanning, acquisition, and signal analysis through a custom MATLAB interface, as shown in Figure 1a.

Quantitative characterization demonstrated stable excitation and reproducible imaging. The 532 nm source exhibited 5.20% RMS variation over 68 min, while QCL measurements at 994–1120 cm^{-1} showed 1.78–2.62% RMS temporal variation, reduced to 0.18–0.23% with 60 s averaging (Figure 1d). Two ultrasound transducers provided axial resolutions of 35–42 µm and 60–66 µm, respectively, while lateral resolution was primarily governed by the optical excitation spot. Continuous line scanning reproduced conventional step-scan imaging with a correlation of 0.979, while reducing acquisition time from 15 to 5 min and improving SNR from 57 to 74, as shown in Figure 1b,c.

Beyond individual component characterization, the platform enables direct comparison of acquisition, acoustic detection, and signal-extraction strategies under matched experimental conditions. Measurements acquired with different transducers were evaluated using complementary signal metrics and depth-resolved analysis, revealing configuration-dependent differences in acoustic response and spatial information. Rather than prescribing a single detection or processing scheme, the developed framework enables application-dependent selection of optoacoustic acquisition and analysis parameters. These results establish a quantitatively characterized platform for ongoing label-free Mid-IR molecular imaging and subsequent biological applications.

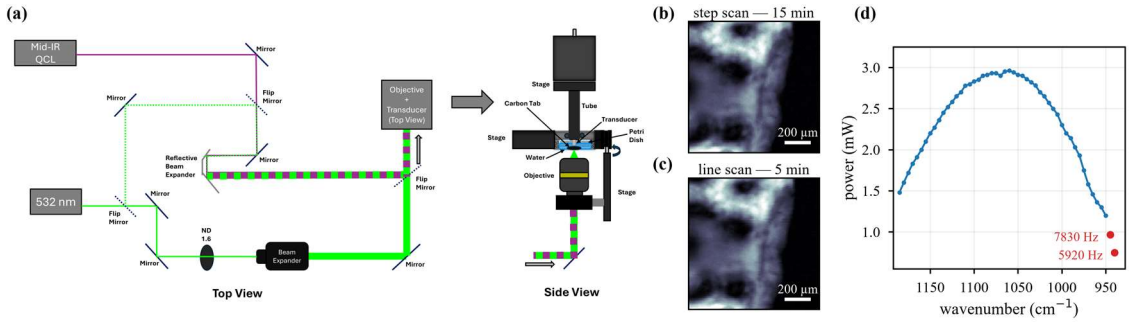

Şekil 1 / Figure 1: (a) Platform layout (top and side views); the 532 nm and mid-IR beams share one expanded path (dotted: alternative routes). (b,c) C-scans of a carbon target (532 nm) in step and continuous line mode (1 × 1 mm, 10 µm step, N = 100). (d) Measured QCL emission spectrum; the two red points were recorded at different pulse repetition rates (7830 and 5920 Hz).

Anahtar Kelimeler / Keywords: Optoacoustic imaging, mid-infrared quantum cascade laser, laser stability, instrument control software, line-scan imaging.

Acknowledgements
This work was supported by TÜBİTAK under the 2232-A International Fellowship for Outstanding Researchers Program (Project No. 124C513). The authors thank Prof. Dr. Alpan Bek and the Environmental Photonics Group at METU for their support.

Referanslar / References

[1] L. V. Wang and S. Hu, Science 335, 1458 (2012).
[2] N. Uluç, S. Glasl, F. Gasparin et al., Nat. Metab. 6, 678 (2024).
[3] J. Shi, T. T. W. Wong, Y. He et al., Nat. Photonics 13, 609 (2019).

Plasmon-Coupled hBN Defects: Scalable Emission Control by Silver Dewetting

***Sinan Genc*[1,2], *Oguzhan Yucel*[2,3], *Furkan Aglarci*[4], *Carlos Rodriguez-Fernandez*[5], *Alpay Yilmaz*[2], *Humeyra Caglayan*[5,6], *Serkan Ates*[4,7], *and Alpan Bek*[2*]**

[1] *Department of Electrical-Electronics Engineering, Abdullah Gül University, 38080, Kayseri, Türkiye*

[2] *Department of Physics, Middle East Technical University, 06800, Ankara, Türkiye*

[3] *Department of Physics, Freie Universität Berlin, 14195, Berlin, Germany*

[4] *Department of Physics, Izmir Institute of Technology, 35430, Izmir, Türkiye*

[5] *Department of Physics, Tampere University, 33720, Tampere, Finland*

[6] *Department of Electrical Engineering, Photonic Integration Group, Eindhoven University of Technology, 5600 MB Eindhoven, The Netherlands*

[7] *Faculty of Engineering and Natural Sciences, Sabancı University, 34956, Istanbul, Türkiye*

bek@metu.edu.tr

Abstract

Defect-based quantum emitters in hexagonal boron nitride (hBN) are promising building blocks for scalable quantum photonics owing to their stable single-photon emission at room temperature [1,2]. However, enhancing their emission intensity and controlling their decay dynamics remain significant challenges, since these emitters exhibit strong emitter-to-emitter variability and are difficult to integrate into photonic structures [3]. In this work, we demonstrate a low-cost, scalable fabrication route that integrates plasmonic nanocavities with defect-based emitters in hBN nanoflakes, building on prior efforts to couple hBN emitters to metallic nanostructures [4-6] but without requiring lithography or deterministic emitter positioning.

Using a thermal dewetting process, silver thin films (5 and 13 nm) are annealed at ~350 °C under nitrogen to form self-assembled Ag nanoparticles (AgNPs) with average diameters of ~35 nm and ~110 nm, following well-established solid-state dewetting behavior [8]. Two distinct configurations are realized: stochastic AgNPs directly on hBN flakes, and hybrid plasmonic nanocavities formed by AgNPs on hBN flakes supported on gold/silicon-dioxide (Au/SiO_2) substrates. The 20 nm SiO_2 spacer and 100 nm Au mirror thicknesses are determined by FDTD simulations to ensure broadband spectral overlap between the hBN zero-phonon-line emission and the scattering-dominated plasmonic response, exploiting the Purcell effect to tailor spontaneous emission [7].

Single-photon character is confirmed by second-order photon correlation measurements, with $g^{(2)}(0)$ values of 0.3 under continuous-wave and 0.1 under pulsed excitation. Small AgNPs quench the emission (up to ~8-fold) through enhanced nonradiative decay, whereas large AgNPs enhance it, driven by scattering-dominated plasmonic modes. While AgNPs on bare hBN yield up to a 2-fold photoluminescence enhancement with reduced emitter lifetimes, the hybrid nanocavity architecture provides a dramatic, up to 100-fold enhancement with improved uniformity across multiple emitters. FDTD simulations and time-resolved measurements confirm size-dependent control over decay dynamics and cavity–emitter interactions, offering a versatile route that overcomes key challenges in quantum photonic device development, including material integration, emission optimization, and spectral multiplexity.

Keywords: Single photon source, photoluminescence, nanocavity, dewetting, hexagonal boron nitride.

Acknowledgements

The authors acknowledge the financial support from the Scientific and Technological Research Council of Türkiye (TÜBİTAK) under Grant No. 118F119, the Middle East Technical University Postdoctoral Research Program (DOSAP-B), the Academy of Finland Flagship Programme (PREIN, 320165), and the Horizon 2020 Marie Skłodowska-Curie Grant Agreement No. 895369. The authors thank Selçuk Yerci for the workstation used in the computations, Vasilis Karanikolas for reviewing the calculations, and Melike Şeyma Tuna for help with the figures.

References

[1] Grosso, G. et al (2017). Nat. Commun., 8, 705. https://doi.org/10.1038/s41467-017-00810-2

[2] Tran, T.T. et al. (2016). Nat. Nanotechnol., 11, 37–41. https://doi.org/10.1038/nnano.2015.242

[3] Kianinia, M. et al. (2022). Appl. Phys. Rev., 9, 011306. https://doi.org/10.1063/5.0072091

[4] Xu, X. et al. (2023). Nano Lett., 23, 25–33. https://doi.org/10.1021/acs.nanolett.2c03100

[5] Nguyen, M. et al. (2018). Nanoscale, 10, 2267–2274. https://doi.org/10.1039/c7nr08249e

[6] Dowran, M. et al. (2023). Adv. Opt. Mater., 11, 2300392. https://doi.org/10.1002/adom.202300392

[7] Purcell, E.M. (1995). Springer, Boston, MA, p. 839. https://doi.org/10.1007/978-1-4615-1963-8_40

[8] Thompson, C.V. (2012). https://doi.org/10.1146/annurev-matsci-070511-155048

Design And Characterizatıon Of A Fiber Bragg Grating Based Hydrophone Array

S. Demiryakan[a*], F. Uyar[a,b], S. Dönertaş[a], S. Aldemir[a], A. Nehir[a], E. Özbay[a,b,c] and İ. Özdür[d]

[a]NANOTAM, Bilkent University, Ankara, Türkiye
[b]Department of Electrical and Electronics Engineering, Bilkent University, Ankara, Türkiye
[c]Department of Physics, Bilkent University, Ankara, Türkiye
[d]Department of Electrical and Electronics Engineering, TOBB ETU, Ankara, Türkiye
*serra.ulug@bilkent.edu.tr

Abstract
Fiber-based underwater acoustic sensors (hydrophones) are increasingly replacing conventional piezoelectric sensors thanks to their compact design, high sensitivity, and superior resistance to electromagnetic interference. In this context, Fiber Bragg Grating (FBG)-based hydrophone arrays have become an important research topic due to their ability to enable multi-point acoustic sensing and direction finding in deep ocean environments.

Hydrophones are fabricated by winding an optical fiber around a cylindrical mandrel and perform sensing through the phase change induced in the fiber by acoustic pressure. The fabrication process of FBG-based fiber optic hydrophones consists of three stages: manufacturing mandrel mechanics, winding the fiber onto the mandrel, and integrating the FBG. Following these stages, mandrel characterization is performed, after which the mandrels become ready for use as individual sensors. The single sensors are then joined by splicing the fiber segments between mandrels at predetermined distances, forming a 16-element array. Underwater tests of the resulting array are conducted using a rotating circular fixture, in which each mandrel is sequentially rotated to face the acoustic projector directly and is tested and characterized in this position.

In this study, the entire process—from the fabrication of individual FBG-based hydrophone sensors, through their integration into an array, to the testing and characterization of the resulting array under real underwater conditions—was demonstrated in practice. The results provide a practical framework for how FBG-based hydrophone arrays can be fabricated and tested for real-world underwater applications, laying the groundwork for future studies on the use of this technology in underwater acoustic sensing systems.

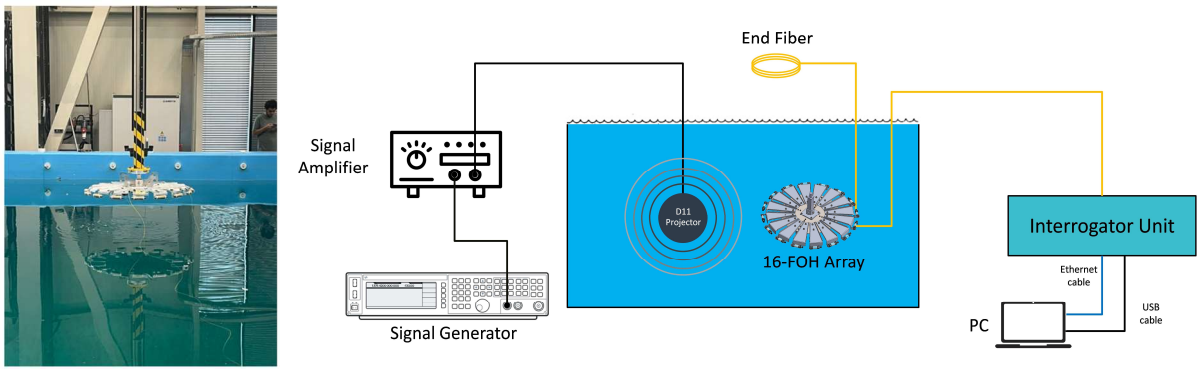

Figure 1: a) Experimental set-up of the underwater test tank with the rotating circular fixture used to characterize the FBG-based hydrophone array. b) Schematic diagram of the underwater acoustic test setup showing the signal generation, hydrophone array, and data acquisition chain.

Keywords: Fiber-optic hydrophone; Underwater acoustic sensing; Mandrel; Hydrophone array; Fiber Bragg Grating (FBG).

References
[1] M. Y. Plotnikov, V. S. Lavrov, P. Y. Dmitraschenko, A. V. Kulikov, and I. K. Meshkovskiy, "Thin Cable Fiber-Optic Hydrophone Array for Passive Acoustic Surveillance Applications," IEEE Sensors Journal, vol. 19, no. 9, pp. 3376–3382, May 2019, doi: 10.1109/JSEN.2019.2894323.

Atomik Oksijenin Silisyum Ve Germanyum Alt Taşlar Üzerindeki Tahribat Analizinin İncelenmesi

Utku Yaman Can ASLAN[1,2] , Süleyman ÖZÇELİK[1,2]
[1]Fotonik Bilimi ve Mühendisliği, Gazi Üniversitesi, 06560, Ankara.
[2]Fotonik Uygulama ve Araştırma Merkezi, Gazi Üniversitesi, 06500, Ankara.
u.yamancan@gmail.com ; sozcelik@gazi.edu.tr

Özet
Yerli uzay kalifiye çok eklemli güneş hücreleri ECSS-E-ST-20-08C Rev.1 standartında uv, proton, elektron ve termal testleri geçse de, Alçak Dünya Yörüngesinin (LEO) en yıkıcı etkeni olan Atomik Oksijen (AO) testlerinde altyapı kısıtı bulunmaktadır. Güneş'ten gelen sert UV fotonlarının ($\lambda < 243$ nm) moleküler oksijeni parçalamasıyla oluşan ve düşük gaz yoğunluğu sebebiyle LEO'da baskın tür haline gelen Atomik Oksijen radikalleri, ~7,8 km/s orbital hız nedeniyle yüzeylere ~5 eV kinetik enerjiyle çarpmaktadır. Bu yüksek enerjili bombardıman; anti-yansıtıcı kaplamaları aşındırarak optik geçirgenliği düşürmekte, hücre içi bağlantı yollarını oksitleyerek seri direnci artırmakta ve elektriksel performansı bozmaktadır. Uzay ajansları atomik oksijenin uzay araçlarının kaplamalarına ve uzay araçlarının enerji sağlayıcısı olan uzay kalifiye güneş hücrelerine etkisini yer gözlem merkezlerinde ürettiği atomik oksijen ile gözlemlemektedir. Vakum ortamında üretilen atomik oksijen miktarı Kapton gibi atomik oksijene karşı davranışı iyi bilinen ve uzay şartlarına uyumlu polimerlerin atomik oksijene karşı erozyonu sonucu kütle değişimleri ile bulunur. Bulunan atomik oksijen miktarı cihaz parametreleri değiştirilerek alçak dünya yörüngesini simüle edecek hale getirilir.

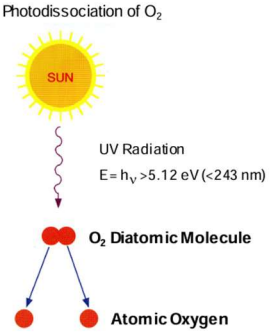

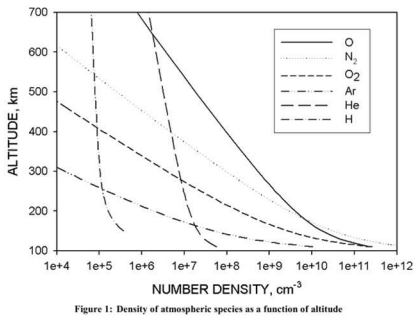

Figure 1: Density of atmospheric species as a function of altitude

Bu çalışmanın amacı; RF plazma ortamında, herhangi bir hedef (target) olmaksızın Argon-Oksijen (20:1) karışımıyla elde edilen plazmadaki atomik oksijenin, güneş hücrelerinde alttaş olarak kullanılan silisyum ve germanyum waferlar üzerindeki etkilerini ve kapton malzemesindeki erozyon davranışını incelemektir. Atomik oksijen maruziyeti öncesinde ve sonrasında gerçekleştirilen FTIR ve UV-Vis spektrometresi analizleriyle malzemelerdeki bağ oluşumları ile optik geçirgenlikler değerlendirilmiştir. Ayrıca, atomik oksijenin yüzey topoğrafyasında meydana getirdiği pürüzlülük değişimleri AFM ile yüzeyde oluşan yeni yapısal fazlar ise XRD analizleriyle belirlenmiştir.

Kapton alttaşın atomik oksijen maruziyeti öncesinde ve sonrasında kütlesi ölçülmüş; elde edilen kütle değişimi, erozyon bağıntısında kullanılarak plazma ortamındaki atomik oksijen akısı hesaplanmıştır.

$$F = \frac{\Delta M_K}{(A_K \rho_K E_K)}$$

F = fluence of atomic oxygen (atoms/cm^2)
ΔM_K = mass loss of Kapton® witness sample (g)
A_K = surface area of Kapton® witness sample exposed to atomic oxygen (cm^2)
ρ_K = density of Kapton® witness sample (1.42 g/cm^3)
E_K = erosion yield of Kapton® witness sample (3.0×10^{-24} cm^3/atom)

Anahtar Kelimeler : RF plazma**,** Atomik Oksijen, Polimer Erozyon, Güneş Hücresi

[1] Low Earth Orbital Atomic Oxygen Interactions With Materials, Bruce A. Banks, Sharon K. Miller, and Kim K. de Groh Glenn Research Center, Cleveland, Ohio
[2] Kim K. de Groh, Donald A. Jaworske, Gary H. Pippin, Phillip P. Jenkins, Robert J. Walters and Sheila A. Thibeault, Experiment (MISSE): Overview, Accomplishments and Future Needs, Discoveries Plenary Presentation at the 3rd Annual International Space Station Research and Development Conference June 17-19, 2014, Chicago,

AsH_3-Controlled InGaAs Epitaxy Toward Strain-Balanced Structures for Extended-SWIR Applications

Muhammet Enes ÇOBAN[1,2], Ferhan Kübra ÖZBAKIR[1,2], İsmail ALTUNTAŞ[1,2,*]
[1] *Sivas Cumhuriyet University Nanophotonics Application and Research Center-CÜNAM, Sivas, Türkiye*
[2] *Department of Nanotechnology Engineering, Faculty of Engineering, Sivas Cumhuriyet University, Sivas, Türkiye*
*Corresponding e-mail:ialtuntas@cumhuriyet.edu.tr

Abstract

InGaAs/InP epitaxial structures are important for short-wave infrared (SWIR) applications because their optical properties can be tuned by varying the In concentration. However, increasing the In concentration introduces lattice mismatch between the InGaAs layer and the InP substrate, which can lead to strain and structural defects. Previous studies have shown that variations in the AsH_3 flow rate during Metalorganic Vapor Phase Epitaxy (MOVPE) growth can affect In incorporation and consequently influence the structural and optical properties of InGaAs/InP structures [1,2]. In this study, the effect of the AsH_3 flow rate on InGaAs epitaxial growth was investigated as a preliminary step toward the development of strain-balanced structures for extended-SWIR applications.

Three different InGaAs/InP epilayers were grown on InP substrate using AsH_3 flow rates of 30, 40, and 50 sccm, while the TMGa and TMIn flow rates were kept constant at 0.4 and 32 sccm, respectively. The structural, optical, and morphological properties of the grown samples were investigated using X-ray diffraction (XRD), photoluminescence (PL), Raman spectroscopy, optical microscopy, and Atomic Force Microscopy (AFM). The measured In concentrations were 0.571, 0.578, and 0.575 for AsH_3 flow rates of 30, 40, and 50 sccm, respectively.

The XRD results showed a slight decrease in the FWHM values from 0.079° at 30 sccm to 0.076° and 0.075° at 40 and 50 sccm, respectively, indicating a slight improvement in crystalline quality with increasing AsH_3 flow rate. AFM characterization revealed uniform surfaces, well-defined atomic steps, and no visible surface defects for all three samples. These results indicate that the AsH_3 flow rate influences the growth behavior of InGaAs, while the In concentration and crystalline quality remain relatively stable within the investigated range. The findings provide a basis for further optimization of InGaAs epitaxial growth and support the development of strain-balanced InGaAs/InP structures for extended-SWIR applications.

Keywords: Extended-SWIR, MOVPE, InGaAs, XRD.

Acknowledgements
This study is supported by the Scientific Research Project Fund of Sivas Cumhuriyet University, Turkey, TÜBİTAK under Project No. 124F464

References
[1] M. Ben Arbia et al. , Experimental insights toward carrier localization in in-rich InGaAs/InP as candidate for SWIR detection: Microstructural analysis combined with optical investigation, Materials Science in Semiconductor Processing 153 (2023) 107149.
[2] E. Kaynar, M. Sayrac, I. Altuntaş, I. Demir, Determination of Optical Properties of MOVPE-Grown $In_xGa_{1-x}As$/InP Epitaxial Structures by Spectroscopic Ellipsometry, Brazilian Journal of Physics 52, 184 (2022).

Femtosecond-Laser-Induced Multiscale Surface Morphologies for Enhanced SERS Performance

İlayda Alparslan[1]*, Ihor Pavlov[1], Arian Goodarzi[2], Alpan Bek[1]

[1] Department of Physics, Middle East Technical University, 06800 Ankara, Türkiye

[2] ODTÜ-GÜNAM, Center for Solar Energy Research and Applications, 06800 Ankara, Türkiye

ilayda.alparslan@metu.edu.tr

Abstract

Raman spectroscopy provides molecule-specific vibrational fingerprints, but weak Raman scattering often limits detection sensitivity. Surface-enhanced Raman spectroscopy (SERS) addresses this limitation by enhancing Raman signals near plasmonic nanostructures, mainly through local electromagnetic field amplification. However, it is limited by the need for reproducible, fast, and large-area fabrication. Conventional methods such as electron-beam lithography and photolithography offer precise control but usually require cleanroom processing, masks or resists, and several fabrication steps. Colloidal nanoparticle-based methods are more accessible, but uncontrolled aggregation can reduce SERS signal uniformity. Laser-induced periodic surface structures (LIPSS) offer a direct and mask-free alternative [1]. During femtosecond-laser irradiation, the interaction between the incident light and the material produces self-organized periodic features within the laser spot. Scanning the beam extends these features across the surface without writing each line separately. Here, crystalline silicon was structured with a 1032 nm femtosecond laser and then coated with approximately 70 nm of Ag, giving a two-step fabrication route. By changing the laser processing parameters, we obtained three distinct surface morphologies, referred to as Nano-LIPSS, Micro-LIPSS, and Hybrid-LIPSS. SERS measurements were performed with Crystal Violet (CV) using 532 nm excitation. The Micro-LIPSS and Hybrid-LIPSS samples produced stronger representative Raman signals than the Nano-LIPSS samples. Using the normal Raman signal of CV solution as the reference, experimental enhancement factors were on the order of 10^7 for Micro-LIPSS and Hybrid-LIPSS and 10^6 for Nano-LIPSS. Three-dimensional surface profiles reconstructed from scanning electron microscopy images were used in finite-difference time-domain (FDTD) electromagnetic simulations. Calculations at 532 nm for different incident polarizations showed morphology-dependent field localization, consistent with the differences observed in the Raman measurements. Together, these findings show that laser structuring followed by Ag coating provides a practical, mask-free route for producing multiscale SERS substrates with morphology-dependent enhancement.

Keywords: surface enhanced Raman spectroscopy, laser-induced periodic surface structures, femtosecond laser processing

Acknowledgements

This work was supported by the Scientific and Technological Research Council of Türkiye (TÜBİTAK) under grant nrs. 123M819 and 124N875. The authors thank the METU Central Laboratory for support with SEM imaging.

References

[1] S.N. Erkızan, F. İdikut, Ö. Demirtaş, A. Goodarzi, A. K. Demir, M. Borra, I.Pavlov, A.Bek (2022). LIPSS for SERS: Metal Coated Direct Laser Written Periodic Nanostructures for Surface Enhanced Raman Spectroscopy. Advanced Optical Materials, 10, 2200233 (2022).

DURO GHz LP30: Ultrafast GHz Laser System with Adjustable Pulse Duration

Alptekin Tanatar[1], Ibrahim Atespare[1], Hamit Kalaycıoğlu[1], Ecem Nur Duman[*1], Gizem Alpakut[2], Seydi Yavas[1,2,3]

[1]Lumos Laser A.S., 34470, Istanbul, Türkiye
[2]Department of Physics, Bogazici University, 34342, Istanbul, Türkiye
[3]Faculty of Engineering, Ozyegin University, 34794 Istanbul, Türkiye
corresponding author, E-mail: ecem@lumoslaser.com

Abstract

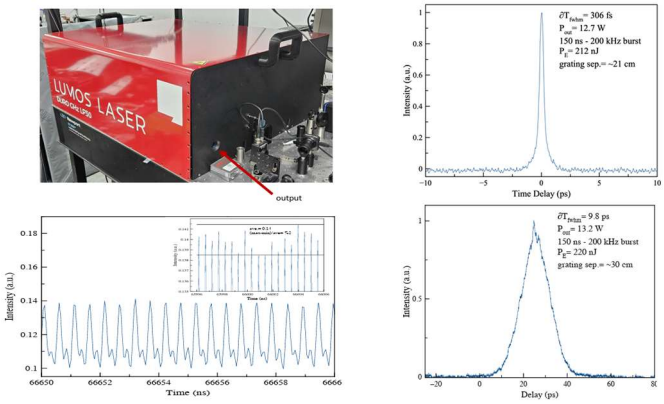

Figure 1: Laser system general view (top left), measured 2-GHz pulse train (bottom left), autocorrelation measurement results of shortest and longest pulse output (top and bottom right, respectively)

We developed a monobloc (Fig.1, top left) ultrafast fiber laser-amplifier system that operates in a burst-mode at an intra-burst repetition rate of ~2 GHz with an average power up to 30 W, able to generate pulses of individual energy above 200 nJ and duration down to ~300 fs (Fig.1, top right). The burst repetition rate is variable between 200 kHz and 1 MHz while the burst duration is adjustable from 300 ns up to 1 µs and the pulse duration is also adjustable up to 10 ps as well ((Fig.1, bottom right). Measured ~2-Ghz pulse train at the output of the repetition rate multiplier has a uniformity of pulse amplitude distribution of ~2% (Fig. 1, bottom left). Laser system generates bursts with pulses of highly uniform pulse energy distribution with standard deviation of ~1% (Fig.2, left side). Further, burst-on-demand operation is available which enables the system to generate a single burst. For this operation, the end-user is given five different burst choices (bursts of 150, 300, 600, 1200 and 2000 ns duration) to select from using the computer interface. Burst-on-demand operation (Fig. 2, right side) is realized by gating the AOM and modulating the pump diodes of the preamplifier and power amplifier, all of which are activated via an external trigger. The system allows from a single pulse up to 50 Hz for the trigger action, meaning that burst-on demand operation is able to produce the selected burst as a single shot or up to a repetition rate of 50 Hz where the number of bursts to be generated is set by setting the number of trigger pulses. All of the laser parameters and functions are controllable by the end-user via computer interface facilitated by the electronic hardware and software developed by Lumos. This laser was developed to investigate applications exploiting ablation cooling phenomenon [1].

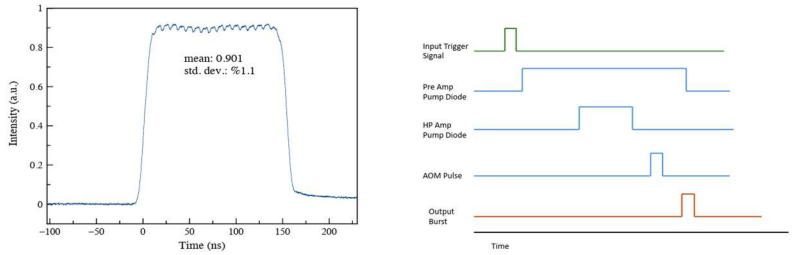

Figure 2: Envelope of 150-ns long bursts where the standard deviation of pulse energy inside the burst is calculated to be ~1% (left side), burst-on demand operation (right side).

Keywords: Ultrafast fiber laser, Femtosecond laser, GHz burst laser, Pulse on demand.

Referanslar / References:

[1] C. Kerse, H. Kalaycıoğlu, P. Elahi, B. Çetin, D. K. Kesim, Ö. Akçaalan, S. Yavaş, M. D. Aşık, B. Öktem, H. Hoogland, R. Holzwarth, and F. Ö. Ilday, Nature 537, 84 (2016).

Structural and Optical Optimization of InAlGaAs Quantum Well Layers Grown on InP Substrate with MOVPE for Laser Diode Structures

Gamze Yolcu*[1,2], İlkay Demir[2,3]

[1]*Department of Department of Metallurgical and Materials Engineering, Sivas Cumhuriyet University, 58140 Sivas, Türkiye*

[2]*Sivas Cumhuriyet University Nanophotonics Research and Application Center-CÜNAM, 58140 Sivas, Türkiye*

[3]*Department of Nanotechnology Engineering, Sivas Cumhuriyet University, 58140 Sivas, Türkiye*

corresponding author, E-mail: gamzeyolcu@cumhuriyet.edu.tr

Abstract

The composition, lattice matching, optical response, and surface morphology of the InAlGaAs quaternary alloy intended for use in the active region of pump laser diode structures are critical to achieving the target emission wavelength and high device performance. In this study, the nominal alloy composition suitable for the target 88x-nm emission band was first determined by comparing RSoft LaserMOD material gain simulations performed over the temperature range of 300–400 K for different In–Ga–Al mole fractions. Based on the simulation results, $In_{0.41}Ga_{0.295}Al_{0.295}As$ was selected as the target composition.

In the experimental study, an InP buffer layer, a lattice-matched InGaAs interlayer, and an InAlGaAs active layer were sequentially grown on an InP substrate by metal-organic vapor phase epitaxy (MOVPE). To approach the target composition, the flow rates of the TMAl, TMGa, and TMIn metalorganic precursors were sequentially optimized. The growth temperature and AsH_3 flow rate were maintained at 600 °C and 35 sccm, respectively. The samples were characterized using in situ reflectance, high-resolution X-ray diffraction (HRXRD), spectroscopic ellipsometry, temperature-dependent photoluminescence (PL), and atomic force microscopy (AFM).

Reducing the TMAl flow rate from 10 to 3 sccm shifted the InAlGaAs XRD peak toward the desired position and significantly improved the crystalline quality of the layer. Consequently, a TMAl flow rate of 3 sccm was selected as the reference condition for the subsequent optimization steps. Under these conditions, increasing the TMGa flow rate from 0.4 to 0.9 sccm generally increased Ga incorporation while decreasing In incorporation, according to the HRXRD-derived trends, and increased the lattice mismatch of the layer relative to InP. The sample grown with the lowest TMGa flow rate exhibited an RMS roughness of approximately 0.11 nm over a 5 × 5 μm² AFM scan area, together with a highly ordered terrace-like surface morphology. Spectroscopic ellipsometry showed that variations in the precursor flow rates affected the refractive index and extinction coefficient of the InAlGaAs layer. The refractive index decreased with increasing wavelength, consistent with normal dispersion, while the extinction coefficient also decreased, indicating weaker absorption at longer wavelengths. Increasing the TMIn flow rate from 15 to 25 sccm systematically enhanced In incorporation. According to the HRXRD modeling, the sample grown with a TMIn flow rate of 23 sccm exhibited an In mole fraction closest to the target value determined by the RSoft LaserMOD simulations ($X_{In} \approx 0.41$) and the strongest InAlGaAs PL emission in the 901–903 nm range. The Ga and Al mole fractions were treated as model-dependent estimates because the similar lattice constants of GaAs and AlAs limit their reliable separation using symmetric HRXRD measurements. The results demonstrate that the sample grown with a TMIn flow rate of 20 sccm exhibited the most favorable surface morphology, whereas the sample grown with a TMIn flow rate of 23 sccm was superior in terms of approaching the target In mole fraction and achieving stronger optical emission. The combined application of theoretical design based on RSoft LaserMOD simulations and sequential MOVPE precursor-flow optimization established the fundamental growth conditions required for the subsequent growth of a complete laser diode epitaxial structure.

Keywords: InAlGaAs, MOVPE, RSoft LaserMOD, material gain, epitaxial growth optimization, surface morphology

Acknowledgements

This work was supported by Projects No. M-2023-857 and 125F147 and was conducted as part of Gamze YOLCU's ongoing Ph.D. thesis, entitled "Development of a GaAs-Based Pump Laser Diode Structure (λ = 88x nm)." The authors gratefully acknowledge Keysight Technologies for providing the RSoft LaserMOD software license used in this study and for their technical support during the licensing and installation processes. Gamze YOLCU is supported by the Council of Higher Education (YÖK) 100/2000 Ph.D. Scholarship Program and the Scientific and Technological Research Council of Türkiye (TÜBİTAK) 2211/A National Ph.D. Scholarship Program.

Interface Engineering of InGaAs/InAlAs Superlattices toward High-Performance QCLs for DIRCM Applications

Merve Nur KOÇAK*[1,3], İlkay DEMİR[2,3]
[1] *Department of Metallurgical and Materials Engineering, Sivas Cumhuriyet University, 58140 Sivas, Türkiye*
[2] *Department of Nanotechnology Engineering, Sivas Cumhuriyet University, 58140 Sivas, Türkiye*
[3] *Sivas Cumhuriyet University Nanophotonics Application and Research Center-CÜNAM, 58140 Sivas, Türkiye*
E-mail: idemir@cumhuriyet.edu.tr

Özet / Abstract
Quantum cascade lasers (QCLs) are promising mid-wave infrared (MWIR) sources for directional infrared countermeasure (DIRCM) systems due to their wavelength-selective emission, compact architecture, and potential for high optical power. The performance of these devices strongly depends on the structural quality of the active region, where electron transport and intersubband transitions occur across numerous nanoscale quantum well/barrier interfaces. Interface roughness and thickness fluctuations can enhance electron scattering, broaden energy states, modify carrier lifetimes, and consequently degrade optical gain and laser performance [1]. Precise control of interface formation is therefore essential for developing high-quality QCL active regions for DIRCM-oriented applications [2].

In this study, $In_{0.68}Ga_{0.32}As/In_{0.34}Al_{0.66}As$ superlattices were investigated as model structures for optimizing the epitaxial growth of QCL active regions. The influence of the V/III ratio, controlled through AsH_3 flow during metal-organic chemical vapor deposition (MOCVD), on interface formation, surface morphology, and structural quality was systematically examined. The structures were characterized by high-resolution X-ray diffraction (HR-XRD), X-ray reflectivity (XRR), atomic force microscopy (AFM), and photoluminescence (PL). The results showed that variations in AsH_3 flow modify surface arsenic coverage and group-III adatom diffusion, thereby governing the interplay between surface kinetics and strain and significantly influencing step-bunching and interface evolution. Well-defined superlattice satellite peaks confirmed that structural periodicity was maintained across the investigated growth conditions, while XRR and AFM revealed pronounced differences in surface and interface morphology. An optimized AsH_3 flow condition provided a favorable balance between surface stabilization and adatom mobility, resulting in improved morphological uniformity without compromising superlattice periodicity. These findings demonstrate that V/III ratio control is a key epitaxial parameter for engineering high-quality InGaAs/InAlAs superlattice interfaces toward the development of MWIR QCL active regions for DIRCM applications.

Figure 1. Schematic illustration of the operating principle of a DIRCM system.

Anahtar Kelimeler / Keywords: Quantum cascade laser, DIRCM, InGaAs/InAlAs, superlattice, V/III ratio, interface engineering, MOCVD

Acknowledgements
This work is based on results obtained during the ongoing Ph.D. thesis of Merve Nur Koçak, titled “Development of Short- and Mid-Wavelength Quantum Cascade Lasers”. Merve Nur Koçak is supported by the YÖK (Council of Higher Education) 100/2000 Ph.D. Scholarship Program and The Scientific and Technological Research Council of Turkey (TÜBİTAK) 2211/A Program. This study supported by The Scientific Research Project Fund of Sivas Cumhuriyet University, Turkey under the project number MRK-2024-004 and The Scientific and Technological Research Council of Turkey (TUBITAK) under the project number 22AG074.

Referanslar / References
[1] Suri, S., Knipfer, B. B., Grange, T., Gao, H., Kirch, J. D., Mawst, L. J., ... & Botez, D. (2024). Modeling with graded interfaces: Tool for understanding and designing record-high power and efficiency mid-infrared quantum cascade lasers. Nanophotonics, 13(10), 1745-1757.
[2] Knipfer, B., Xu, S., Kirch, J. D., Botez, D., & Mawst, L. J. (2022). Analysis of interface roughness in strained InGaAs/AlInAs quantum cascade laser structures (λ~ 4.6 μm) by atom probe tomography. *Journal of Crystal Growth*, *583*, 126531.

Thickness Optimization of MOCVD-Grown InGaAs/InAlAs Superlattices for Quantum Cascade Laser Structures

Ömer SÜR[1], Merve Nur KOÇAK[1,3], İlkay DEMİR[1,2,*]

1 Sivas Cumhuriyet University Nanophotonics Application and Research Center-CUNAM, Sivas, 58140, Türkiye

2 Department of Nanotechnology Engineering, Faculty of Engineering, Sivas Cumhuriyet University, 58140 Sivas, Türkiye

3 Department of Metallurgy and Materials Science, Faculty of Engineering, Sivas Cumhuriyet University, 58140 Sivas, Türkiye

corresponding author, E-mail: idemir@cumhuriyet.edu.tr

Abstract

Quantum cascade lasers (QCLs) are unipolar semiconductor lasers based on intersubband transitions in nanometer-scale quantum well and barrier heterostructures. Since their electronic states and carrier transport are strongly dependent on the dimensions and interfaces of the constituent layers, precise thickness control is a critical requirement in QCL epitaxy [1]. InGaAs/InAlAs/InP is an established material system for mid-infrared QCLs, and metal-organic chemical vapor deposition (MOCVD) has been successfully employed for the growth of these multilayer structures [2].

In this study**,** thickness control in MOCVD-grown InGaAs/InAlAs superlattices is investigated by varying the InAlAs growth time while maintaining the principal growth conditions at comparable values. The approach is intended to examine the relationship between deposition time, individual layer thickness, and the resulting superlattice periodicity. Previous studies have demonstrated that HRXRD can be effectively used to determine layer and period thicknesses in InGaAs/InAlAs superlattices and to evaluate their structural periodicity [3].

High-resolution X-ray diffraction (HRXRD) is therefore employed as the primary structural characterization technique, with emphasis on superlattice satellite peaks and period thickness. Photoluminescence (PL) spectroscopy is used to evaluate the emission characteristics of the structures, while Raman spectroscopy provides complementary information on their phonon characteristics [4,5]. PL studies have shown that the optical response of InGaAs/InAlAs heterostructures can be sensitive to quantum-well geometry and interface fluctuations, whereas Raman spectroscopy has been used to investigate phonon behavior in InGaAs/InAlAs superlattices. The combined characterization aims to assess growth-time-based thickness control and its relationship with the structural and optical characteristics of InGaAs/InAlAs superlattices relevant to QCL applications.

Keywords: Quantum Cascade Laser, MOCVD, InGaAs/InAlAs, Superlattice, Thickness Control, HRXRD, Photoluminescence, Raman Spectroscopy

Acknowledgements

This work is based on results obtained during the ongoing Ph. D. thesis of Merve Nur Koçak, titled “Development of Short- and Mid-Wavelength Quantum Cascade Lasers”. Merve Nur Koçak is supported by the YÖK (Council of Higher Education) 100/2000 Ph. D. Scholarship Program and The Scientific aSnd Technological Research Council of Turkey (TÜBİTAK) 2211/A Program. This study supported by The Scientific Research Project Fund of Sivas Cumhuriyet University, Turkey under the project number MRK-2024-004 and The Scientific and Technological Research Council of Turkey (TUBITAK) under the project number 22AG074.

References

[1] Y. Yao, A. J. Hoffman, and C. F. Gmachl, “Mid-infrared quantum cascade lasers,” Nature Photonics, 6, 432–439 (2012).

[2] Y. Huang et al., “Optimization of growth conditions for InGaAs/InAlAs/InP quantum cascade lasers by metalorganic chemical vapor deposition,” *Journal of Crystal Growth*, 316, 75–80 (2011).

[3] İ. Demir and S. Elagöz, “Growth of InGaAs/InAlAs superlattices by MOCVD and precise thickness determination via HRXRD,” *Gazi University Journal of Science*, 29(4), 947–951 (2016).

[4] Y. Wang et al., “Photoluminescence Study of the Interface Fluctuation Effect for InGaAs/InAlAs/InP Single Quantum Well with Different Thickness,” *Nanoscale Research Letters*, 12, 229 (2017).

[5] Y. Hu et al., “Micro-Raman study on chirped InGaAs–InAlAs superlattices,” *Physica Status Solidi A*, 210, 2364–2368 (2013).

Quantum and Strain Engineering of InAs/InP Short-Period Superlattices for e-SWIR Photodetection

Izel Perkitel[1,2] and Ilkay Demir[*1,2]

[1] *Sivas Cumhuriyet University Nanophotonics Application and Research Center-CÜNAM, 58140 Sivas, Türkiye*

[2] *Department of Nanotechnology Engineering, Sivas Cumhuriyet University, 58140 Sivas, Türkiye*

corresponding author, E-mail: idemir@cumhuriyet.edu.tr

Abstract

Extended short-wave infrared (e-SWIR) photodetectors are of increasing interest for applications such as spectroscopy, gas sensing, remote sensing, and biomedical imaging. III–V semiconductor heterostructures are particularly attractive for this spectral region due to their tunable band structures and favorable carrier transport properties. Among these, InAs/InP digital alloys offer a promising platform for extending the spectral response through the combined effects of strain and quantum confinement [1].

However, the large lattice mismatch between InAs and InP introduces significant strain into the active region, strongly affecting the conduction and valence band alignment and limiting the achievable spectral range. Metamorphic InAsP graded buffers provide an effective approach to overcome this limitation by gradually changing the lattice constant from InP toward an InAs-rich virtual substrate. Step-graded compositions, together with overshoot and step-back layers, can promote strain relaxation and provide a more suitable template for the subsequent growth of highly mismatched active regions [2].

In this study, the strain-dependent electronic and quantum properties of an InAs/InP digital alloy with a nominal $InAs_{0.85}P_{0.15}$ composition were investigated using Sentaurus TCAD. Different relaxation conditions were first analyzed to determine their influence on the band structure and confined carrier states. Subsequently, a step-graded InAsP metamorphic buffer incorporating overshoot and step-back layers was introduced beneath the digital-alloy active region. Schrödinger calculations revealed a systematic red-shift with increasing relaxation, while the metamorphic-buffer structure extended the calculated fundamental transition wavelength to approximately 2.75 µm while maintaining a high electron–hole wavefunction overlap. These results demonstrate that metamorphic-buffer and strain engineering provide an effective route for tailoring InAs/InP digital-alloy structures toward e-SWIR photodetection applications.

Keywords: e-SWIR, InAs/InP digital alloy, strain engineering, quantum confinement, metamorphic InAsP buffer

Acknowledgements

The authors acknowledge the use of the facilities of the Sivas Cumhuriyet University Nanophotonics Application and Research Center (CÜNAM). This study was supported by Scientific and Technological Research Council of Türkiye (TUBITAK) under the COST Support Program, Grant Number 125F362. The authors thank to TUBITAK for their supports.

This work is based on results obtained as part of the ongoing Ph.D. thesis of İzel PERKİTEL, entitled *"Development of Digital Alloy $InAs_xP_{1-x}$-Based Photodetectors for e-SWIR Applications."* İzel PERKİTEL is supported by the Scientific and Technological Research Council of Türkiye (TÜBİTAK) under the 2211/A National Ph.D. Scholarship Program.

References

[1] Guo, B., Liang, B., Zheng, J., Ahmed, S., Krishna, S., Ghosh, A., & Campbell, J. (2024). Digital alloy-grown InAs/GaAs short-period superlattices with tunable band gaps for short-wavelength infrared photodetection. ACS photonics, 11(4), 1419.

[2] Park, S., Kim, Y., Nguyen, P. D., Jeon, J., Chun, B. S., & Lee, S. J. (2024). Toward Ga-free wavelength extended 2.6 µm InAsP photodetectors with high performance. Advanced Functional Materials, 34(9), 2309897.

Machine Learning-Assisted Optimization of Ultrafast Laser Micromachining

H. Berk Demir*[1] , Ecem Nur Duman[2], Alptekin Tanatar[2], Burak Arayit[1], Sema Demirel[1], Gizem Alpakut[3], Ibrahim Atespare[2], Seydi Yavas[1,2,3], Bora Akgün[3], Hamit Kalaycıoğlu[2]

[1]Faculty of Engineering, Ozyegin University, 34794 Istanbul, Türkiye

[2]Lumos Laser A.S., 34470, Istanbul, Türkiye

[3]Department of Physics, Bogazici University, 34342, Istanbul, Türkiye

corresponding author, E-mail: berk.demir.33432@ozu.edu.tr

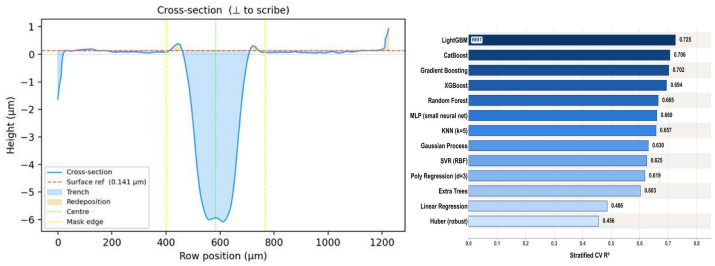

Figure 1: Left Side: Cross section of the ablation line. Right Side: Model comparison for depth prediction on silicone wafer.

Micromachining is one of the main applications of ultrafast laser technology, where achieving high-quality and damage-free processing depends on operating with optimized laser and scanning parameters. In most micromachining processes, the initial characterization of the material is performed through ablation line tests, in which a matrix of laser and scanning parameters is systematically investigated. The resulting data are then used to identify optimized processing conditions that provide low heat-affected zones (HAZ), minimal material damage, and high machining quality. However, this parameter optimization process is time-consuming and becomes challenging when the same characterization procedure must be repeated for each new material.

In this research, we investigate the use of machine learning to reduce the experimental workload required for laser parameter optimization [1]. Several regression models were trained using experimental ablation line tests (Figure 1, left side) performed on silicon wafers with a 1030 nm, 350 femtosecond ultrafast laser operating at a repetition rate of 400 kHz and a 15 µm focal spot diameter. A comprehensive parameter matrix covering different laser powers, scanning speeds, and numbers of passes was generated to provide the training dataset. The models were trained to establish predictive relationships between laser power, scanning speed, and number of passes and the resulting ablation depth. Their performance was evaluated using stratified 5-fold cross-validation. A total of 13 regression algorithms were investigated, including Linear Regression, Polynomial Ridge Regression, Support Vector Regression with an RBF kernel, Random Forest, Gradient Boosting, Gaussian Process, XGBoost, LightGBM, CatBoost, Extra Trees, K-Nearest Neighbors (KNN), Huber Regression, and Multi-Layer Perceptron (MLP). The comparative results are presented in Figure 1 (Right side). Among the evaluated models, the LightGBM model achieved the highest coefficient of determination, with an R^2 value of 0.72. These results demonstrate the potential of machine learning-based approaches for predicting ablation depth .

As a next step, transfer learning was investigated to determine whether the process relationships learned from silicon wafers could be transferred to a new material, stainless steel, using only a limited amount of additional experimental data. The previously trained LightGBM model was used as the source model, with the learned relationship between laser power, scanning speed, number of passes, and ablation depth transferred to the stainless-steel dataset. The goal is to reduce the experimental workload required for each new material by reusing previously learned process relationships rather than rebuilding the model. For initial results, it has been seen that as the amount of stainless-steel data increases, a model approaches and, in some cases, matches or outperforms the transferred model. These results suggest that transfer learning is particularly promising when only a small number of experimental measurements are available for a previously uncharacterized material.

Keywords: Ultrafast laser, Ultrashort pulsed laser, Femtosecond laser, Machine Learning, Micromachining, Transfer learning, Ablation quality, Silicon wafer, Stainless steel

Acknowledgements

This research is supported by TÜBİTAK TEYDEB 1501 (Project No: 3231665) and Cumhurbaşkanlığı SSB (Project No: 2009K120520).

References

[1] Deng, J., Zhu, Y., Miao, Y., & Li, Z. (2026). Progress and opportunities of machine learning in metal laser additive manufacturing. *The International Journal of Advanced Manufacturing Technology, 145*, 1553–1584.

Kuantum Şifrelemede Optik Kayıp ile Ağ Anahtar Oluşturma Veriminin Artırılması

Muhammed Kaan Yildiz[1]*, Ekmel Ozbay[1,2,3] and Ibrahim Ozdur[4]
[1]Department of Electrical and Electronics Engineering, Bilkent University, Ankara, Türkiye
[2]Nanotechnology Research Center, Bilkent University, Ankara, Türkiye
[3]Department of Physics, Bilkent University, Ankara, Türkiye
[4]Department of Electrical and Electronics Engineering, TOBB University of Economics and Technology, Ankara, Türkiye
Sorumlu yazar, E-mail: mkaan.yildiz@bilkent.edu.tr

Özet

Kuantum mekaniği kullanılarak güvenli şifre paylaşımı birimler arası teorik güvenliği olan anahtar paylaşımı sağlar [1]. Ancak güvenli anahtarın paylaşılan sinyallere oranı birçok etmen nedeniyle azalmaktadır. Örneğin, hata oranının yüksek olması, optik yapılar, verimliliği düşük hata ayıklama mekanizmasının kullanılması gibi durumlar güvenli anahtar oranını düşürmektedir. Bu faktörlerin yanında algılanan sinyallerinin entropisinin düşük olması da güvenli anahtar oranını düşürmektedir. Detektör ölü-zamanı, kuantum anahtar dağıtımında foton algılandıktan sonra detektörün yeni bir fotonu bir önceki fotondan bağımsız olarak ölçmesi için gereken zamandır. Kuantum kanalı kuantum durumlarından birine diğerinden daha fazla kayıp uygulayabilmektedir. Ölü-zaman ve kuantum kanalının sönümleme oranının kuantum durumları için farklı olması gibi faktörler gönderici tarafından hazırlanan kuantum durumunun entropisinin azalmasına neden olur. Birimler arası kanala uygulanan optik kayıp, algılanan sinyal sayısını azaltmasına rağmen ölü-zaman sırasında oluşan ölçüm verimi farklı azaltılarak entropi yükseltilebilmektedir. Bu yükseliş güvenli anahtar oranını artmaktadır. Kuantum şifreleme ağlarında ise bir gönderici çoklu alıcı durumunda pasif optik elemanlar ile kanallara giden foton miktarları değiştirilerek ağın anahtar oluşturma verimi artırılabilmektedir. Bu çalışmada farklı topolojilerde optik ayırıcının ayırma oranları değiştirilerek kuantum ağlarının anahtar oluşturma verimi artırılmıştır. Alıcılarda güvenli anahtar oranı [2]'te verilen yöntem ile formül (1) üzerinden hesaplanmıştır. Hata ayıklama adımında ortaya çıkan bilgi miktarı [3]'de verilen yöntem ile tahmin edilmiştir. Alıcıların güvenli anahtar oranları metrik, optik ayırıcının fotonu farklı alıcıları gönderme oranları ise değişken olarak kullanılarak gradyan yükselme algoritması üzerinden kuantum ağının anahtar oluşturma oranı optimize edilmiştir.

$$l = nH_{min}(Z) - H(Z_A|Z_B) - nf_{EC}\big(H(Z_A|Z_B)\big)H(Z_A|Z_B) + log_2(5)\sqrt{3nlog_2\left(\frac{2}{\varepsilon_{EC}}\right)} - log_2\frac{2}{\varepsilon_{cor}} - 2log_2\frac{1}{2\varepsilon_{PA}} \qquad (1)$$

Kaynakça

[1] Portmann, Christopher, and Renato Renner. "Security in quantum cryptography." *Reviews of Modern Physics* 94.2 (2022): 025008.
[2] Lim, Charles Ci Wen, et al. "Concise security bounds for practical decoy-state quantum key distribution." *Physical Review A* 89.2 (2014): 022307.
[3] Bunandar, Darius, et al. "Numerical finite-key analysis of quantum key distribution." *npj Quantum Information* 6.1 (2020): 104.

Development of an Optical Probe for Controlled Irradiance Distribution in High-Intensity Laser Therapy

Kaan TURAN[1,2], Erhan AKMAN[3], Merve TURAN[4], Ahmet İREN [1], Levent CANDAN[5],
[1] Kocaeli University, Department of Electro-Optical Systems Engineering, Kocaeli, Türkiye
[2] FARBA Automotive Inc., Gebze/Kocaeli, Türkiye
[3] Kocaeli University, Faculty of Aeronautics and Astronautics, Department of Aviation Electrics and Electronics, Kocaeli, Türkiye
[4] Department of Physical Medicine and Rehabilitation, Kocaeli City Hospital, Kocaeli, Türkiye
[5] Kocaeli University, Laser Technologies Research and Application Center, Kocaeli, Türkiye
corresponding author, E-mail: turankaan08@gmail.com

Abstract
High-Intensity Laser Therapy (HILT) is increasingly used in physical medicine and rehabilitation because of its ability to deliver relatively high optical power to deeper tissue regions. Although treatment parameters such as wavelength, output power, irradiation time, spot size, and energy density are commonly considered in therapeutic protocols, the spatial distribution of irradiance across the treatment area may also influence local energy deposition, thermal response, and treatment reproducibility. This study presents the development and evaluation of a novel optical probe designed to control the spatial irradiance distribution of an existing HILT system without modifying the primary laser source. The probe was developed through optical modelling, numerical simulation, and prototype-based experimental evaluation. Its optical performance was compared with that of the conventional delivery configuration under equivalent laser operating conditions. The investigated parameters included spot size, spatial irradiance distribution, peak irradiance, beam uniformity, optical efficiency, and working-distance dependence. In addition, tissue-equivalent and/or ex vivo models were used to investigate the relationship between spatial optical energy distribution and the resulting thermal response. The developed probe provides a platform for systematically investigating spatial irradiance distribution as an additional parameter in HILT dosimetry. This approach may contribute to the development of more controlled, predictable, and reproducible therapeutic laser delivery systems.

Keywords: High-Intensity Laser Therapy, HILT, optical probe, irradiance distribution, laser-tissue interaction, therapeutic laser, medical optics.

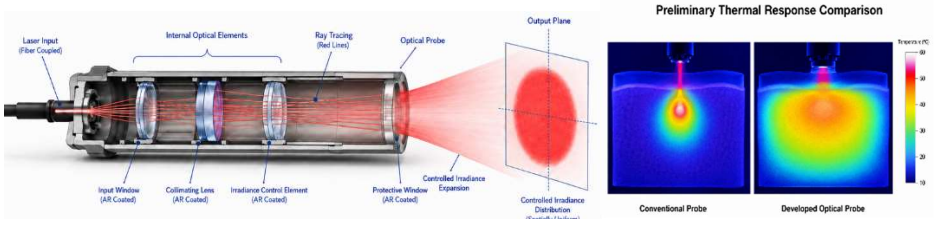

a) b)

Figure 1: a) Conceptual optical layout of the developed HILT probe showing the internal optical elements, ray propagation, and controlled irradiance distribution at the output plane b) Conceptual comparison of thermal response and spatial irradiance distribution for the conventional and developed optical probes

Controlling the spatial distribution of laser energy may provide an additional approach for improving the predictability of HILT applications. In this study, a novel optical probe was developed to modify and control the irradiance distribution of an existing HILT system without altering the primary laser source [1]. Compared with the conventional delivery configuration, the proposed probe produced a broader and more controlled optical distribution over the target area and reduced the dominant concentration of optical energy around the central region of the beam [2]. Preliminary optical evaluations indicated that the developed configuration increased the effective irradiation area and improved the spatial uniformity of the delivered optical energy. In addition, the redistribution of optical power resulted in a lower localized peak irradiance while preserving the overall energy delivery characteristics required for therapeutic application.

References
[1 [1] A. Amaroli, P. Arany, C. Pasquale, S. Benedicenti, A. Bosco, S. Ravera, Improving Consistency of Photobiomodulation Therapy: A Novel Flat-Top Beam Hand-Piece versus Standard Gaussian Probes on Mitochondrial Activity, Int. J. Mol. Sci. 22(15), 7788 (2021).
[2] P. Zielińska, M. Soroko, K. Howell, M. Godlewska, W. Hildebrand, K. Dudek, Comparison of the Effect of High-Intensity Laser Therapy (HILT) on Skin Surface Temperature and Vein Diameter in Pigmented and Non-Pigmented Skin in Healthy Racehorses, Animals 11(7), 1965 (2021).

SBS-Corrected Distributed Temperature Sensing Through Landau-Placzek Ratio

Rahmetullah Durgun*[1], Volkan Türker[1], Ali Emre Yılmaz[1], Faruk Uyar[1,2], Ekmel Özbay[1,2,3], İbrahim Özdür[4]

[1]NANOTAM, Bilkent University, Ankara, Türkiye

[2]Department of Electrical and Electronics Engineering, Bilkent University, Ankara, Türkiye

[3]Department of Physics, Bilkent University, Ankara, Türkiye

[4]Department of Electrical and Electronics Engineering, TOBB ETU, Ankara, Türkiye

*rahmetullah.durgun@bilkent.edu.tr

Brillouin Optical Time Domain Reflectometers (BOTDR) are based on Brillouin scattering from an optical fiber and utilize properties of the Brillouin spectrum to estimate the local temperature and the strain along the sensor. Measurements of the Brillouin frequency shift (BFS) and Brillouin intensity (BI) enable independent measurements of both variables. Landau-Placzek ratio (LPR) is the ratio of Rayleigh scattering intensity to BI, and it is significantly more sensitive to temperature than to strain. Therefore, LPR can be utilized to estimate temperature independently, facilitating subsequent determination of strain through BFS alone [1-2]. In BOTDR systems, uncertainty in the BI measurement is significantly larger than that of BFS measurements, and therefore the major driver of total system uncertainty. In this study, we increase the signal-to-noise ratio (SNR) of BOTDR BI measurements by launching optical powers nearing the stimulated Brillouin scattering (SBS) threshold.

As optical power is increased to improve SNR, the SBS threshold is quickly reached where Brillouin Stokes line faces nonlinear amplification, and thus the inversely proportional dependence on temperature of the LPR measurement gets disturbed. It has been noted in regards to SBS that pump power amplifies the Stokes line while attenuation is observed on the anti-Stokes line [3] as the latter amplifies the pump beam. For small SBS gain, this effect can be quantified and reversed. In this study, we launch power near the SBS threshold, utilize the relative ratio of Stokes and anti-Stokes lines to deduce the level of SBS amplification, and consequently recover the original spontaneous BI while simultaneously improving SNR to levels not achievable in a native spontaneous measurement of LPR. Compared to the condition where SBS is minimal, the effective sensing range has been improved by more than 15 km or by 6 dB.

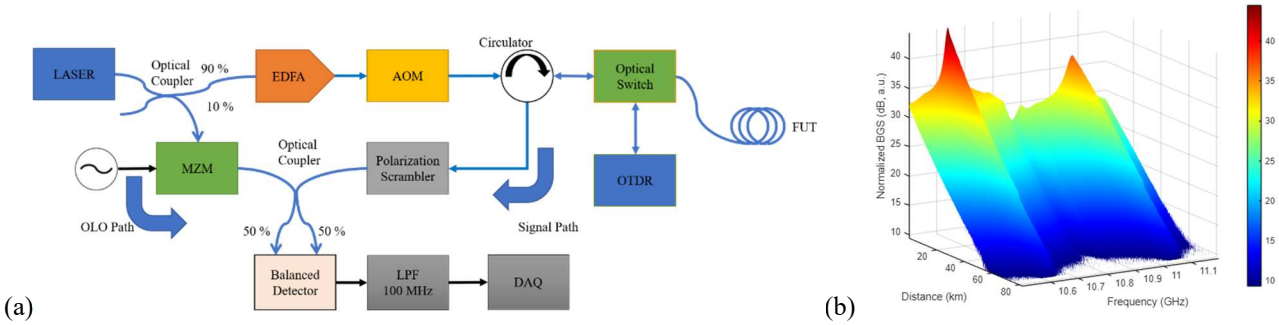

Figure 1: a) Experimental setup FUT (fiber under test), EDFA (Erbium-doped fiber amplifier), AOM (acousto-optic modulator), DAQ (data acquisition unit), MZM (Mach-Zehnder modulator) **b)** Obtained Brillouin gain spectrum

Fig. 1a shows the experimental configuration for the measurement. Coherent detection is used and a local oscillator is beaten with the backscattered Brillouin signal. MZM is used to generate sidebands of the carrier frequency, making both the Stokes and the anti-Stokes beat spectrum fall into the baseband. A low bandwidth detection system is used to measure subsections of the BGS, and a sequence of measurements is conducted by sweeping the MZM sideband frequency to stitch together the entirety of the BGS. Frequency upshift introduced by the AOM allows separation of the Stokes and anti-Stokes lines. A separate OTDR module is used to collect the Rayleigh traces.

Keywords: Distributed sensing, Brillouin frequency shift, strain, temperature, Landau-Placzek ratio, BOTDR

References

[1] P. C. Wait and T. P. Newson, "Landau Placzek ratio applied to distributed fibre sensing," Optics Communications, vol. 122, no. 4-6, pp. 141–146, Jan. 1996.

[2] A. H. Hartog, An Introduction to Distributed Optical Fibre Sensors, 1st. ed., (CRC Press, Boca Raton, 2017)

[3] N. Lalam et al., "Analysis of Brillouin frequency shift in distributed optical fiber sensor system for strain and temperature monitoring," Proc. PHOTOPTICS, pp. 333–340, 2016.

Atmosferik Türbülans Koşullarında 1064 nm Lazer Işının Yayılımının Sayısal Modellemesi

Serpil Yağmur YILMAZ[*1,2], Barış POLAT[2], Aydan YELTİK[1,3], İbrahim Tuna ÖZDÜR[4]
[1]TOBB Ekonomi ve Teknoloji Üniversitesi, Mikro ve Nanoteknoloji Mühendisliği Bölümü, Ankara, Türkiye
[2] ASELSAN Elektronik Sanayi ve Ticaret A.Ş.
[3]TOBB Ekonomi ve Teknoloji Üniversitesi, Malzeme Bilimi ve Nanoteknoloji Mühendisliği Bölümü, Ankara, Türkiye
[4]TOBB Ekonomi ve Teknoloji Üniversitesi, Elektrik ve Elektronik Mühendisliği Bölümü, Ankara, Türkiye
E-mail: serpilyagmuryilmaz@etu.edu.tr

Özet
Atmosferde meydana gelen sıcaklık değişimleri ve düzensiz hava hareketleri, kırılma indisinin değişmesine neden olarak atmosferik türbülansı oluşturmaktadır. Atmosferik türbülans, atmosferde yayılan lazer ışınlarının performansını etkileyen önemli çevresel faktörlerden biridir. Bu etkiler ışın genişlemesi (beam spreading), ışın gezinmesi (beam wander) ve ışın şiddetinde zamana bağlı dalgalanmalar (scintillation) şeklinde ortaya çıkabilmektedir. Bu çalışmada, 1064 nm dalga boyuna sahip bir lazer ışınının farklı atmosferik türbülans koşullarındaki yayılımının sayısal olarak modellenmesi ve türbülans kaynaklı parıldama (scintillation) etkisinin incelenmesi amaçlanmaktadır. Gaussian lazer ışını ve rastgele faz ekranları ile atmosferik türbülansın etkisi modellenerek yayılım modeli oluşturulacaktır. Türbülanslı atmosferde oluşan farklı büyüklüklerdeki hava girdaplarını temsil etmek üzere iç ve dış ölçek parametreleri kullanılacaktır. Farklı yayılım mesafeleri ve türbülans seviyeleri için alıcı düzlemindeki ışın şiddeti dağılımları incelenecek ve şiddet dalgalanmaları parıldama indisi üzerinden nicel olarak değerlendirilecektir. Bu şekilde C_n^2, yayılım mesafesi ve parıldama arasındaki ilişkinin ortaya konulması ve atmosferik türbülansın 1064 nm lazer ışını üzerindeki etkilerinin sayısal olarak değerlendirilmesi hedeflenmektedir. Elde edilen sayısal sonuçların, atmosferik ortamda çalışan lazer tabanlı sistemlerin performansının değerlendirilmesine katkı sağlaması amaçlanmaktadır.

Anahtar Kelimeler: Atmosferik Türbülans, Lazer Işını Yayılımı, Parıldama (Scintillation)

Referanslar
[1] Tatarski, V. I. (1961). Wave propagation in a turbulent medium. McGraw-Hill.
[2] Clifford, S. F. (1978). The classical theory of wave propagation in a turbulent medium. Optics Letters.
[3] Kolmogorov, A. N. (1941). Dissipation of energy in locally isotropic turbulence. Doklady Akademii Nauk SSSR.
[4] Fried, D. L. (1965). Statistics of a geometric slope of a wavefront over a circular aperture. Journal of the Optical Society of America, 55(11), 1427–1431.
[5] Fante, R. L. (1975). Electromagnetic beam propagation in turbulent media. Proceedings of the IEEE, 63(12), 1669–1692.

Advanced Optimization of Nanosecond-Laser Induced Nanostructured Surfaces for Large Area, Highly Uniform SERS Substrates

Batuhan Balkan*[1], Melis Atlıer[2], İlayda Alparslan[1], Doğaç Tüzel[1], Alpan Bek[1]
[1]Department of Physics, Middle East Technical University, 06800 Ankara, Türkiye
[2]Department of Mathematics and Science Education, Faculty of Education, Middle East Technical University, 06800 Ankara, Türkiye
batuhanbalkan07@gmail.com

Abstract
This study demonstrates a practical, low-cost method for preparation of large area, low relative standard deviation Surface Enhanced Raman Spectroscopy (SERS) substrates prepared by nanosecond pulsed laser. Silicon surface topography is tailored for high uniformity large area applications by optimization of available 1064nm pulsed nanosecond (ns) laser parameters. Different regimes of laser induced surface topographies were analyzed using dark field microscopy. Laser parameters and surface topographies are mapped and later optimized based dark field microscopy observations. SERS performance and high uniformity of active regions on the obtained nano-scale surface structures were characterized by large area Raman scattering mappings. Raman analyses across different laser structuring parameters indicate that laser textured surface nano-topographies provide an enhancement factor in the order of 10^6 across multiple different samples. Furthermore, the low relative standard deviation (RSD) from a Raman spectroscopy mapping collected from different places on a 1x1cm^2 area indicates homogeneity of the silver coated nanosecond-laser induced nanostructured surfaces. SEM analyses were conducted on best performing SERS substrates. SEM images indicate highly uniform generation of nanostructures on silicon substrate. Raman intensity mappings SEM analyses conducted on best performing samples indicate to a region of laser textured surface topographies which provide an enhancement factor on the order of 10^7. Experimental findings are supported by electromagnetic field simulations of finite domain time difference method for best performing samples. Simulations are generated by using images from SEM analysis. Large processing area, short preparation time and high enhancement factors resulting from the homogeneity of the active regions makes this pulsed nanosecond (ns) laser surface structure morphologies a candidate for practical and rapid alternative for SERS substrates compared to high-cost laser systems[1] and complex processes[2].

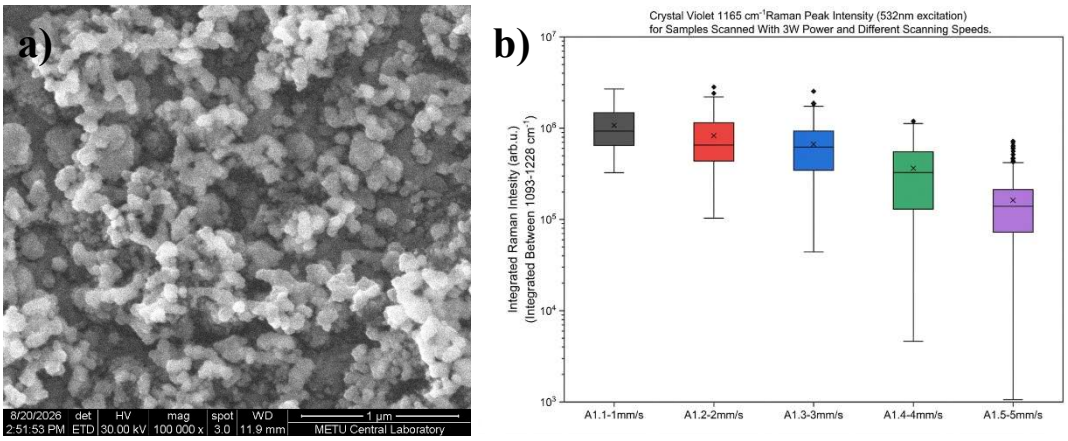

Figure 1: (a) SEM image of silver coated nanostructured surface, (b) Raman spectra of 10^{-5} M CV molecules drop casted on silver coated nanostructured surfaces.

Keywords: Self-Assembled Structures, Nanosecond Laser, Direct-Laser Writing, SERS.

Acknowledgements
The authors gratefully acknowledge the financial support from the Scientific and Technological Research Council of Türkiye (TÜBİTAK) under Grant No. 123M819. We thank METU Central Laboratory for SEM analysis.

References
[1]C. Huang, H. Li, and X. Zhang, "Direct Writing of SERS Substrates Using Femtosecond Laser Pulses," *ACS Omega*, vol. 9, no. 35, pp. 37188–37196, Sep. 2024, doi: 10.1021/ACSOMEGA.4C04588.
[2]Y. Zhang *et al.*, "High Sensitivity SERS Substrate with Femtosecond Laser-Printed Nanohole Arrays," *Sensors 2025, Vol. 25, Page 3680*, vol. 25, no. 12, p. 3680, Jun. 2025, doi: 10.3390/S25123680.

Bağlanma Dinamik Uygulamaları için Kılavuzlu-Mod Rezonans Platformu

Rozalin Celik[1], Meryem Beyza Avci[1,3,4], Furkan Kocer[1], Nimet Yildirim-Tirgil[2], Arif E. Cetin[*1,3,4,5]

[1]Izmir Biomedicine and Genome Center, Balcova, Izmir 35340, Türkiye
[2]Department of Biomedical Engineering, Ankara Yildirim Beyazit University, Kecioren, Ankara 06010, Türkiye
[3]Izmir International Biomedicine and Genome Institute, Dokuz Eylul University, Balcova, Izmir 35340, Türkiye
[4]Department of Biophysics, Faculty of Medicine, Dokuz Eylul University, Izmir 35340, Türkiye
[5]Department of Electrical and Electronics Engineering, Istanbul Atlas University, Kagithane, Istanbul 34408, Türkiye

[*]corresponding author, E-mail: arifengin.cetin@ibg.edu.tr

Özet

Kılavuzlu-mod rezonans (KMR) sensörleri, çevresel kırılma indisindeki küçük değişimleri rezonans dalga boyu kaymaları üzerinden izleyerek etiketsiz ve gerçek zamanlı biyomoleküler analiz yapılmasına olanak sağlar. Bu çalışmada, bağlanma kinetiğinin hassas ve tekrarlanabilir biçimde incelenmesi amacıyla optofluidik bir KMR platformu geliştirilmiştir. Sistem; özel tasarlanmış ters mikroskop düzeni, 0,15 nm spektral çözünürlüğe sahip yüksek çözünürlüklü çoklu spektrometre ve otomatik çoklu pompa akış kontrol altyapısını bir araya getirmektedir. Akış otomasyonu; sensör çipinin hazırlanması, ligand ve analit inkübasyonu ile deney sonrası temizleme basamaklarını standartlaştırarak manuel müdahaleyi ve kullanıcı kaynaklı değişkenliği azaltmaktadır. Platformun kırılma indisi duyarlılığı 201,73 nm/RIU olarak belirlenmiş; IgG proteini için 0,15 ng/mL tespit limitine ulaşılmıştır. Ayrıca Protein A/G ile IgG arasındaki etkileşim gerçek zamanlı olarak izlenmiş ve bağlanma sürecine ait asosiyasyon parametresi belirlenerek sistemin kinetik analiz yeteneği gösterilmiştir. Entegre kendi kendini temizleme yaklaşımı, ardışık deneylerde kontaminasyon riskini azaltarak yeniden kullanımı desteklemektedir. Elde edilen sonuçlar, platformun tıbbi tanı, biyomoleküler etkileşim analizi ve diğer yüksek hassasiyet gerektiren etiketsiz biyosensör uygulamaları için güçlü ve tekrarlanabilir bir araç olduğunu göstermektedir.

Anahtar Kelimeler: Bağlanma dinamikleri, Kılavuzlu-mod rezonans (KMR), etiketsiz biyosensör, nanoteknoloji, optofluidik

Referanslar

[1] M. B. Avci vd., "An Optofluidic Guided-Mode Resonance Platform for Binding Kinetics Applications," *IEEE Sensors Journal*, c. 25, sy. 3, ss. 4481–4493, 2025, doi: 10.1109/JSEN.2024.3515653.

[2] R. Magnusson ve S. S. Wang, "New principle for optical filters," *Applied Physics Letters*, c. 61, sy. 9, ss. 1022–1024, 1992, doi: 10.1063/1.107703.

Label-Free Preoperative Discrimination of Odontogenic Keratocysts from Cyst-Aspirate ATR-FTIR Spectra Using Riemannian–Biochemical Fusion

Sarp Hasan Ün[1], Meryem Beyza Avci[2,3], Furkan Kocer[2], Bilge Can[6], Arif E. Cetin[2,3,4,5*]

[1]Department of Biomedical Engineering, TOBB University of Economics and Technology, Ankara, Türkiye

[2]Izmir Biomedicine and Genome Center, Balcova, Izmir 35340, Türkiye

[3]Izmir International Biomedicine and Genome Institute, Dokuz Eylul University, Balcova, Izmir 35340, Türkiye

[4]Department of Biophysics, Faculty of Medicine, Dokuz Eylul University, Izmir 35340, Türkiye

[5]Department of Electrical and Electronics Engineering, Istanbul Atlas University, Kagithane, Istanbul 34408, Türkiye

[6]Department of Biomedical Engineering, Atlas University, Istanbul, Türkiye

*Corresponding author: Arif E. Cetin, E-mail: arifengin.cetin@ibg.edu.tr

Abstract

Odontogenic keratocysts (OKCs) can resemble radicular and dentigerous cysts during routine clinical and radiographic assessment, yet their recurrence profile can alter surgical planning and follow-up. We therefore asked whether a small volume of preoperative cyst aspirate could reveal a label-free biochemical signature of OKC. To investigate this question, we combined attenuated-total-reflection Fourier-transform infrared (ATR-FTIR) spectroscopy [1] with a patient-level model designed to capture both global spectral relationships and targeted relative absorbance.

This single-center proof-of-concept secondary analysis included 46 adults with histopathologically confirmed lesions: 12 OKCs, 24 radicular cysts, and 10 dentigerous cysts. Spectra were acquired over 4000–400 cm^{-1} at 4 cm^{-1} resolution using 32 co-added scans, and technical repeats were averaged within patient before validation. The locked RCov–Ratio model fused two complementary probabilities with equal weights. RCov encoded patient-wise SNV-transformed covariance across nine contiguous fingerprint intervals between 900 and 1800 cm^{-1} plus 2800–3000 cm^{-1}, combining an affine-invariant Riemannian centroid path [2] with a tangent-space radial-basis-function support-vector machine. Ratio used class-balanced logistic regression on two training-selected log-ratios from chemically constrained Amide III/carbohydrate and CH_2/COO^- windows in the unnormalized fingerprint spectrum. The decision threshold was fixed at 0.5. Primary performance was estimated by patient-level nested leave-one-out cross-validation (LOOCV), with every feature-selection, transformation, tuning, and augmentation step confined to the corresponding outer-training set. Robustness was examined in 100 unique stratified 80/20 outer splits with complete pipeline refitting.

Nested LOOCV correctly classified 44 of 46 patients, yielding 95.65% accuracy (95% Wilson confidence interval, 85.47–98.80), 91.67% sensitivity, 97.06% specificity, and a receiver-operating-characteristic area under the curve (ROC AUC) of 0.9118. Across the 100 repeated holdouts, pooled descriptive accuracy was 87.90%, ROC AUC was 0.9133, sensitivity was 75.67%, and specificity was 93.14%. Because these 1,000 held-out predictions reuse the same 46 patients, they are correlated and do not constitute external validation. These findings show that cyst-aspirate ATR-FTIR spectra contain a reproducible patient-level signal capable of supporting OKC discrimination and establish technical feasibility for a label-free photonic sensing approach. They do not establish expected clinical accuracy: the cohort was small and class-imbalanced [3], the study was a secondary analysis, and no compatible independent cohort was accessible. Prospective multicenter validation of the frozen acquisition and analysis pipeline is therefore required before clinical utility can be inferred.

Validation	Accuracy	Sensitivity	Specificity	ROC AUC
Nested LOOCV	95.65%	91.67%	97.06%	0.9118

Keywords: odontogenic keratocyst, ATR-FTIR spectroscopy, cyst aspirate, Riemannian geometry, machine learning, nested cross-validation

References

[1] Baker MJ, Trevisan J, Bassan P, et al. Using Fourier transform IR spectroscopy to analyze biological materials. Nat Protoc. 2014;9:1771–1791. doi:10.1038/nprot.2014.110.

[2] Pennec X, Fillard P, Ayache N. A Riemannian framework for tensor computing. Int J Comput Vis. 2006;66:41–66. doi:10.1007/s11263-005-3222-z.

[3] Varoquaux G. Cross-validation failure: small sample sizes lead to large error bars. NeuroImage. 2018;180:68–77. doi:10.1016/j.neuroimage.2017.06.061.

Morphological Index Integration for White Blood Cell Classification: Beer Boundary Index and Beer Area Index as Discriminative Features

Fahad Naari Ibrahim [1], Atif Eren Arikan[2], Zeki Kus[3], Berna Kiraz[4], and Alper Kiraz[1,2]

[1] Koç University, Department of Physics, Sarıyer, İstanbul
[2] Optofil A.Ş., Esenler, İstanbul
[3] Fatih Sultan Mehmet Vakif University, Department of AI and Data Engineering, Zeytinburnu, İstanbul
[4] Istanbul Technical University, Department of AI and Data Engineering, Sarıyer, İstanbul

Abstract

This work presents two novel morphological indices - the Beer Boundary Index (BBI) and the Beer Area Index (BAI) - computed from segmented neutrophil nuclei, and their integration into a deep learning late fusion pipeline for binary classification of Band and Segmented Neutrophils. By combining these handcrafted morphological features with embeddings from two pre-trained DenseNet121 backbones, we demonstrate a significant improvement in the detection of the clinically important but underrepresented Band Neutrophil class.

Methodology

Nucleus segmentation was performed on raw purple-stained blood smear images using a MATLAB-based active contour algorithm (Chan-Vese), producing binary nucleus masks. Two morphological indices were then computed from each mask:

Beer Boundary Index (BBI): Measures the complexity and irregularity of the nucleus boundary. For each pair of boundary pixels, a line-of-sight visibility check is performed. Time complexity: $O(n^2 \times D)$ per image, where n is the number of boundary pixels and D is the image diagonal. Parallelised using Numba prange across CPU cores.

Beer Area Index (BAI): Measures the area and mass distribution of the nucleus via pixel-level scanning. Time complexity: O(W x H) per image, where W and H are image dimensions. Significantly faster than BBI.

The computed BBI and BAI scores were subsequently integrated as a third feature group into an existing late fusion pipeline. Two pre-trained DenseNet121 backbones - one binary (Band vs. Segmented) and one morphological (7-class) - extract 1032 deep features per image. The BBI and BAI scores are concatenated to form a final 1034-dimensional feature vector, on which XGBoost and LightGBM classifiers are trained.

Datasets

Three experimental configurations were evaluated: (1) Original dataset - 199 Band Neutrophils and 16,256 Segmented Neutrophils; (2) Combined dataset - augmented with approximately 600 newly acquired Band Neutrophil images; (3) New Only - the 600 new Band Neutrophil images paired with the existing Segmented Neutrophils. Each configuration was processed through the full pipeline independently.

Results : *Green rows indicate best performance. Seg. = Segmented Neutrophil.*

Dataset	Model	Band F1	Seg. F1	Macro F1	Accuracy
Original	LightGBM	0.8333	0.9975	0.9154	0.9951
Original	XGBoost	0.9492	0.9994	0.9743	0.9988
Combined	LightGBM	0.9635	0.9979	0.9807	0.9961
Combined	XGBoost	0.9740	0.9986	0.9863	0.9973
New Only	LightGBM	**0.9952**	0.9998	**0.9975**	0.9996
New Only	XGBoost	**1.0000**	1.0000	**1.0000**	1.0000

Conclusion

The integration of BBI and BAI scores into the late fusion pipeline produced a substantial improvement in Band Neutrophil detection across all experimental configurations. XGBoost achieved a Band Neutrophil F1 of 0.9492 on the original dataset, improving to 1.0000 on the new dataset. LightGBM demonstrated perfect recall with zero missed Band Neutrophils on the original dataset, which is of particular relevance in clinical diagnostic settings where missed detections carry greater risk than false positives. These results validate the discriminative value of nucleus boundary complexity as a morphological feature for neutrophil subtype classification.

Acknowledgements

The authors would like to thank Koc University and the Optofil workstation laboratory for providing the computational resources and infrastructure used in this work

References

[1] A. Kiraz, A. E. Arikan, Z. Kus, and B. Kiraz, Morphology-Based Hybrid Hierarchical Classification of Peripheral Blood Cells, SIU 2026.

Thin-Film-Assisted Laser-Induced Defect Engineering in Diamond

Rumeysa Salci[1], Okan Ozdemir[2,3], Muhammed Bilgin[4,5], Leyla C. Arslan[1,2,3*]

[1]Department of Physics, Gebze Technical University, 41400, Kocaeli, Türkiye
[2]Institute of Nanotechnology, Gebze Technical University, 41400, Kocaeli, Türkiye
[3]Nanotechnology Research and Application Center (NAUM), Kocaeli, 41400, Türkiye
[4]Nanomagnetics Instuments Inc, 06530, Ankara, Türkiye
[5] Department of Physics, Middle East Technical University, 06800 Ankara, Türkiye

corresponding author, E-mail: r.salci2021@gtu.edu.tr

Abstract
Diamond, together with its controllably engineered color centers, offers a promising platform for next-generation quantum applications owing to its exceptional optical, thermal, electrical, and spin properties. However, the controlled and scalable formation of optically active color centers over large areas remains a significant challenge. Laser-based processing provides a versatile route for spatially selective defect engineering while offering the potential for rapid and large-area processing. In this study, we investigate a thin-film-assisted approach for the controlled formation and modification of color centers in diamond using sub-bandgap nanosecond laser irradiation. 350 µm-thick, double-side-polished, type IIa, [100]-oriented single-crystal CVD diamond samples were used. Three sample sets were prepared for comparative analysis: an uncoated and two samples coated with 10 nm Si and 10 nm Ge thin films, respectively, both grown by molecular beam epitaxy (MBE). All samples were irradiated under identical conditions using a 1064 nm nanosecond pulsed laser. For both the single-crystal diamond and thin-film-coated diamond samples, irradiation is performed from the surface opposite to the coated side, enabling localized laser energy deposition and controlled modification within the diamond. Laser irradiation is expected to generate mobile vacancies while simultaneously providing the thermal energy required for their migration through the lattice. These vacancies can subsequently be trapped at substitutional nitrogen or incorporated silicon sites, resulting in the formation of NV and SiV centers, respectively.

The irradiated regions and pristine regions were characterized using photoluminescence (PL) spectroscopy, optically detected magnetic resonance (ODMR), Raman spectroscopy, X-ray diffraction (XRD), and atomic force microscopy (AFM). Our results demonstrated that nanosecond sub-bandgap laser irradiation increases the density of optically active NV and SiV color centers in single-crystal CVD diamond, with the thin-film-coated samples showing a more pronounced enhancement compared to the uncoated reference. AFM revealed clear ablation-related surface modification in all three sample sets; in the coated samples, the thin film underwent evaporation at the irradiated surface. In the uncoated sample, PL measurements additionally showed a decrease in NVH-related emission alongside the increase in NV-related emission, consistent with laser-induced hydrogen release and NVH-to-NV conversion[1,2]. ODMR measurements confirmed that the laser-induced NV centers remain spin-active, while Raman and XRD analyses showed that the single-crystal structure was preserved despite localized surface ablation. These findings suggest that thin-film-assisted laser processing offers a simple and scalable route for engineering optically and spin-active color centers in diamond, with potential applications in quantum sensing and photonic devices.

Keywords: Diamond, color centers, quantum sensing, laser irradiation

References

[1] R. Salci, O. Ozdemir, M. Bilgin, M. Mansoor, A. Oral, A.G. Ozbay, L.C. Arslan, Boosting the density of NV centers in diamond through nanosecond sub-bandgap laser irradiation, Diam. Relat. Mater. 168 (2026) 113914. https://doi.org/10.1016/j.diamond.2026.113914.

[2] M. Mansoor, K. Czelej, M. Mansoor, M. Mansoor, R. Salci, T. Linzmeyer, Y. Sorkhe, K.S. Moe, O. Ozyildirim, K. Kitajima, M.A. Sarsil, G. Hamamci, E. Taylan, O. Ergen, A. Kurt, A. Akhavan, Z. Er, S. Rubanov, N.M. Kazuchits, A. Gokce, N. Davies, S. Timur, S. Prawer, A. Zaitsev, M. Urgen, Engineering NV centers via hydrogen-driven defect chemistry in CVD diamonds for quantum applications: NVHx dissociations into NV,origin of 468 nm center, cause of brown coloration, ArXiv.Org (2025). https://arxiv.org/abs/2%0A507.00300.

MRG Cihazları İçin Silisyum Fotonik Tümdevre Ve Alıcı Eş Tasarımı

Erol Tunahan Gedik*[1], Seçkin Ata Sezgin[1], Onur Ferhanoğlu[2], Arda D. Yalçınkaya[1]
[1]Elektrik ve Elektronik Mühendisliği, Boğaziçi Üniversitesi, İstanbul, Türkiye
[2]Elektronik ve Haberleşme Mühendisliği, İstanbul Teknik Üniversitesi, İstanbul, Türkiye
erol.gedik@std.bogazici.edu.tr

Özet

Geleneksel bakır bağlantıların yol açtığı elektromanyetik kuplaj, ortak mod akımları ve RF ısınma risklerini ortadan kaldıran optik MRG sistemleri, güvenli ve düşük gürültülü iletim için popülerleşen bir alternatiftir. Bu çalışmada, doğrudan bobin üzerine tümleştirilen iki farklı RFoF alıcı ön katı mimarisi sunulmaktadır: analog MRG işaretlerinin doğrudan optik domaine aktarıldığı yapı (Şekil 1.a) ve sinyallerin ADC ile sayısal domaine çevrilerek harici modülasyonlu optik linklerle iletildiği yapı (Şekil 1.b). CMOS ve Silisyum Fotonik (SiPh) kırmıkların eş-tasarımına dayanan bu sistemlerde modülatör seçimleri mimarinin gereksinimlerine göre optimize edilmiştir. Analog yaklaşımda proses varyasyonlarına dayanıklılığı, hassas akortlanabilme imkânı ve sunduğu yüksek dinamik aralık nedeniyle MZM kullanılmıştır (Şekil 1.c). Sayısal yaklaşımda ise, kısıtlı dinamik aralığına ve üretim toleransı hassasiyetine rağmen sunduğu yüksek alan verimliliği ve yüksek EO kazancı sayesinde RRM, bir EO anahtar olarak tercih edilmiştir. Her iki yaklaşım da DWDM ile birden fazla kanalı tek fiberden iletmeye imkan verir [1]. LNA, ADC ve EO modülatör sürücü bloklarından oluşan CMOS kırmığın SiPh ile bobin üzerine tümleştirilmesi, düşük genlikli MRG işaretlerini EMI hassaslığı olmayan optik sinyallere çevirerek geleneksel RF akım koruma devrelerine olan ihtiyacı da kaldıran avantajlı bir çözüm önerisidir.

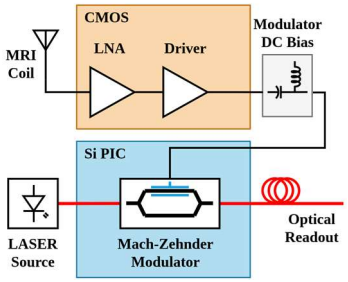

(a) Analog Yaklaşım

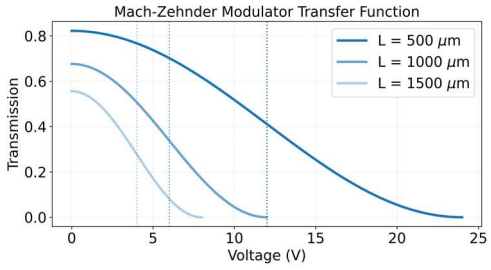

(c) MZM Transfer Fonksiyonu

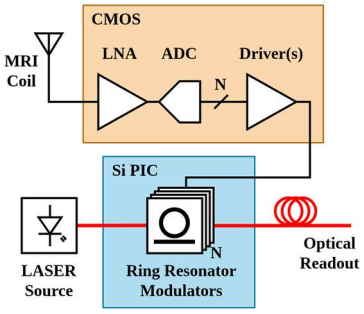

(b) Sayısal Yaklaşım

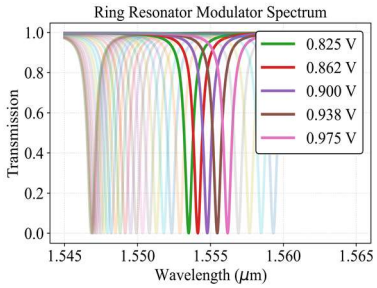

(d) RRM Spektrumu

Şekil 1: MRG sistemleri için önerilen on-coil alıcı ön katı mimarileri (a, b) ve tasarımlarda kullanılan elektro-optik modülatörlerin transfer karakteristikleri (c, d).

Anahtar Kelimeler: Silisyum Fotonik (SiPh) Tümdevre, Manyetik Rezonans Görüntüleme (MRG), Mach-Zehnder Modülatörü (MZM), Halka Rezonans Modülatörü (RRM), Yoğun Dalgaboyu Bölmeli Çoğullama (DWDM).

Acknowledgements
Bu çalışma BAP 25A02P4 ve TÜBİTAK 22AG016 kodlu projelerle desteklenmiştir.

Referanslar
[1] Asadi, H., A. D. Yalcınkaya and O. Ferhanoglu, “Implementation of a Scalable Multi-Channel WDM Optical Link for MRI Signal Transmission Using Ring Resonators a
nd MZI Switches”, 2025 International Conference on Optical MEMS and Nanophotonics (OMN), pp. 1–2, 2025.

Effect of Optical Path Length Asymmetry on the Performance of a Fiber Optic Gyroscope

İrem DİNÇ[1*], Seren KESMEN[1], Başak Çağlayan ŞAHİNER[1], Erkut Emin AKBAŞ[1] , Aylin YERTUTANOL[1], Ekmel ÖZBAY[1,2,3]

[1]Bilkent University, Nanotechnology Research Center-NANOTAM, Ankara, Türkiye
[2]Bilkent University, Department of Physics, Ankara, Türkiye
[3]Bilkent University,Department of Electrical and Electronic Engineering, Ankara, Türkiye

corresponding author, E-mail: irem.dinc@bilkent.edu.tr

Abstract

Fiber optic gyroscopes (FOGs) are high-precision inertial sensors that measure angular velocity based on the Sagnac effect. The accuracy and bias stability of a FOG are strongly influenced by non-reciprocal phase errors arising from asymmetries in the optical path. Among these asymmetries, differences in the pigtail fiber lengths of the multifunction integrated optical chip (MIOC) can contribute to phase imbalance and consequently affect the bias stability of the gyroscope.[1]

In this study, the effect of optical path length (l_1, l_2, l_3) asymmetry on the bias stability of a 1550 nm fiber optic gyroscope is investigated. Two different configurations are compared to evaluate the relationship between optical path length mismatch and FOG bias. In the first configuration, the optical path lengths are intentionally asymmetric, whereas in the second configuration, the lengths are set equal. Differences in optical lengths may lead to increased sensitivity to environmental effects, particularly temperature variations, resulting in additional non-reciprocal phase errors and bias instability.

In the first configuration, the input pigtail lengths were set to $l_1 = 0{,}6\ l_2 = 0{,}6\ l_3$, whereas in the second configuration, all optical path lengths were set equal $l_1 = l_2 = l_3$.
The effect of optical path length asymmetry on the bias of a fiber optic gyroscope was investigated. Different configurations with equal and unequal optical path lengths were evaluated to determine the relationship between optical path length mismatch and bias stability.

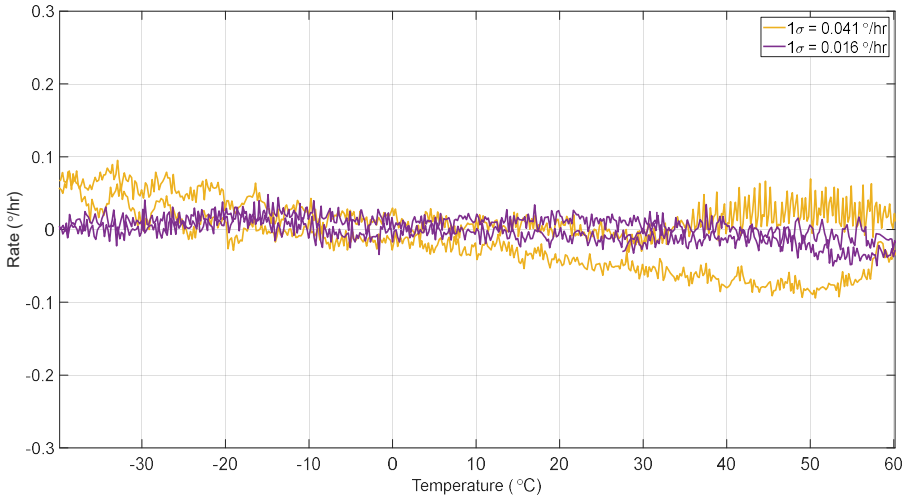

Figure-1: Comparative Rate Measurement

Keywords: Interferometric fiber optic gyroscopes / optical path length / bias stability

References

[1] Zheng, T., Xu, A., Xu, X., & Liu, M. (2023). Modeling and Compensation of Inertial Sensor Errors in Measurement Systems. Electronics, 12(11), 2458

Phase-Based Detection of Surface-Induced Errors in Fixed-WMS Methane Sensing

Emre Güralp*[1], Süheyl Töken*[1], Anıl Nehir*[1], Ekmel Özbay[1,2,3], İbrahim Özdür[4]

[1]NANOTAM, Bilkent University, Ankara, Türkiye
[2]Department of Electrical and Electronics Engineering, Bilkent University, Ankara, Türkiye
[3]Department of Physics, Bilkent University, Ankara, Türkiye
[4]Department of Electrical and Electronics Engineering, TOBB ETU, Ankara, Türkiye
*emre.guralp@bilkent.edu.tr

Abstract
This study presents a phase-based approach for reducing surface-induced measurement errors in fixed wavelength modulation spectroscopy (Fixed-WMS) methane sensing. The output of a single modulated diode laser was divided into two simultaneous optical channels. The reference channel passed through a fixed methane gas cell, while the measurement channel propagated through the open path and was collected from a Lambertian target using an independent photodetector. The first- and second-harmonic components of both channels were synchronously demodulated, and the differential harmonic phases between the open-path and reference-cell signals were extracted.

Surface-condition tests were performed using dry matte, reflective, oily, and wet targets under controlled methane concentrations. In addition to conventional harmonic-amplitude-based methane retrieval, the differential first- and second-harmonic phases were analyzed. Received optical power was independently varied and matched between surface conditions to distinguish phase variations caused by the optical/electronic detection chain from those associated with the target surface. The second-harmonic differential phase was used as the primary discrimination parameter, while the first-harmonic response was employed as a complementary indicator of wavelength detuning and surface-dependent harmonic distortion.

The measurements showed that changes in target surface condition produced characteristic deviations in the differential harmonic response that were not explained solely by variations in received optical power. In particular, surface conditions associated with erroneous methane indications produced measurable deviations from the phase behavior obtained for the dry reference surface. Comparison of conventional methane retrieval with the phase-resolved measurements demonstrated that reference-to-measurement harmonic phase information provides an additional criterion for identifying surface-induced measurement artifacts. The results establish differential harmonic phase analysis as a practical method for improving the robustness and measurement validity of Fixed-WMS methane sensing over varying target surfaces.

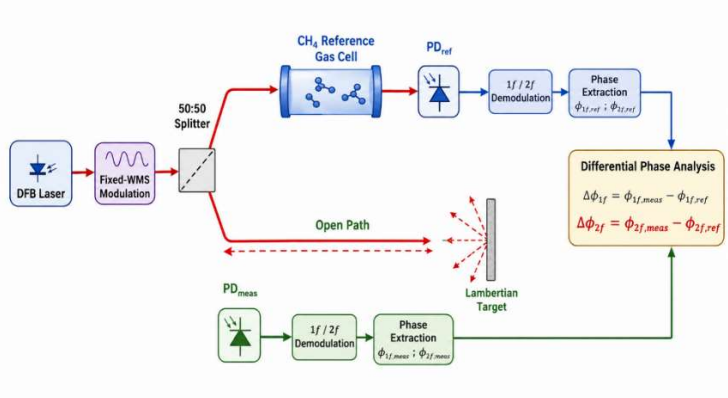

Figure 1: Schematic of the Fixed-WMS methane sensing system.

Keywords: Methane sensing, Fixed-WMS, harmonic phase, phase-sensitive detection,optical modulation

References
[1] J. Li, W. Ma, Z. Wang, Y. Zhou, L. He, M. Lin, and Y. Ji, "Miniaturized and portable laser gas sensor for standoff methane detection with non-cooperative targets," Appl. Spectrosc., 78(1), 76–83 (2024).
[2] S. Shen, W. Li, M. Wang, D. Wang, Y. Li, and D. Li, "Methane near-infrared laser remote detection under non-cooperative target condition based on harmonic waveform recognition," Infrared Phys. Technol., 120, 103977 (2022).
[3] C. Zhu, P. Wang, T. Chu, F. Peng, and Y. Sun, "Second harmonic phase angle method based on WMS for background-free gas detection," IEEE Photonics J., 13(5), 1–6 (2021).

Halka Optik Ağlarda Trafik Ağırlıklı Kuvvetlendirici Yerleşimi

Neda Naderi, N. Özlem Ünverdi
Yıldız Teknik Üniversitesi, Elektrik - Elektronik Fakültesi
Elektronik ve Haberleşme Mühendisliği Bölümü, 34220 Esenler, İstanbul, Türkiye
neda.naderi@std.yildiz.edu.tr , unverdi@yildiz.edu.tr

Özet

Dalga boyu bölmeli çoğullama (Wavelength Division Multiplexing, WDM) tabanlı optik omurga ağlarında iletim kalitesi; fiber zayıflaması, kuvvetlendirici gürültüsü, doğrusal olmayan girişimler ve optik sinyal-gürültü oranı (Optical Signal-to-Noise Ratio, OSNR) gibi fiziksel katman etkilerinin birlikte değerlendirilmesini gerektirir [1]. Erbiyum katkılı fiber kuvvetlendiriciler (Erbium-Doped Fiber Amplifier, EDFA), uzun mesafeli iletimde sinyal gücünü yeniden yükseltirken aynı zamanda kuvvetlendirilmiş kendiliğinden yayılım gürültüsü oluşturur. Bu nedenle, EDFA yerleşimi sadece güç bütçesi açısından değil, ağ genelindeki iletim kalitesi ve uygulanabilir bağlantı oranı açısından da kritik bir tasarım kararıdır. İletişim teknolojileri içinde kilit konumda bulunan 5G ve benzeri yüksek trafik yoğunluklu servislerde, ortalama ağ başarısının yanı sıra yoğun trafik taşıyan ve işletme açısından öncelikli kaynak-hedef çiftlerinin korunmasının da dikkate alınması büyük önem taşır.

Makine öğrenmesi yöntemleri, son yıllarda optik ağlarda kalite tahmini ve planlama süreçlerini hızlandırmak amacıyla yaygın biçimde incelenmektedir [2]. Önceki çalışmamızda, fiziksel katman doğrulamasını koruyarak aday EDFA yerleşimlerini makine öğrenmesi ile sıralayan taramalı bir planlama çerçevesi sunulmuştur [3]. Bu çalışmada, söz konusu yaklaşım, eşit trafik varsayımının ötesine taşınarak trafik ağırlıklı yoğunlaşma (hotspot) talep profilleri altında değerlendirilmiştir. Böylece yöntemin genel uygulanabilirliğinin yanında yüksek öncelikli bağlantıları koruma yeteneği de irdelenmiştir [4].

Analizde, Ring-8 ile Ring-16 arasındaki WDM halka topolojilerinde, dengeli referans (uniform_reference), tek merkezli 5G trafik yoğunlaşması (core_5g_hotspot), çift trafik yoğunlaşmalı karma trafik (dual_hotspot_mixed) ve kritik omurga yükü (critical_backbone_stress) olmak üzere dört trafik profili kullanılmıştır. Aday EDFA maskeleri, Rastgele Orman (Random Forest) modeli ile sıralanmış, ancak son kararlar, her durumda kesin fiziksel katman iletim kalitesi (Quality of Transmission, QoT) doğrulamasına uygulanmıştır. BASELINE, GREEDY, ML_SCREENED, ML_SCREENED_IMPROVED ve tam arama esaslı OPTIMUM yöntemleri; klasik uygulanabilirlik oranı, trafik ağırlıklı uygulanabilirlik, kritik trafik kapsaması, optimumdan sapma ve kesin QoT değerlendirme sayısı açısından karşılaştırılmıştır.

Toplu hotspot deneylerinde, ML_SCREENED_IMPROVED yönteminde, 0,5609 trafik ağırlıklı uygulanabilirlik ve 0,5491 kritik trafik kapsaması elde edilmiş, OPTIMUM yönteminde ise söz konusu olan bilgiler için sırasıyla 0,5655 ve 0,5582 değerlerine ulaşılmıştır. Buna karşılık önerilen yöntem, 266 kesin QoT değerlendirmesi kullanmış ve tam arama, 3981 değerlendirme gerektirmiştir. Bu sonuç, kesin fiziksel katman değerlendirme yükünde yaklaşık olarak %93,3 azalma sağlanırken optimum trafik ağırlıklı uygulanabilirlik seviyesinin yaklaşık olarak %99,2'sinin korunduğunu açıklamaktadır. Bulgular, trafik farkındalıklı makine öğrenmesi destekli taramanın, özellikle yoğun trafik taşıyan kritik optik bağlantıları koruyarak EDFA planlamasında kesin fiziksel katman değerlendirme yükünü önemli ölçüde azaltabilecek etkili bir karar destek yaklaşımı olduğunu göstermektedir.

Anahtar Kelimeler: İletişim teknolojileri, halka optik ağ, dalga boyu bölmeli çoğullama, erbiyum katkılı fiber kuvvetlendirici, makine öğrenmesi

Bilgilendirme: Bu çalışma, Yıldız Teknik Üniversitesi Bilimsel Araştırma Projeleri Koordinasyon Birimi (BAP) tarafından FYL-2025-6850 numaralı proje kapsamında desteklenmiştir.

Referanslar

[1] Agrawal G. P., Fiber-Optic Communication Systems, 4th Edition, Wiley, 2010.
[2] Ayassi R. et al., "Survey on the use of machine learning for quality of transmission estimation in optical transport networks," Journal of Lightwave Technology, 40(17), 5803-5815, 2022, doi: 10.1109/JLT.2022.3184178.
[3] Naderi N. and Ünverdi N. Ö., "Analysis of Erbium-Doped Fiber Amplifiers Used in Ring Backbone Optical Networks Using Machine Learning," AURUM Journal of Engineering Systems and Architecture, 10(1), 89-103, 2026, doi: 10.53600/ajesa.1957573.
[4] Naderi N., "Optik Ağların Performans Analizi ve Modellenmesi", Yüksek Lisans Tezi, Yıldız Teknik Üniversitesi, Fen Bilimleri Enstitüsü, İstanbul, 2026.

Haberleşme Ağlarının Omurga Yapısındaki Optik Haberleşme Sistemlerinin Performans Analizi

N. Özlem Ünverdi [1], N. Aydın Ünverdi[2]

[1]Yıldız Teknik Üniversitesi, Elektrik - Elektronik Fakültesi
Elektronik ve Haberleşme Mühendisliği Bölümü, 34220 Esenler, İstanbul, Türkiye
unverdi@yildiz.edu.tr

[2]İstanbul Teknik Üniversitesi, Makina Fakültesi
Makina Mühendisliği Bölümü, 34437 Gümüşşsuyu, İstanbul, Türkiye
unverdi@itu.edu.tr

Özet

Optik haberleşme sistemleri, sağladıkları avantajlar nedeniyle veri iletimi, telefon ağları, ulaşım, sağlık, savunma ve güvenlik amaçlı çalışmalar gibi birçok farklı alanda tercih edilmektedir. Haberleşme ağlarındaki optik haberleşme sistemleri, ağların omurgasında kilit konumda bulunmaktadır. Bu çalışmada, optik haberleşme yapısı, sistem bazında incelenmiştir. Sistem, OptiSystem 23.0 simülasyon programı ile tasarlanarak analiz edilmiştir [1-8].

Optik haberleşme sisteminin optimizasyonunda, verici katında, lazer, darbe üreteci ve modülatör kullanılmıştır. Sistemde dalga boyu bölmeli çoğullama (Wavelength Division Multiplexing, WDM) mekanizmasından yararlanılmıştır. Fiber optik kablodan iletilen veri kuvvetlendirilmiştir. Alıcı katında, fotodiyot ve filtre yer almıştır. Sistemin performansı değerlendirilmiştir. Analizde, optik spektrum analizör, RF spektrum analizör, WDM analizör, BER analizör, zaman domeninde görselleştirici ve güçölçer ile ölçümler yapılmıştır. Lazer, darbe üreteci, modülatör, kuvvetlendirici, izolatör, fotodiyot, filtre ve kanal sayısı konusunda optimizasyon çalışmaları yapılmıştır. Sürekli dalga lazeri (continuous wave laser, CW laser), Sıfıra Dönüşsüz (Non Return to Zero, NRZ) darbe üreteci, Mach-Zehnder (MZ) modülatörü, EDFA (Erbium-Doped Fiber Amplifier, Erbiyum Katkılı Fiber Kuvvetlendirici), ideal izolatör, PIN fotodiyot ve Gaussian optik filtrenin bulunduğu sistemin yüksek verimle çalıştığı gözlenmiştir. Kanal sayısının artmasıyla veride bozulmalar izlenmiştir. BER analizörü ile incelenen sistemin göz diyagramı irdelenmiş ve maksimum kalite faktörü değeri belirlenmiştir. Sistemin yüksek performansla çalıştığı görülmüştür.

Analizlerde, optik devre elemanlarının haberleşme ağlarının performansını etkilediği ve bu bileşenlerin optimizasyonunun yüksek hızlı ağ altyapıları için çok önemli olduğu saptanmıştır. Optik haberleşme sistemlerinin, haberleşme ağlarının anahtarı olduğu sonucuna varılmıştır.

Anahtar Kelimeler: İletişim teknolojileri, haberleşme ağları, optik haberleşme, çoğullama, optik devre elemanları

Referanslar

[1] Agrawal G. P., Fiber-Optic Communication Systems, Wiley Interscience, New York, 2002.
[2] Keiser, G., Optical Communication Essentials, McGraw-Hill Companies, New York, 2004.
[3] Simmons J. M., Optical Network Design and Planning, Springer, New York, 2008.
[4] Kazovsky L. G., Cheng N., Shaw W-T., Gutierrez D. and Wong, S-W., Broadband Optical Access Networks, John Wiley & Sons, New Jersey, 2011.
[5] Pachnicke S., Fiber-Optic Transmission Networks: Efficient Design and Dynamic Operation, Springer-Verlag, Heilderberg, 2012.
[6] Ünverdi N. Ö., "Düz ve Bükülmüş Optik Dalga Kılavuzlarının Karşılıklı Kuplajına Kılavuzlanmış Modların Evanescent Alanlarının ve Sızıntılı Modların Etkisi", Doktora Tezi, Yıldız Teknik Üniversitesi, 1998.
[7] Unverdi N. O., Unverdi N. A., "Signal Analysis of Optical Circuit Elements", Third International Symposium on Engineering, Artificial Intelligence and Applications (ISEAIA 2015), Girne, North Cyprus Turkish Republic, November 4-6, 2015.
[8] Unverdi N. O., Unverdi N. A., "Analysis and Modelling of Optical Circuit Elements", Fourth International Symposium on Engineering, Artificial Intelligence and Applications (ISEAIA 2016), Girne, North Cyprus Turkish Republic, November 2-4, 2016.

Experimental Investigation of PBS-Induced Antipodality in Polarization-Encoded QKD

Abdulhay Can Kara*[1,2], Yusuf Kayra Gül[2], Ekmel Özbay[1,2,3], İbrahim Özdür[4]

[1]*NANOTAM, Bilkent University, Ankara, Türkiye*

[2]*Department of Physics, Bilkent University, Ankara, Türkiye*

[3]*Department of Electrical and Electronics Engineering, Bilkent University, Ankara, Türkiye*

[4]*Department of Electrical and Electronics Engineering, TOBB ETÜ, Ankara, Türkiye*

*abdulhay.kara@bilkent.edu.tr

Abstract

Quantum key distribution (QKD) is a method that enables the creation of symmetric keys between two points, whose security is based on quantum physics [1]. Although its security has been proven theoretically, imperfections in practical devices may cause deviations from ideal system behavior [2]. In polarization-encoded QKD, one such imperfection is the non-ideal generation and separation of orthogonal polarization states. Since ideal orthogonal states are represented by antipodal points on the Poincaré sphere, a loss of antipodality provides a direct indication of imperfect polarization-state geometry.

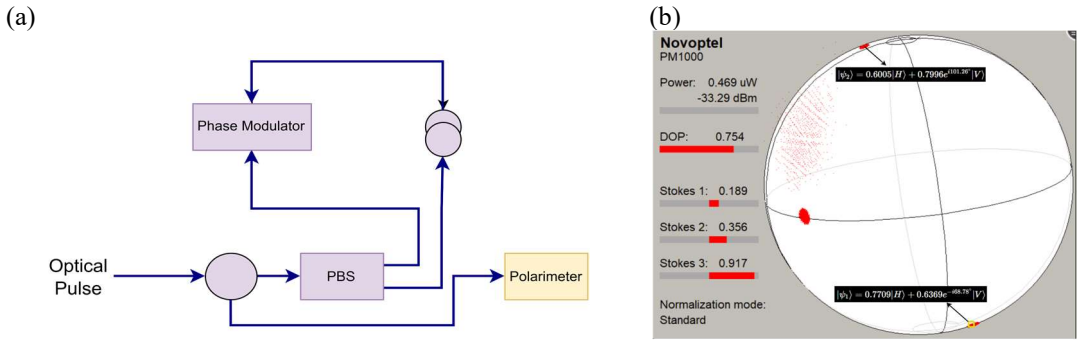

Figure 1: (a) iPOGNAC-based polarization encoder. (b) Example polarization states measured on the Poincaré sphere for a selected PBS configuration.

In this work, we experimentally investigate how the splitting behavior of a polarization beam splitter (PBS) affects the antipodality of states generated in an iPOGNAC-based polarization encoder. The structure considered here is shown in Fig. 1(a), following the self-compensating Sagnac polarization-encoding principle [3]. Experimentally, the PBS is first characterized through its output-power separation, and the polarization states encoded with that PBS are then measured on the Poincaré sphere, as illustrated in Fig. 1(b).

The key idea is that the effective 45° splitting condition of the PBS directly influences the orthogonality of the encoded states. Ideally, a 45° polarized input is equally projected onto the two orthogonal PBS axes. As the 45° alignment and the associated power separation deviate from the ideal case, the relative amplitudes of the two optical components change, and the generated state pair can move away from the antipodal condition. This degradation of orthogonality is expected to increase the discrimination error at the receiver and therefore contribute to QBER.

As a next step, the measured antipodality will be compared directly with the measured QBER for the different PBS configurations.

Keywords: Quantum Key Distribution (QKD), polarization encoding, iPOGNAC, polarization beam splitter, Poincaré sphere, antipodality

References

[1] Bennett, Charles H., and Gilles Brassard. "Quantum cryptography: Public key distribution and coin tossing." Theoretical Computer Science 560 (2014): 7-11.

[2] Tamaki, Kiyoshi, Marcos Curty, Go Kato, Hoi-Kwong Lo, and Koji Azuma. "Loss-tolerant quantum cryptography with imperfect sources." Physical Review A 90.5 (2014): 052314.

[3] Agnesi, C., Avesani, M., Stanco, A., Villoresi, P., & Vallone, G. (2019). All-fiber self-compensating polarization encoder for quantum key distribution. Optics Letters, 44(10), 2398-2401.